WASHINGTON UNIVERSITY
SEVER INSTITUTE OF TECHNOLOGY
DEPARTMENT OF CHEMICAL ENGINEERING

GAS HOLDUP AND LIQUID PHASE MIXING IN TRAYED BUBBLE COLUMN REACTORS

by Javier Alvaré
Prepared under the direction of Professor Muthanna H.Al-Dahhan

---

A thesis presented to the Sever Institute of
Washington University in partial fulfillment
of the requirements of the degree of
MASTERS OF SCIENCE
August 2002
St. Louis, Missouri

WASHINGTON UNIVERSITY
SEVER INSTITUTE OF TECHNOLOGY
DEPARTMENT OF CHEMICAL ENGINEERING

ABSTRACT

GAS HOLDUP AND LIQUID PHASE MIXING IN TRAYED BUBBLE COLUMN REACTORS

by Javier Alvaré Castro

ADVISOR: Professor Muthanna.H. Al-Dahhan

August 2002
St. Louis, Missouri

The sectionalization of conventional Bubble Columns into Trayed Bubble Columns by perforated trays has been used in chemical, biochemical, and petroleum processes as an effective way to reduce the liquid axial backmixing, and to improve the gas-liquid contacting efficiency (*Maretto et al., 2000; Palaskar et al., 2000;* and *Dreher et al., 2001)*.

The objective of this work is to investigate the effect of tray hole diameter, tray open area, superficial gas and liquid velocities, gas sparger design, and liquid phase on gas holdup, pressure drop across the trays, and overall liquid-phase backmixing.

An experimental co-current Trayed Bubble Column set-up has been constructed. The column, which has a diameter of 20 cm and total height of 274 cm, is sectionalized into five stages by four perforated plates. The effect of gas sparger was analyzed by

comparing the performance of a perforated plate with a single nozzle. Air-water and air with an aqueous solution of surfactants were used as gas-liquid systems.

The overall gas holdup was determined by the Gas Disengagement Technique, whereas the staged gas holdup and the pressure drop across the trays were measured by Differential Pressure Transducers. The extent of liquid-phase overall mixing was investigated in light of model interpretation of tracer response experiments. The N-CSTR in Series with Backmixing Model and the Axial Dispersion Model (ADM) were used.

The trays significantly increase the overall gas holdup, without introducing a significant pressure drop penalty. The tray hole diameter and the superficial gas velocity were found to be the most important factors. The effect of the studied variables on the overall liquid backmixing was quantified by fitting the experimental E-curves of the injected tracer to the models. The N-CSTR in Series with Backmixing model matches the experimental tracer response curves better than the ADM. The effect of operating conditions and tray design was analyzed based on the values of the parameters of the former model. The axial mixing of the liquid phase is largely reduced by the presence of the trays. A decrease in the superficial liquid velocity and in the tray open area reduces the liquid backmixing.

Contents

Tables

Figures

Nomenclature

$C(t)$	[gm cm^{-3}]	Tracer concentration
$C^*(\theta_i)$	[-]	Dimensionless tracer concentration (N-CSTR with Backmixing Model)
$\overline{C}(Z,\theta)$	[-]	Dimensionless tracer concentration (ADM)
D_c	[cm]	Column diameter
D_L	[cm^2 s^{-1}]	Liquid phase axial dispersion coefficient
$D_{L,i}$	[cm^2 s^{-1}]	Liquid phase axial dispersion coefficient in the i^{th} stage
d_{BP}	[cm]	Primary bubble size
d_{BS}	[cm]	Secundary bubble size
d_o	[cm]	Tray hole diameter
$E(t)$	[s^{-1}]	Exit age density function
$E_D(\theta)$	[-]	Dimensionless exit age density function
$\overline{E}(s)$	[-]	Dimensional Laplace transfer function
$\overline{E}(s^*)$	[-]	Dimensionless Laplace transfer function
$f_{cut-off}$	[Hz]	Cut-off frequency
g	[cm^2 s^{-1}]	Acceleration of gravity
H_c	[cm]	Height of the column
H_{gas}	[cm]	Height of the gas-phase bed
H_{liquid}	[cm]	Height of the liquid-phase bed
H_S	[cm]	Height of the stage (tray spacing)
H_{SR}	[cm]	Height of the sparger region
h	[cm]	Distance between pressure drop probes
k	[-]	Backmixing coefficient
k_T	[ohm^{-1} cm^{-1}]	Conductivity at temperature T
k_{25}	[ohm^{-1} cm^{-1}]	Conductivity at $T=25^0C$

m_T	[gm]	Total mass of tracer
N	[-]	Total number of stages in the column
N_t	[-]	Total number of trays in the column
n_B	[-]	Order of the Butterworth filter
n_i	[-]	n^{th} stage in a column with N total stages
L	[cm]	Length of the column
P	[inches of water]	Absolute pressure
Q_B	[$cm^3\ s^{-1}$]	Backward liquid flowrate
Q_F	[$cm^3\ s^{-1}$]	Forward liquid flowrate
Q_L	[$cm^3\ s^{-1}$]	Net liquid flowrate
R^L	[-]	Laplace domain residual function
R^t	[-]	Time domain residual function
S_d	[-]	Standard deviation
s	[s^-1]	Dimensional Laplace Transform variable
s*	[-]	Dimensionless Laplace Transform variable
T	[^0C]	Temperature
t	[t]	Time variable
$\bar{t}$	[s]	Mean residence time
$\bar{t}_n$	[s]	Mean residence time at the n^{th} stage
U_g	[cm s^{-1}]	Superficial gas velocity
U_l	[cm s^{-1}]	Superficial liquid velocity
$U_{l,h}$	[cm s^{-1}]	Superficial liquid velocity at the tray holes
V_c	[cm^3]	Volume of the column
V_{gas}	[cm^3]	Volume of the gas-phase bed
V_i	[cm^3]	Volume of the i^{th} stage
V_{liquid}	[cm^3]	Volume of the liquid-phase bed
V_S	[cm/s]	Slip velocity
W_0	[cm s^{-1}]	Superficial gas velocity at the tray holes
Z	[-]	Dimensionless axial location coordinate
z	[cm]	Axial location coordinate

Greek symbols

δ	[cm]	Thickness of the tray
$\delta(\theta)$	[-]	Dirac impulse function
Δl	[cm]	Length of the cloud of tracer
Δl_i	[cm]	Length of the i^{th} stage
ΔP	[inches of water]	Pressure drop
ΔT	[^oC]	Temperature gradient
Δt	[s]	Injection time
$\Delta\theta$	[-]	Dimensionless time step
ε_g	[-]	Overall gas holdup
ε_l	[-]	Overall liquid holdup
$\bar{e}_g$	[-]	Mean gas holdup
ε_g^{exp}	[-]	Experimental overall gas holdup
ε_g^{pred}	[-]	Predicted overall gas holdup
$\varepsilon_g(z)$	[-]	Axial gas holdup profile
Γ	[-]	Gamma function
$\Phi(p_j)$	[-]	Objective function (Equation 4.4)
μ_l	[gm cm^{-1} s^{-1}]	Viscosity of the liquid phase
μ_1	[s]	First moment of E-curve
μ_2	[s^2]	Second moment of E-curve
ρ_{gas}	[g cm^{-3}]	Density of the gas phase
ρ_{liquid}	[g cm^{-3}]	Density of the liquid phase
σ^2	[s^2]	Dimensional variance
σ^2_D	[-]	Dimensionless variance
$\sigma^2_{D,n}$	[-]	Dimensionless variance at the n^{th} stage
σ_l	[dyn cm^{-1}]	Surface tension of the liquid phase

θ	[-]	Dimensionless time
θ_n	[-]	Dimensionless time at the n^{th} stage

Dimensionless Numbers

Fr_l	$\frac{U_l}{\sqrt{g\,d_0}}$	Froude number of the liquid phase
Fr_g	$\frac{U_g}{\sqrt{g\,d_0}}$	Froude number of the gas phase
Mo	$\frac{\mu_l^4\, g}{\rho_l\, \sigma_l^3}$	Morton number
Pe	$\frac{U_l\, L}{D_L\,(1-\varepsilon_g)}$	Peclet number

Abbreviations

ADM	Axial Dispersion Model
CMC	Carboxyl Methyl Cellulose
B	N-CSTR with Backmixing Model
BC	Bubble Column
D	Dimensionless
d.f.	degrees of freedom
E	Experimental
FFS	Final Filtered Signal
FP	Flow Parameter
FS	Filtered Signal
FTS	Filtered plus Thresholded Signal
G-L	Gas Liquid
G-L-S	Gas-Liquid-Solid
g	gas

l	liquid
L	Laplace domain
M	Model
MRF	Mean Relative Error
O.A.	Open Area
RES	Residual
RS	Raw Signal
RT	Residence Time
S.E.	Standard Error
SCFH	Standard Cubic Feet per Hour
SDS	Sodium Dodecyl Sulfate
T	Time domain
TBC	Trayed Bubble Column
TOL	Tolerance
wt	Weight fraction

Acknowledgements

I would like to deeply thank my advisor, Professor Muthanna Al-Dahhan, for giving me the opportunity and the economic support to make this research work possible. His constant supervision and advice helped me to always keep focused on the objectives of my work during all the steps of this effort.

I also owe a great deal to Professor Milorad Dudukovic, Chairman of the Department of Chemical Engineering, for many different reasons, but in special for providing me with the theoretical tools needed to achieve the goals of this project.

I would like to express my gratitude to my all CREL colleagues and fellow graduate students, and in special to Aravind Rammohan, Puneet Gupta, Shantanu Roy, and Abdenour Kemoun for being available all the time and for giving me the pleasure of their friendship.

I am very grateful to Steve Picker, technician of the Units Operation Laboratory, for his advice and hands-on help to solve many of challenging problems encountered in the development of the experimental part of this work.

None of this would have been possible without the support and patience of my fiancée, Michele, and my parents who always were there to cheer me up in the moments when I most needed it.

Finally, I want to especially dedicate this thesis to my friend and fellow graduate student, Piuyush Gigras, who recently has passed away in a terrible car accident.

Chapter 1 General Introduction

1.1 General Introduction and Motivation

Bubble Columns are widely used as gas-liquid, or gas-liquid-solid reactors in chemical, petrochemical, biotechnological and waste treatment industrial processes (*Shah et al., 1982*). Their advantages over other contacting devices are the simplicity of their construction and maintenance, low energy consumption, and minimal space requirements due to their vertical design.

The addition of trays to conventional bubble columns helps to further improve the intensity of interfacial transport and to reduce the axial dispersion of the gas and liquid phases, which is needed in some industrial processes. The operating mode, flow arrangement, and plate internals have a strong effect on the performance of these reactors, as well as on the extent of axial backmixing reduction. The columns can be operated in a semi-batch or continuous mode. In the continuous mode, two different flow arrangements are possible: co-current (upward or downward flow direction), and counter-current. Many different types of internals can be used to achieve the desired sectionalization. A general classification could be based on whether the internals have downcomers or not. These two generic groups, with and without downcomers, can be further classified by the design of the plate openings and the length of the downcomer tubes. Within the classification of trays based on the plate openings, the following types can be used: perforated Karr plates, porous plates, and bubble-cup plates. Also, it has been proposed the use of trays made from woven fibrous catalytic layers (*Hoeller et al., 2001*), or structural packing (*Urseanu et al., 2001*).

The presence of the trays introduces a number of advantages, and minor disadvantages, to the performance of multistage bubble columns compared to single stage or conventional bubble columns. The main advantages of sectionalization are the increase

in the holdup of the dispersed phase, and the reduction of the axial backmixing of the gas and liquid phases. There is an energetic disadvantage due to the pressure drop losses introduced by the trays. However with proper tray design, this effect can be minimized.

The lack of fundamental and experimental information regarding the hydrodynamics and mixing of multistage bubble columns have made the design and scale-up of these reactors a difficult task. Their use among the Chemical Process Industries (CPI) has been much more limited than the conventional single stage bubble columns for these reasons.

Trayed Bubble Columns (TBC) have been applied in biotechnology, where low backmixing is required to achieve high substrate conversion. For instance, *Schugerl et al., 1977* analyzed their performance as biological fermentors in aerated slurry systems (e.g. continuous single-cell protein production). *Bakopoulos, 1998* described a very promising application as photo-bioreactors by employing algae to produce fine chemicals. Other chemical processes that have benefited from the unique hydrodynamic and mixing characteristics of TBC include: ozonation of drinking and waste water (*Munter et al., 1990*), oxidation of anthraquinone to produce hydrogen peroxide (*Eickhoff et al., 2000*), Fischer-Tropsch synthesis of paraffins from syngas using a slurry catalyst (*Maretto et al., 2000)*. A petrochemical process where trayed bubble columns have recently found a very important application is in the Visbreaking operation of petroleum residues (*Dassori, 1999; and Palaskar et al., 2000*). Visbreaking is an important application of thermal cracking because it reduces the viscosity of the residue fed into the process. Traditionally, the process was entirely carried out in a furnace, where the necessary cracking temperatures (450-460 C) could be achieved. However, a more efficient alternative is to substitute for the furnace a preheating stage followed by a soaker where the cracking reactions take place. The soaker allows for a much longer residence time for the cracking reactions to occur than in the furnace. Thus, the required working temperature conditions (300-400 C at 2-5 bar of pressure) can be lowered. As a result, the operating costs and coke formation are considerably reduced. Pressurized bubble columns are the ideal

reactors to be used as soakers because of their extraordinary high mass and heat transfer properties. During the cracking process, the low molecular weight components formed during the chain scission reactions are in gaseous form, and thus bubble through the liquid bed. The intense gassing is responsible for axial liquid backmixing, which causes an undesirable overcracking of the residue. As explained earlier, the addition of internals to conventional bubble columns can significantly reduce this problem by reducing the axial liquid backimixing.

1.2 Overall Objectives

As already stated, there is a lack of information about the effect of partition on the hydrodynamics and liquid mixing behavior of bubble columns. Only a few authors have reported specific aspects of the hydrodynamics, operation, design and scale-up of these reactors (*Vinaya 1995*; *Kastanek et al., 1992*; *Poncin et al., 1990*; *Chen et al., 1988; Chen et al., 1986; and Nishikawa et al., 1985*).

Therefore, the goal of the present study is to provide experimental knowledge about the effect of the perforated tray design, operating conditions, liquid phase properties and gas sparger on key hydrodynamic parameters, such as overall gas holdup, gas holdup axial profile, pressure drop across the trays and overall liquid phase mixing.

1.3 Outline of the Thesis

This thesis has been divided in two main sections. Part I deals with the experimental study of the effect of tray design, superficial gas and liquid velocities, liquid phase and gas sparger type on overall gas holdup, axial gas holdup profile and pressure drop across the trays. Part II focuses on the effects of tray design and superficial gas and liquid velocities on the overall liquid phase mixing characteristics of Trayed Bubble Columns.

Each part is individually structured and covers the following aspects: introduction, motivation, objectives, literature survey, experimental setup and apparatus, experimental results, and interpretation of results. Chapter 9 summarizes the main conclusions of this study and suggests some ideas for future work. In addition, several appendixes have been added at the end.

Chapter 2 Gas Holdup and Pressure Drop: Introduction, Objectives, and Literature Review

2.1 Introduction

Overall Gas Holdup e_g is an important parameter in the design and scale-up of bubble columns. It represents the volumetric fraction of the dispersed phase in the two-phase flow system. The gas holdup coupled with the knowledge of the mean bubble diameter allows the determination of the gas-liquid interfacial area, which is necessary, for instance, in the prediction of the gas-liquid mass transfer coefficient (*Shah et al., 1982*). The average bubble size, bubble rise velocity, and the rate of coalescence and break-up are the important factors that govern the extent of the gas holdup in bubble column reactors.

The effects of design and scale-up variables, and of the operating conditions on gas holdup should be properly characterized for reliable design and scale-up of trayed bubble columns. In these columns, the gas volumetric fraction mainly depends on the superficial velocity of the dispersed and continuous phases, physical properties of the gas and liquid phases, column dimensions (diameter, total height, and stage height), geometric design of the trays (hole diameter, and total open area), flow operation arrangement (batch, upward/downward co-current or counter-current), and type of gas sparger (single or multi nozzle, perforated plates, and others). While some authors have conducted experimental studies in Trayed Bubble Column reactors (*Yang et al., 1989; Chen et al., 1986, Schugerl, 1977*; and a few others), only *Vinaya (1994)* developed a correlation for the estimation of the overall gas holdup in counter-current columns as a function of most of the factors listed above. As mentioned in Section 1.1, a petrochemical process where trayed bubble columns have recently found a very important application is the Visbreaking operation of the petroleum residue (*Dassori, 1999; and Palaskar et al., 2000*). In this process, the upward co-current flow arrangement is preferred over the

counter-current scheme because of the larger degree of liquid backmixing reduction achieved by the former. Therefore, a systematic investigation in co-current conditions is needed to facilitate the design of these reactors.

The average bubble size in the column is set by the balance between coalescence and external break-up forces. Coalescence is significantly influenced by the physical properties of the liquid phase, whereas the break-up phenomenon is mainly due to disturbances at the interface caused by external factors. Therefore the use of non-coalescing liquid systems helps to control the bubble size growth, which in turn increases the overall gas holdup.

In the Visbreaking process, the columns can be usually operated at very high gas holdup conditions because of the non-coalescence nature and low surface tension of the liquid systems encountered. In fact, we can simulate these conditions in a cold flow model by using an aqueous mixture of chemical surfactants (*Liang et al., 1987*). Surfactants lower the surface tension of the medium, prompting the formation of small bubbles, and promoting non-coalescing tendency in the rising gas bubbles. The reactors are usually operated at large superficial gas velocities in the so-called churn-turbulent regime. In this regime, there are large radial density variations that give rise to an intense liquid phase recirculation pattern (*Myers, 1986*). In addition, a variation of the gas holdup in the axial direction has also been reported (*Joshi et al., 1998*). The axial gas holdup profile is steeper in the sparger region than in the rest of the column due to the bubble size adjustment that occurs in this zone. The measurement of the pressure profile along the height of the column (i.e. by differential pressure transducers) can be used to determine the gas holdup axial profile (*Hewitt, 1982*).

The trays introduce an additional pressure drop to the normal operation of the bubble column. This fact negatively affects the economics of the process by increasing the costs of operation. Thus, aspects such as tray design and operating ranges should be studied to minimize the pressure drop losses across the trays.

2.2 Objectives

The specific objectives of the gas holdup and pressure drop study can be summarized as follows:

1. Investigate the effect of the gas and liquid superficial velocities on both overall and staged gas holdups. The overall holdup can be measured via Gas Disengagement Technique (DGT), whereas the staged holdup can be determined via Differential Pressure Transducer (DPT) measurements.

2. Study the effect of the tray design (hole diameter and open area) by comparing the overall gas holdup obtained with three different tray designs to the column without trays.

3. Investigate the effect of the liquid phase physical properties on the overall gas holdup via testing two different liquid systems: tap water and an aqueous solution of a surfactant mixture (1 % Butanol, and 0.01 % wt. Sodium Dodecyl Sulfate). This surfactant system mimics the physical properties (surface tension) of the heavy oil fractions fed into the Visbreaking Process *(Dassori, 1999)*.

4. Study the effect of the gas sparger geometry on the overall and staged gas holdup by testing two different gas-distributing systems: single nozzle, and perforated plate spargers.

5. Characterize the pressure drop across the trays, and evaluate the effect of tray geometry, gas and liquid superficial velocities, and gas sparger on the measured pressure drop.

6. Develop, if needed, an expression for the prediction of the overall gas holdup as a function of the studied variables.

2.3 Literature Review

As it was mentioned in Section 1.1, the amount of scientific literature available on this topic is quite scarce. The addition of perforated trays into conventional single stage bubble columns was suggested to reduce the liquid phase backmixing and hence to increase process efficiency, especially in biological fermentation processes (*Schugerl et al., 1977*). Recently bubble columns were used as gas-liquid soakers in the petrochemical industry to promote the cracking of heavy oil residues (*Dassori, 1999*).

Table 2.1 summarizes most of the published work in the open literature regarding the overall gas holdup in multistage bubble columns.

Schugerl et al., 1977 studied the effect of tray geometry, number of stages, and physical properties of the liquid phase on the overall gas holdup and volumetric mass transfer coefficient. They reported that the highest gas holdup is obtained with the smallest tray hole diameter and tray open area. An aqueous solution of 1% ethanol gave higher gas holdups than water in both single stage and multi-stage columns. The authors recommended larger stage height for coalescence suppressing media (e.g. methanol-air systems), while recommending smaller stage height for coalescence systems (e.g. water-air). A significant increment in the residence time of the dispersed phase was obtained in both co-current, and counter-current multistage columns as compared to a single stage bubble column.

Kato et al., 1984 investigated the effect of tray design, stage height, superficial gas and liquid velocities, and column diameter on the overall gas holdup in a gas-liquid liquid co-current tray bubble column. Air, tap water and kerosene were used as gas, continuous liquid and dispersed liquid, respectively. The trays consisted of perforated brass plates with the holes drilled in an equilateral triangular pitch arrangement. The tray hole diameters and open areas ranged between 0.65-1.20 cm and 6.0-28.9%, respectively. The

authors found the mean gas holdup nearly independent of the trays and the superficial velocity of the liquid phase. They correlated the measured mean gas holdup with the gas velocity.

Nishikawa et al., 1985 confirmed the suppression of bubble coalescence in a spouted vessel when trays were added. They also reported that a decrease of 40% in the tray hole diameter yielded an increase of up to 5 % in gas holdup.

Chen et al., 1986 studied two types of plates in two different co-current trayed bubble columns. One of them was the Karr tray design with a 53 % of open area, whereas the second design was a perforated plate made out of meshed screen with 64% open area. They found that the Karr type yielded higher gas holdups. Also the superficial liquid velocity was observed not to have a significant effect on the gas phase volumetric fraction. They observed the formation of a cushion or layer of bubbles underneath the trays at low superficial liquid velocities. In the correlations presented by these authors (Table 2.1), only the effect of the superficial velocities is considered.

Chen et al., 1989 studied the overall gas holdup for various gas-liquid systems in both batch and co-current upward multistage units. They reported that the volumetric fraction of the dispersed phase significantly increases with each tray addition, that it was independent of the viscosity of the liquid phase, and that the variation of the surface tension of the liquid phase slightly changed the gas holdup. In addition to this, they found that an increase in the net liquid flow rate decreases the gas holdup. This effect was explained as a result of the bubble acceleration through the plates by the flowing liquid.

Yang et al., 1989 correlated the experimental overall gas holdup obtained in a co-current upward trayed bubble column (sectionalized with screen plates, 64% O.A.) with both the superficial gas and liquid velocities using the slip velocity concept. The range of superficial gas velocities was restricted to low values (U_g~0-7 cm/s). However, as mentioned in the introduction section, most of the industrial applications described for

trayed bubble columns occur well within the churn-turbulent regime. Therefore, the use of their correlation should be handled with extreme care.

More recently, Vinaya, 1994 considered the study of several hydrodynamic parameters on the performance of a counter-current multistage bubble column. It was found that the tray open area has less influence than the tray hole diameter on the increment of gas holdup when both parameters are independently reduced. The tray hole diameter controls the bubble size and hence the residence time of the gas phase. The author correlated the overall gas holdup for counter-current units separately for the bubbly and churn-turbulent regimes as a function of the superficial velocities of the phases, the dimensions of the trays and the stages (open area, tray hole diameter and stage height), and the liquid phase physical properties (surface tension, viscosity, and density). The previous factors were grouped into dimensionless groups for proper use.

Yamada et al., 1998 studied the effect of superficial gas and liquid velocities, stage height, and catalyst weight in a gas-liquid-liquid-solid (G-L-L-S) co-current bubble column partitioned into a number of stages using stainless steel mesh (0.2 mm wire diameter an 73% O.A.). They reported that only gas velocity had an influence on the gas holdup, which they correlated using the same type of expression introduced by Kato et al., 1984 (Table 2.1).

As we have seen, the information available in the open literature for TBC's is limited and very scattered. In fact, only Vinaya 1994 took into consideration the effect of the flow regime, tray and column design, liquid phase properties, and operating conditions on the study of the gas holdup in a counter-current trayed bubble column. However, the co-current mode of operation is preferred for industrial applications such as the Visbreaking operation (Dassori, 1999) because of the advantage to operate in a much more flexible and wider range of conditions. Therefore, this work helps to fill the current gap that exists in the information available to the design and scale-up of co-current trayed bubble-column.

Table 2.1 Summary of Published Correlations and Experimental Data for Overall Gas Holdup in Multistage Bubble Columns.

References	Gas-Liquid System	Range of Parameters and Operating Conditions	Results
Schugerl et al., 1977	Air 0.5 %-2 % methanol 0.5 %-1 % ethanol 0.5 %-2 % glucose	Counter-current U_g =1-8 cm/s U_l = 2 cm/s D_c= 20 cm, H_c=381 cm 6 Stages H_s=10, 50 cm d_o=0.2, 0.4 cm O.A. = 12.5, 28%	Experimental Data
Kato et al., 1984	Air-Water-Kerosene	Co-current upflow U_g =1.5-13 cm/s U_l = 0.1-1.0 cm/s H_c=200, 220 cm D_c= 6.6, 12.2 cm, 4, and 8 stages H_s=25, 50 cm, d_o=0.65, 0.90, and 1.20 cm, O.A.= 6, 12.8, 28.9%	$\varepsilon_g = \frac{U_g}{30 + 3.3U_g^{0.8}}$ U_g (=) cm/s

Table 2.1 Summary of Published Correlations and Experimental Data for Overall Gas Holdup in Multistage Bubble Columns (Continued).

References	Gas-Liquid System	Range of Parameters and Operating Conditions	Results
Nishikawa et al., 1985	Air-N_2 Tap water Carboxyl Methyl Cellulose 10-60 % sugar solution	Counter-current U_g = 1-7 cm/s U_l = 0-3 cm/s D_c=15, 10 cm H_c=140, 115 cm 3 and 4 Stages H_S=40, 35 cm d_o=0.5, 0.75, 0.8, 0.5, 0.3 cm	Experimental data
Chen et al., 1986	Air Water	Co-current upflow U_g =0-8.22 cm/s U_l =0-6.12 cm/s H_c=300 cm, D_c=7.5 cm Plates made of stainless steel wire screen: 38 stages, d_o=0.058 cm, O.A. = 64%, H_S=5 cm Karr type trays: 85 stages, d_o=1.27 cm, O.A.=53%, H_S=2.54 cm	Stainless steel wire screen mesh $\varepsilon_g = 0.0416\, Ug^{1.23} U_l^{-0.092}$ Perforated plates (Karr type) $\varepsilon_g = 0.0448\, Ug^{0.81} U_l^{-0.055}$ U_g (=) cm/s, U_l (=) cm/s

Table 2.1 Summary of Published Correlations and Experimental Data for Overall Gas Holdup in Multistage Bubble Columns (Continued).

References	Gas-Liquid System	Range of Parameters and Operating Conditions	Results
Chen et al., 1989	Air Water Alcohol Ethylene-glycol Carboxyl Methyl Cellulose	Batch, and Co-current upflow U_g =0-8 cm/s, U_l =0-2.2 cm/s D_c=7 cm, H_c=240cm 38 stages, O.A.= 64% H_S=5 cm	Experimental data
Yang et al., 1989	Air Tap water 0.2 % Carboxyl Methyl Cellulose	Co-current upflow U_g = 0-7 cm/s U_l =not specified D_c=5, 7.5, 15 cm H_c=300 cm 6-mesh stainless steel sheets 38 stages O.A.=64 %, H_S= 5 cm	$V_S = 0.115 e_g^{-0.182}$ $V_S = \frac{U_g}{e_g} - \frac{U_l}{1-e_g}$ V_S = Slip Velocity (=) m/s

Table 2.1 Summary of Published Correlations and Experimental Data for Overall Gas Holdup in Multistage Bubble Columns (Continued).

References	Gas-Liquid System	Range of Parameters and Operating Conditions	Results
Vinaya, 1994	Air-Water / Air-Kerosene	Counter-current U_g = 0.42-11.6 cm/s U_l = 0.7-1.2 cm/s D_c=9.8-15.4 cm H_c=110, 180 cm Perforated Trays d_o= 0.3, 0.5, 1, 1.2 cm O.A.= 10, 12.5, 20, 30, 38, 52% H_S= 5, 12, 20, 85 cm	Air-Water /Air-Kerosene Bubbly Regime: $\varepsilon_g = 2.4\left[\frac{U_g^{\,2}}{g\,d_0}\right]^{0.54}\left[\frac{d_o}{H_s}\right]^{0.26} O.A.^{-0.22}\left[\frac{\sigma}{\sigma_w}\right]^{-0.3}$ Churn Turbulent Regime: $\varepsilon_g = 0.59\left[\frac{U_g^{\,2}}{g\,d_0}\right]^{-0.4}\left[\frac{U_l^{\,2}}{g\,d_0}\right]^{0.03} O.A^{-0.03}\, H_S^{-0.21}\left[\frac{\sigma}{\sigma_w}\right]^{-0.41}$ S.I. Units

Chapter 3 Determination of Gas Holdup and Pressure Drop across the Trays

3.1 Experimental Facility and Setup

A co-current Trayed Bubble Column setup has been arranged (Figure 3.1) to achieve the goals set for this study. The column is made of four intermediate sections plus a top (disengagement) and bottom (plenum) section, all built in plexiglas and attached together by flanges. The intermediate sections have an inside diameter of 19 cm and a total height of 52 cm inches each. The upper section has the same diameter as the intermediate ones, but it is only 33 cm tall. There is also a 33 cm tall cone-shaped plenum section where the gas and liquid phases enter the column and mix. The total height of the column from the base of the plenum to the top of the disengagement section is 241 cm. This is a five-stage setup unit with a total of four trays, which are mounted between the flanges. The design of the column does not provide the flexibility to change the distance between the trays. Determination of gas holdup and pressure drop across the trays. Three different types of trays were designed and utilized (Figure 3.2). Their design was chosen in such a way that it would permit the independent study of the tray hole diameter and the tray open area. In order to study the effect of the design of the gas distributing system, two different gas spargers have been chosen: a 9.5 mm diameter single point nozzle, and a perforated plate with a tray hole diameter of 0.4 mm, 163 holes, and 0.07% of total open area.

As mentioned in Section 2.1, the high gas holdup conditions of the liquid phase systems found for instance in the Visbreaking Process of petroleum residues can be mimicked by using aqueous mixture of surfactants. Two liquid phase systems have been selected: tap water and an aqueous solution of a surfactant mixture (1% butanol, and 0.01 wt% of sodium dodecyl sulfate). Their physical properties are listed in Table 3.1. Filtered and compressed air was used as the gas phase. When using the surfactant mixture, the

appearance of foam was anticipated. In fact, the formation of foam, especially at the highest gas flow rate conditions, was so large that it completely filled the column and caused it to flood. Therefore, it was necessary to modify the upper section of the column in order to bring the foam and the liquid, together with the gas, to the recycle tank, where the air could then be disengaged and the foam destabilized. Handling the foam in the system was very cumbersome, and as it will be shown later, the experimental reproducibility with this liquid system was not as good as that obtained with the air-water system. Due to the high formation of foam, two different experimental setups were used for the tap water and the surfactant mixture. The corresponding schematics are shown in Figures 3.3, and 3.4, respectively.

For the tap water system (Figure 3.3), the recycle tank was filled with 200 gallons at room temperature. Two centrifugal pumps arranged in series were in charge of pumping water to the column, up to a maximum flow rate of 10 gallons per minute. The flow rate could be varied and measured by a rotameter. Once the water filled the column, it overflowed through the side of the column's upper section and then was returned to the recycle tank by a 5 cm in diameter hose. The unit was hooked to a high-pressure air line, which provided a constant flow rate up to a pressure of 200 psig. A pressure regulator and a rotameter allowed for the air to be set at the required working pressure, which was usually the value at which the rotameter has been calibrated, 150 psig in this case. The reading of the gas rotameter was in SCFH (Standard Cubic Feet per Hour). There were two ball valves with fast open-close mechanisms in the air and liquid lines. The location of the valves was close enough to each other so that they can be shut off simultaneously. These valves were used for the overall gas holdup measurement experiments. The content of the column could be drained directly to the room sewer by opening the draining valve.

A slightly different experimental set-up was prepared for use with the surfactant mixture to be able to measure the overall gas holdup under foamy conditions (Figure 3.4). A forty-gallon tank and a new centrifugal pump connected to it were added to the system. This tank was used to prepare the solution of the surfactant mixture. The mixture was

then pumped to the recycle/feed tank, where tap water was added to bring the solution to the required concentration. In order to leave enough clearance for the foam to settle, it was decided not to fill the recycle/feed tank more than one third of its total capacity. As mentioned before, the upper section of the column was redesigned. Basically, the side outlet was eliminated, and the lid of the top section was perforated and connected to a 7.6 cm diameter PVC reinforced hose with the help of a 90^{o} stainless steel elbow. The hose run all the way to the recycle tank, where it discharged the foam, liquid and gas mixture.

Even with the modifications described above, the column could only be operated with the single nozzle sparger. The large pressure drop created across the perforated plate sparger enhanced the foam formation process in such a way that made the steady state operation of the column impossible under the planned experimental conditions.

Table 3.1 Physical Properties of the Liquid Systems Used in this Work at T=20 C

	Density (ρ_l)	**Viscosity (μ_l)**	**Surface Tension (σ_l)**
Liquid System #1 Tap water	0.997 g/cm^3	10^{-4} g/cm s	72 dyn/cm
Liquid System #2 Water + 1 % vol. Butanol + 0.01 w.t% Sodium Dodecyl Sulfate (SDS)	0.997 g/cm^3	10^{-4} g/cm s	34 dyn/cm

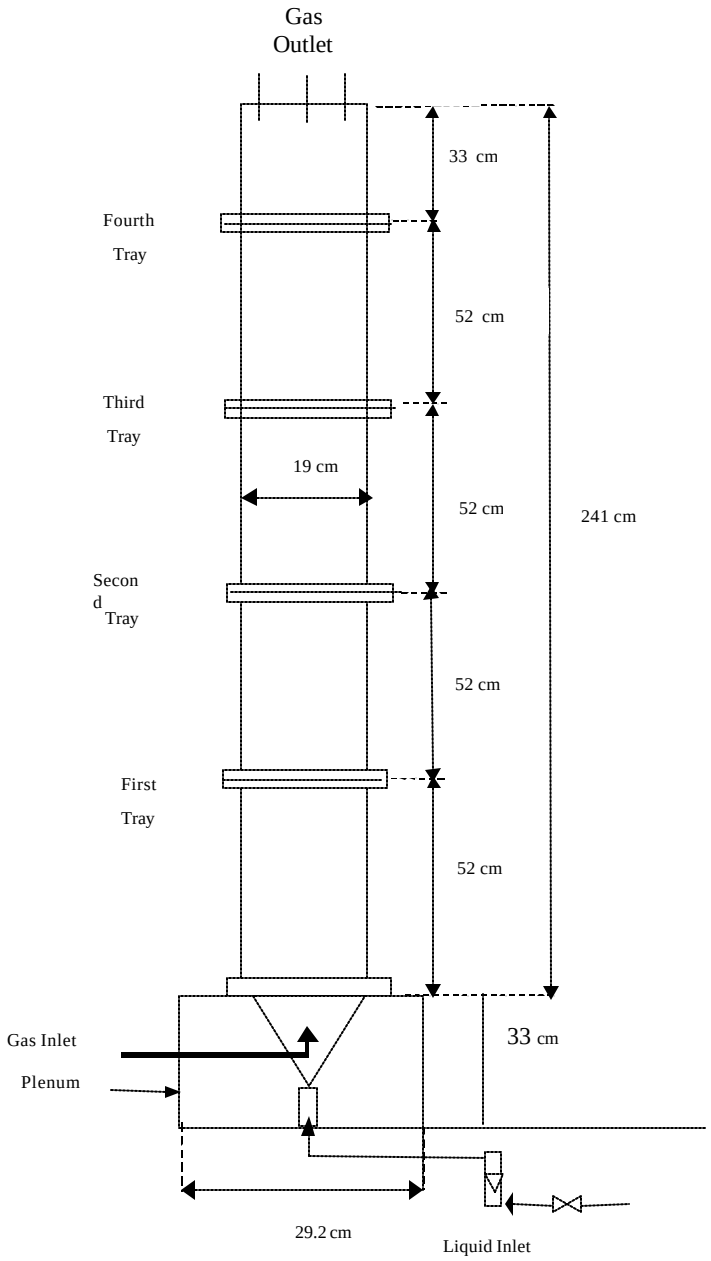

Figure 3.1 Schematic Diagram of the Trayed Bubble Column.

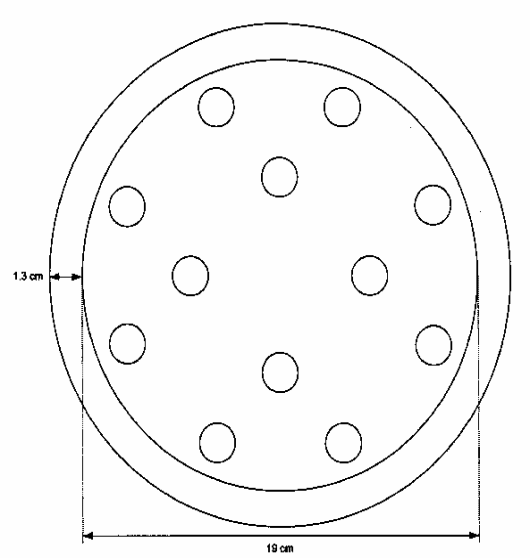

Tray # 1: 12 holes, 1.74 cm Tray Hole Diameter, 10.2 % Open Area

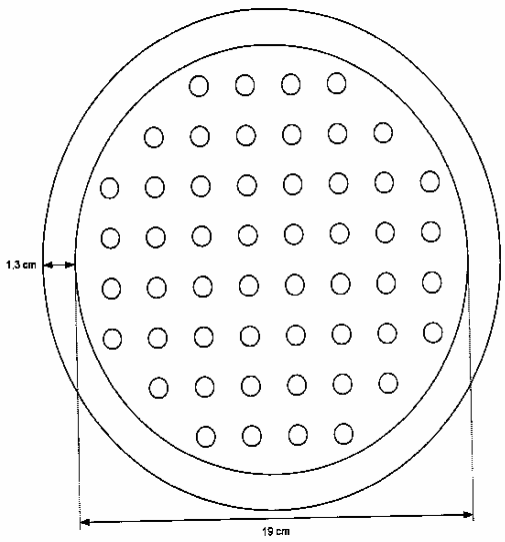

Tray # 2: 52 holes, 0.6 cm Tray Hole Diameter, 5.2 % Open Area

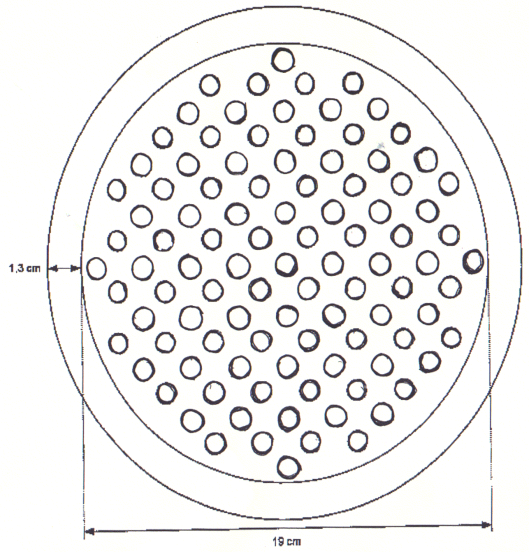

Tray # 3: 105 holes, 0.6 cm Tray Hole Diameter, 10.2 % Open Area

Figure 3.2 Tray Designs

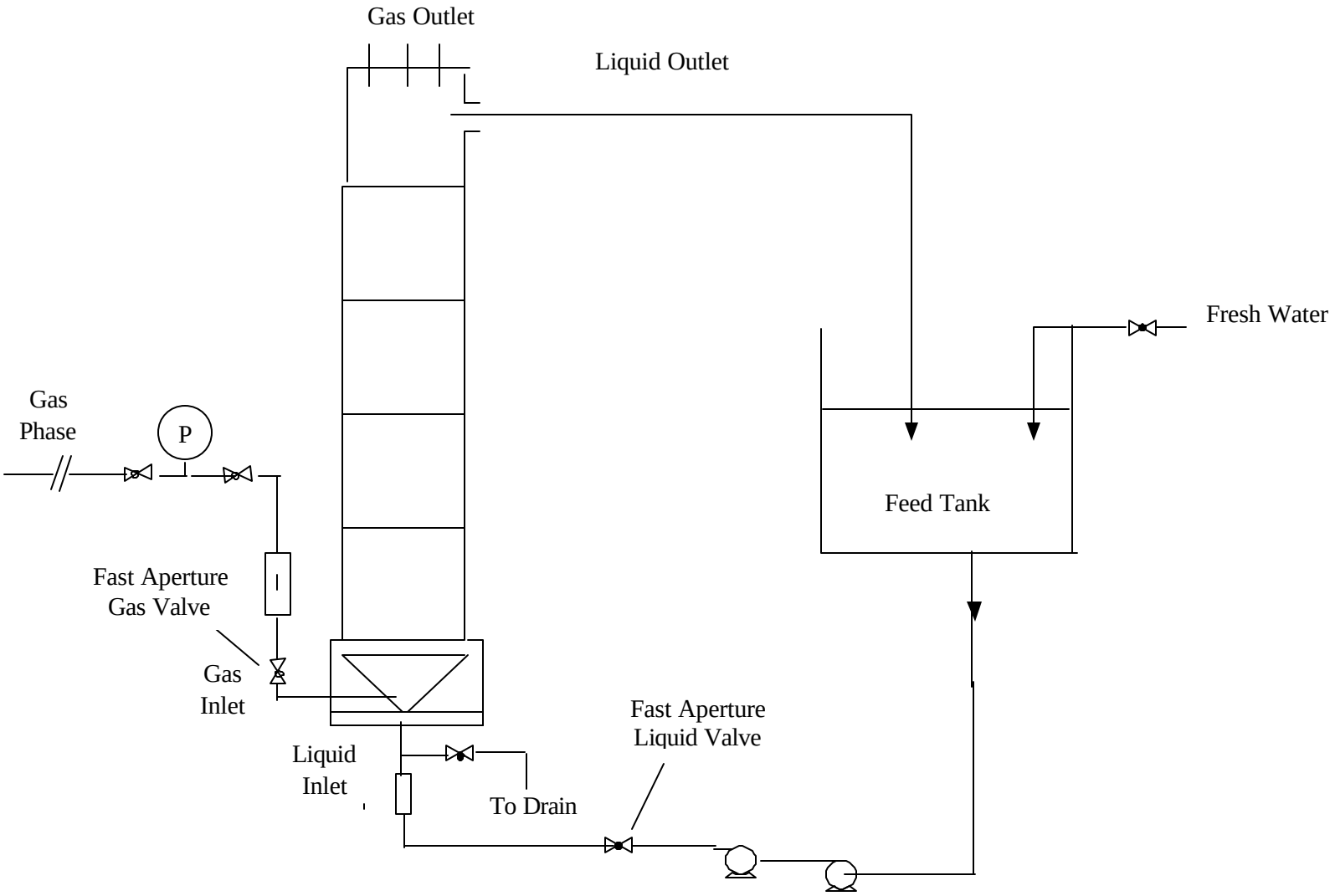

Figure 3.3 Experimental Setup for the Air-Water System.

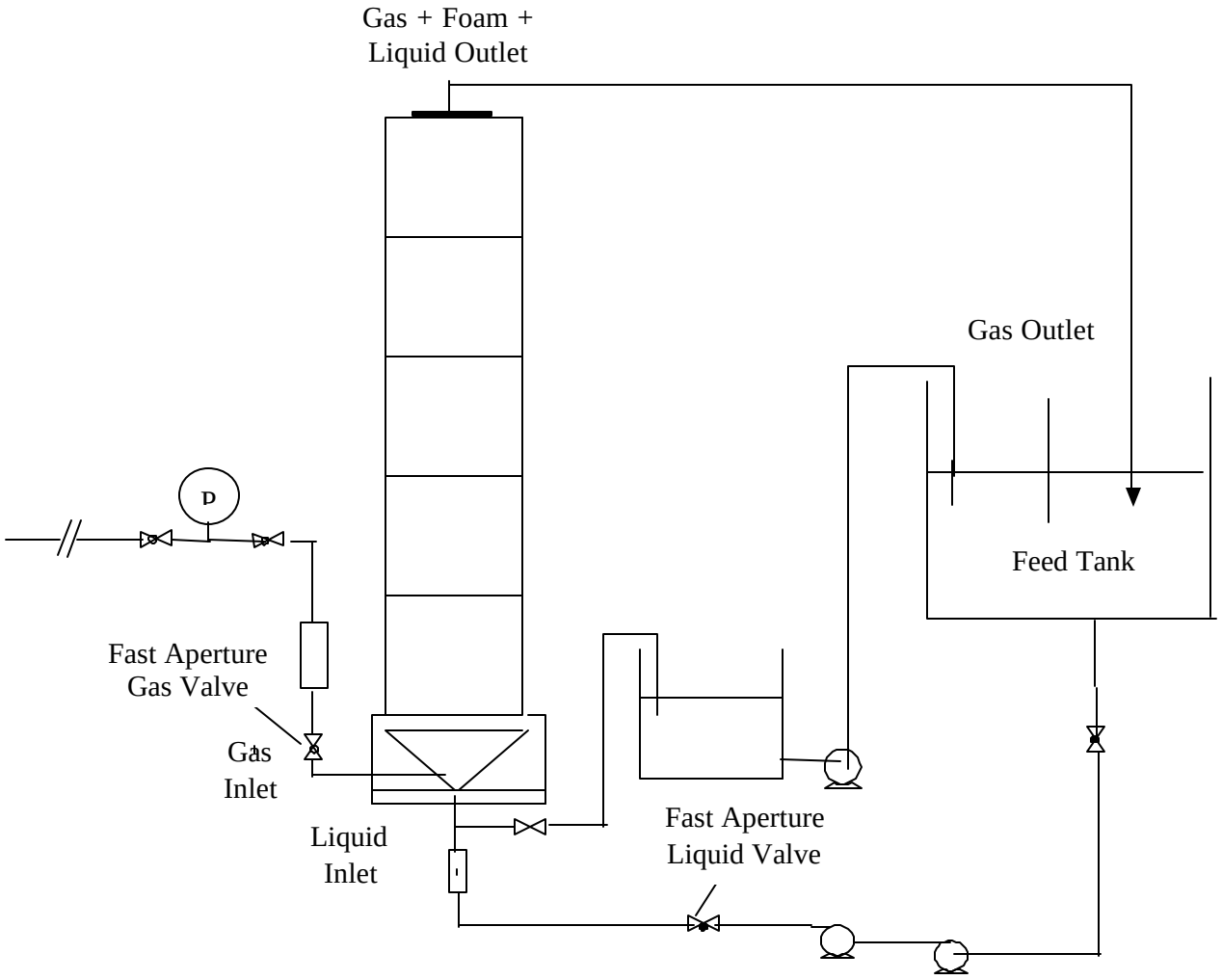

Figure 3.4 Experimental Setup for the Air-Surfactant System

Chapter 4 Experimental Results and Analysis

4.1 Overall Gas Holdup

The experimental overall gas holdup values as measured by the Gas Disengagement Technique (GDT), are displayed in Table A.1.1 (Appendix A.1) for all the studied conditions. The experimental findings regarding the effect of the following parameters: superficial gas and liquid velocities, geometry of the trays (open area, and tray hole diameter), liquid phase physical properties, and gas sparger design on the overall gas holdup are presented in the next sections. The analysis of the effect of each of the studied factors should also consider the variation of the rest in order to account for their potential interaction. Further, the experimental data collected in this work have been used to develop an empirical expression to predict the overall gas holdup in trayed bubble columns.

4.1.1 Effect of the Superficial Gas Velocity and Flow Regime Transition

Figures 4.1 and 4.2 show the overall gas holdup versus the superficial gas velocity U_g in the single stage and multi-stage bubble columns at a superficial liquid velocity of U_l=*0.5* cm/s using the single nozzle sparger in air-water and air-surfactant systems, respectively. In all the figures, two different regions can be clearly distinguished. In the low superficial gas velocity region (U_g<5-8 cm/s), known as Bubbly Flow regime, there is almost a linear relationship between superficial gas velocity and gas holdup. The trays have little effect on the gas holdup, because in this regime the diameter of the holes is larger than the average bubble size diameter, and the gas can easily travel across the trays. In fact, the overall gas holdup shows the following type of dependency with the superficial gas velocity:

$$e_g a U_g^n \tag{4.1}$$

Where n ranges between 0.7 and 1.2 in the Bubbly Regime (*Shah et al., 1982*).

As the gas velocity is increased, the gas-liquid flow becomes turbulent and the hydrodynamic properties of the system radically change. The bubbles now present a wide distribution of sizes, shapes, and rise velocities. In this regime, also known as Churn-Turbulent, the almost linear behavior between gas holdup and superficial gas velocity is no longer observed. Instead, the exponent *n* can take values between 0.4, and 0.7. It is in this turbulent region where the introduction of perforated trays in the column significantly increases the overall gas holdup as compared to the column without trays (Figures 4.1 and 4.2). The redistribution of the gas phase by the trays helps to readjust the bubble size and to reduce the bubble coalescence and break-up. Also, the competition between the gas and liquid phases to move across the trays enhances the overall staging effect of the gas in the column, subsequently increasing the residence time of the latter in the column.

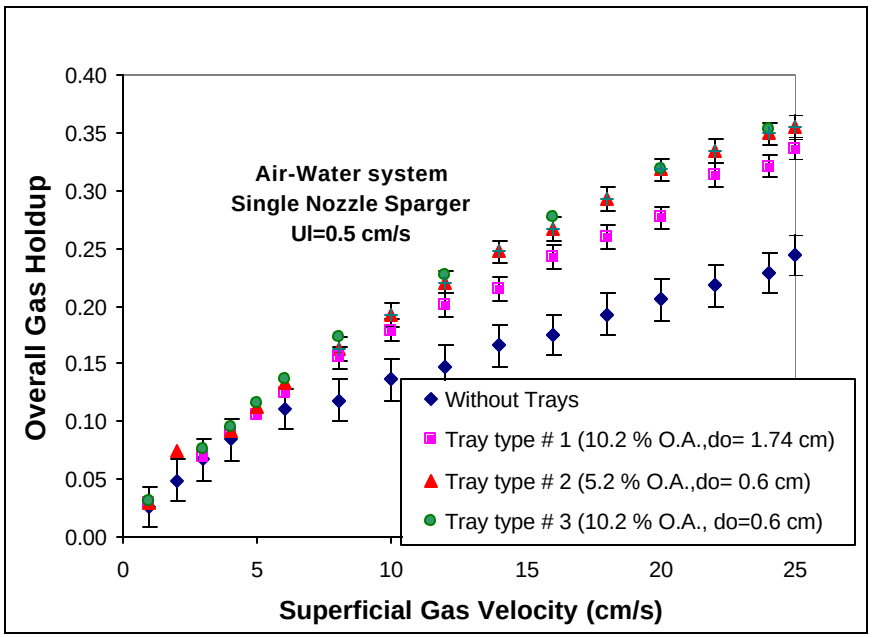

Figure 4.1 Overall Gas Holdup versus Superficial Gas Velocity at U_l=0.5 cm/s. Air Water System and Single Nozzle Sparger.

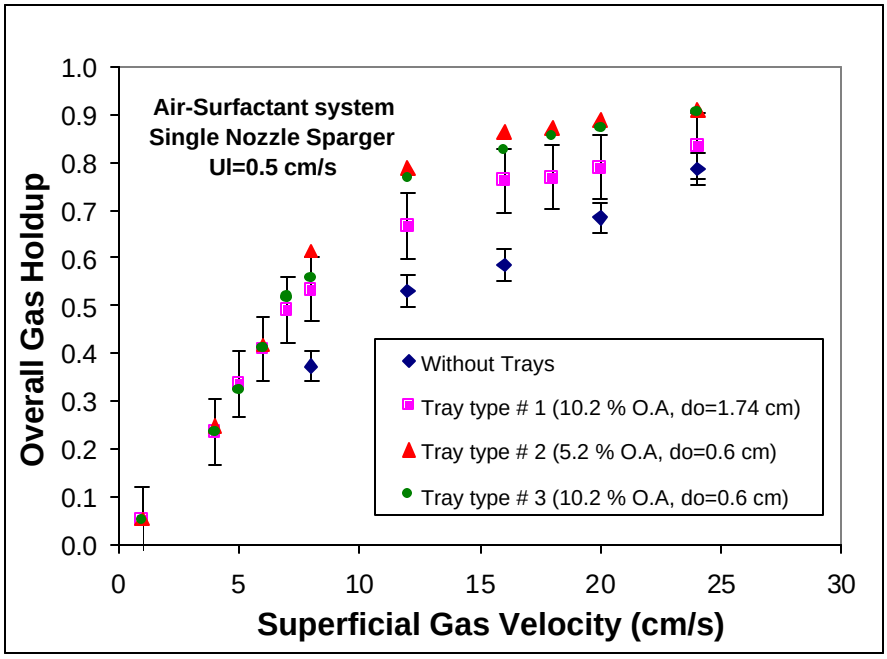

Figure 4.2 Overall Gas Holdup versus Superficial Gas Velocity at U_l=0.5 cm/s. Air Surfactant System and Single Nozzle Sparger.

The exact determination of the regime transition in bubble columns is still an open issue. Although many approaches such as frequency and chaos analysis (*Letzel et al., 1996*) have been suggested, none of them can still unequivocally predict the transition. However, a good approximation can be obtained by plotting e_g versus U_g in logarithmic scale. In this type of representation, the data points belonging to different regimes would fall into straight lines with different slopes. Then the regime transition superficial gas velocity can be considered to be the point given by the intersection of the two straight lines. Moreover, the slope of the lines would directly give the exponents of Equation 4.1 (n_1 for bubbly and n_2 for churn-Turbulent Regimes, respectively). Figure 4.3 graphically illustrates the described procedure. Table A.1.2 in Appendix A.1 list the estimated regime transition velocities and the slopes of the straight lines (n_1 and n_2) resulting from plotting *log* (e_g) versus *log* (U_g). From careful analysis of the data reported in Table A.1.2, it can be concluded that the trays delay the transition from the Bubbly to the Churn-Turbulent Regimes and shift it toward higher superficial gas velocities as compared to the column

without trays. This is mainly due to the redistribution of the gas phase in each of the trays, which helps to control both the bubble size and their rise velocity. The increase in the regime transition velocity, which in some cases reached up to 100%, was also observed with different G-L systems (air-surfactant and air-water) and different gas spargers (single nozzle and perforated plate spargers). It seems that tray hole diameter has a more important effect in the transition velocity shift than tray open area, as it can be seen from the comparison of the results for trays types #1 (10.2% O.A, d_0=1.74 cm), #2 (5.2% O.A, d_0=0.6 cm), and #3 (10.2% O.A, d_0=0.6 cm). As mentioned earlier, smaller holes produce smaller bubbles and hence the Bubbly Regime can exist at larger gas velocities. The nature of the liquid phase also affects the location of the regime transition velocity, and the magnitude of the slopes of the straight lines n_1, and n_2. The non-coalescent properties of the liquid surfactant mixture, and its low surface tension (Table 3.1) reduce the average bubble size. This fact can also explain the delay in the appearance of the Turbulent Regime as the superficial gas velocity is increased. In addition, it can be noticed that the rate of increase of the gas holdup with U_g in the Bubbly Regime is consistently larger ($n_1>1$) than the values measured for the air-water system. This implies that in the Bubbly Regime the effect of increasing the gas flow rate is to form more bubbles of small size, which do not break-up or coalescence in their journey along the column. Thus, in this regime a much larger increment of the overall gas holdup is measured than in turbulent conditions. The presence of the trays in the column delays the transition even more.

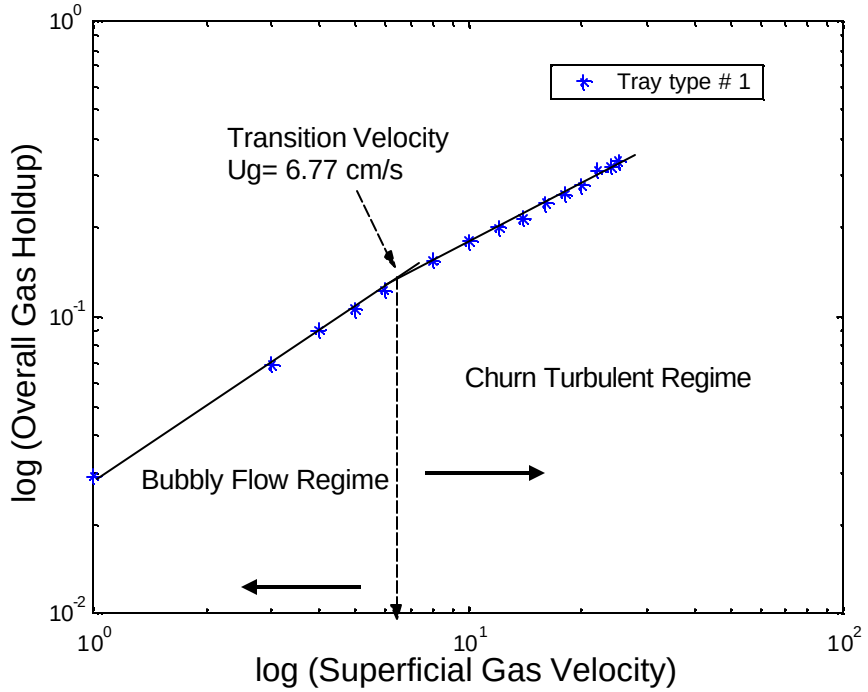

Figure 4.3 Logarithmic Plot of the Overall Gas Holdup versus the Superficial Gas Velocity in Tray Bubble Column with Tray Type #1 (d_o=1.74 cm, 10.2% O.A.) at U_l=0.5 cm/s.

4.1.2 Effect of the Trays

As it was explained in Section 4.1.1, in the Churn-Turbulent Regime the effect of the trays on the overall gas holdup as compared to the empty column is very significant (Figures 4.1-4.2). The average gas holdup increment due to the presence of the trays (averaged over the range of superficial gas velocities in the Turbulent Regime) varies between 20% and 50% depending upon the liquid phase system, gas sparger, and the superficial liquid velocity used. The larger gas volumetric fraction achieved in the column due to the presence of the trays can be explained as follows: First, the competition between the gas and liquid phases to travel across the trays increases the residence time of the gas phase. Second, the gas is redistributed in each of the trays and therefore the overall bubble size is smaller.

The most important parameters for design are the tray hole diameter d_o, and the tray open area *O.A.* The former controls the bubble diameter entering each of the stages, whereas the latter is related to the total energy dissipation in the tray. In addition, the nature of the liquid phase is also a very important factor to consider since it is directly responsible for the coalescing/non-coalescing properties of a given G-L system. In this sense, *Lucke et al., 1977* reported that for a coalescing system (e.g. pure water) the local bubble size is determined by the local dynamic equilibrium bubble diameter. Since the energy dissipation is mainly caused by turbulence, then the dynamic equilibrium bubble diameter will decrease at every perforated tray but quickly increase again. On the contrary, for non-coalescing systems (e.g. surfactant liquid systems) the bubble diameter is largely preserved in each of the stages.

From Figure 4.2, we can observe that the air-surfactant system with tray type #1 (10.2% O.A., d_o=1.74 cm) yielded statistically significant lower overall gas holdups than tray type #2 (5.2% O.A., d_o=0.6 cm), and type # 3 (10.2% O.A., d_o=0.6 cm). In contrast, the overall gas holdups measured in the column with trays #2, and #3 can not be distinguished. Therefore, the experiments confirm the fact that in non-coalescing gas-liquid systems such as the air-surfactant system tested in this work, the bubble size diameter generated at the tray is maintained along the stage. Thus, the tray hole diameter becomes the most important parameter for tray design since it controls the diameter of the bubbles formed in the trays. Conversely, in a coalescing medium such as the air-water system, the tray hole diameter does not have such a strong effect. However, it is still more important than the tray open area as it can be seen in Figure 4.1. In the Churn-Turbulent Regime, a smaller tray open area promotes a higher rate of energy dissipation in the trays. However, it should be also noted that for trays of equal hole diameters but different open areas, a larger number of bubbles is formed in the tray with the most free open area. More bubbles means more gas-liquid interfacial area, and therefore it counterbalances the increase in the overall gas holdup due to the energy dissipation effect. The latter may explain the trend exhibited in this work, where tray type #3 (10.2%, d_o=0.6 cm, and 105 holes) gave always slightly higher overall gas

holdups than tray type #2 (5.2%, d_o=0.6 cm, and 52 holes) for the air-water system (Figure 4.1). In any case, it should be pointed out that the differences are always in the order of magnitude of their 95% confidence intervals, and therefore no statistically significant differences can be claimed.

The effect of the trays on the overall gas holdup is slightly affected by the superficial liquid velocity as it is shown in Figures 4.4-4.7. The pairs of Figures 4.4-4.5, and 4.6-4.7 display the experimental data at U_l=1 cm/s, and U_l=1.5 cm/s for the air-water and the air-surfactant systems, respectively. Although, there is a small decrease in the overall gas holdup as the superficial liquid velocity is increased, the trends of the curves are identical to the data at U_l=0.5 cm/s (Figures 4.1, and 4.2). This observation implies that an increase on U_l does not affect the flow structure significantly except for the reduction in the overall gas holdup. This is discussed in more detail in the following section.

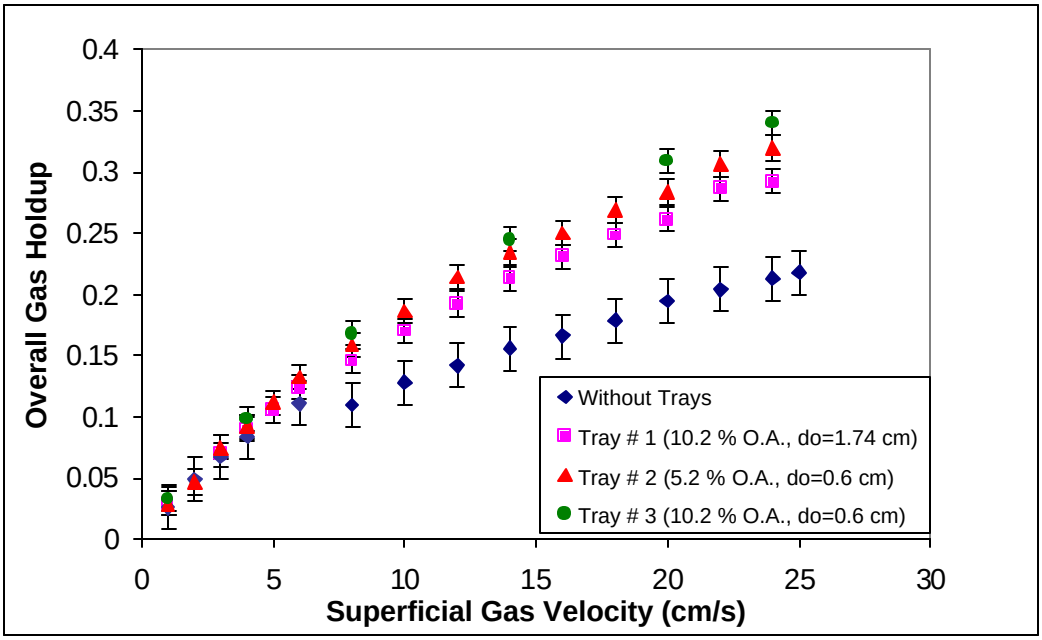

Figure 4.4 Overall Gas Holdup versus Superficial Gas Velocity at U_l=1 cm/s. Air-Water System and Single Nozzle Sparger.

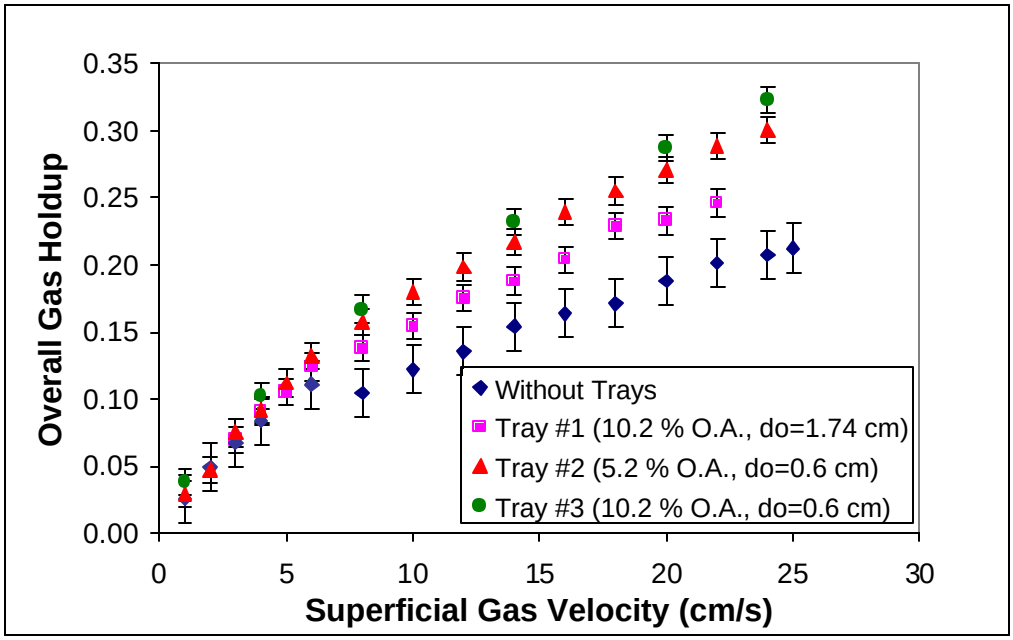

Figure 4.5 Overall Gas Holdup versus Superficial Gas Velocity at U_l=1.5 cm/s. Air-Water System and Single Nozzle Sparger.

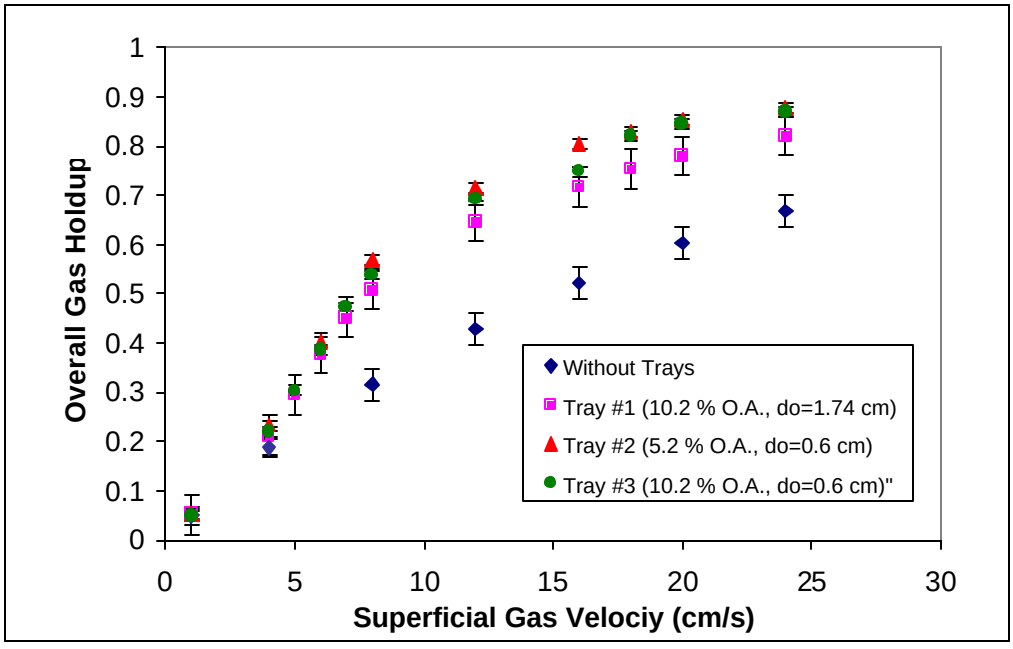

Figure 4.6 Overall Gas Holdup versus Superficial Gas Velocity at U_l=1 cm/s. Air-Surfactant System and Single Nozzle Sparger.

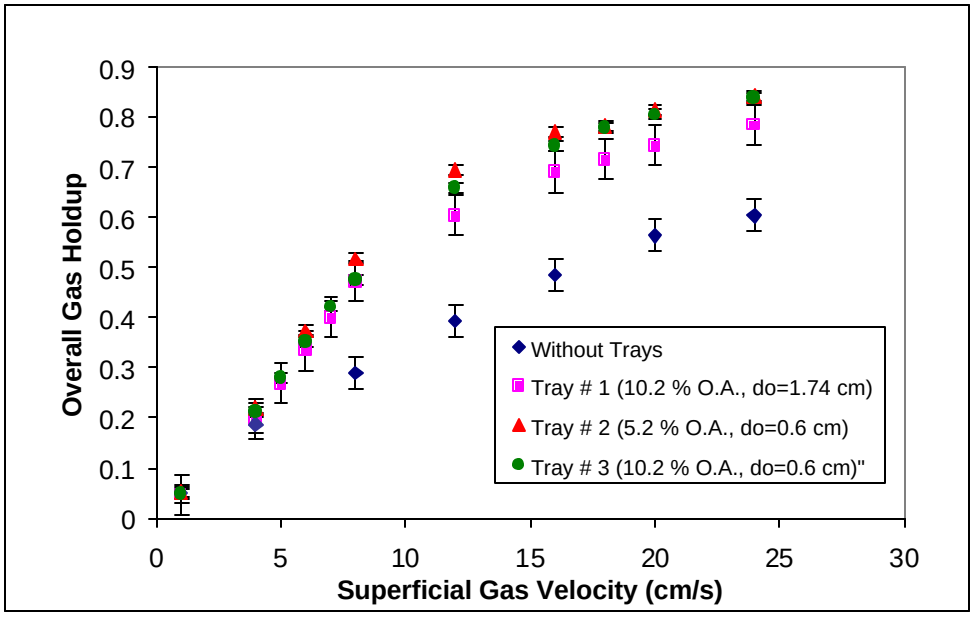

Figure 4.7 Overall Gas Holdup versus Superficial Gas Velocity at U_l=1.5 cm/s. Air Surfactant System and Single Nozzle Sparger.

4.1.3 Effect of the Superficial Liquid Velocity

Figures 4.8-4.11 show the effect of changing the superficial liquid velocity on the overall gas holdup in the single and multistage bubble columns for the air-water and air-surfactant systems. In all the figures, there is a slight decrease in the overall gas holdup (from 2% to 10%) for each increment of 0.5 cm/s in the superficial liquid velocity. Thus, it seems that a change in U_l does not significantly change the flow structure, but it only reduces the residence time of the gas phase and hence the overall gas holdup.

For single stage bubble columns, *Joshi et al., 1998* reported that with an increase in the superficial liquid velocity the extent of liquid downflow near the wall decreases. Thus, the overall effect of the net liquid flow is to increase the upward liquid velocity in the riser area and decrease the downward velocity in the downcomer area. The liquid flows upward where the gas holdup is high and that is in the central region of the column. As a result, the overall bubble rise velocity is higher in the central region where the gas

fraction is also high and this reduces the gas residence time. Although, in trayed columns the plates break the large liquid macro circulation pattern, some authors such as *Joshi et al., 1979; and Patil et al., 1984* have postulated the formation of multiple circulation cells inside the column stages. In the same manner as in a single stage bubble column, an increase in the superficial liquid velocity will also enhance the circulation of the liquid in the upward direction, with the subsequent acceleration of the bubble motion.

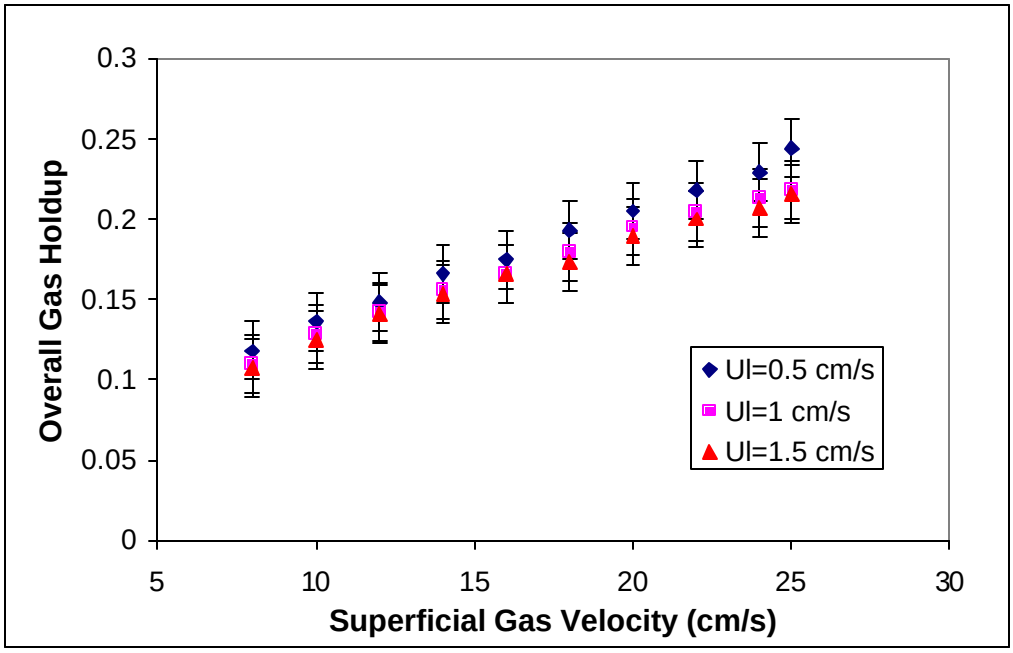

Figure 4.8 Overall Gas Holdup versus Superficial Gas Velocity in Single Stage Bubble Column. Air-Water System and Single Nozzle Sparger.

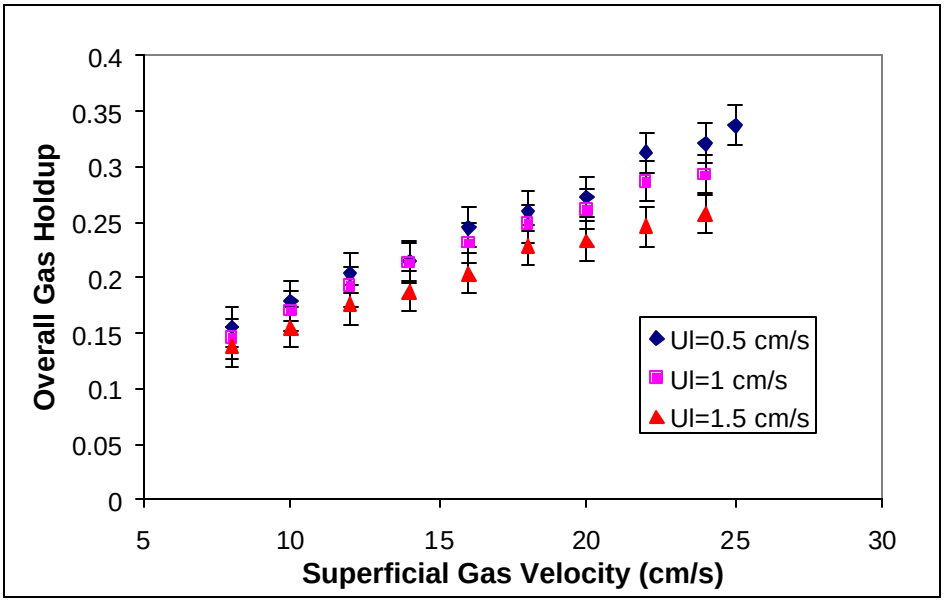

Figure 4.9 Overall Gas Holdup versus Superficial Gas Velocity in Multistage Bubble Column with Tray Type #1 (d_o=1.74 cm and 10.2% O.A.). Air-Water System and Single Nozzle Sparger.

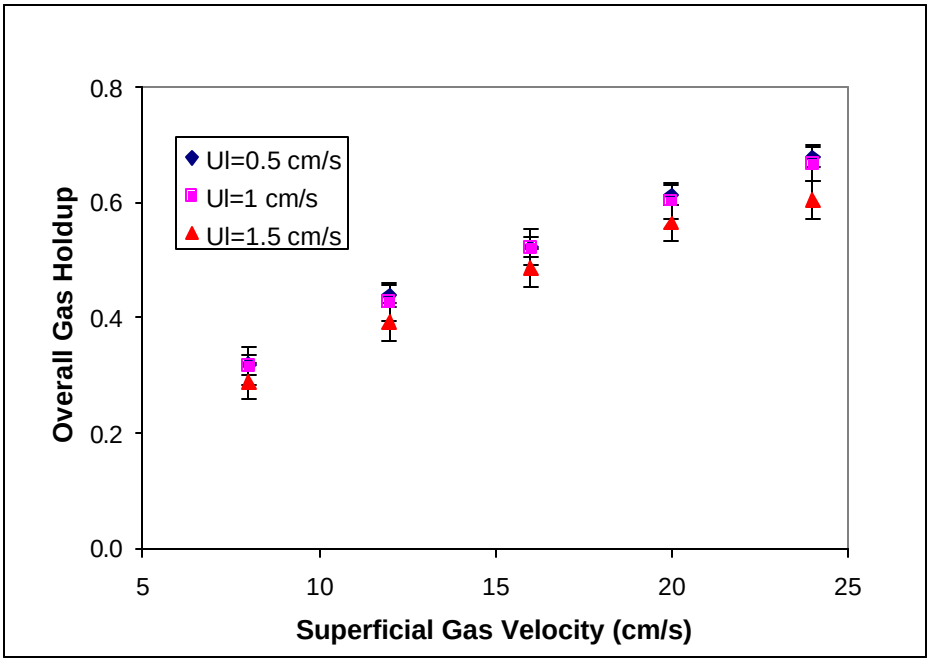

Figure 4.10 Overall Gas Holdup versus Superficial Gas Velocity in Single Stage Bubble Column. Air- Surfactant System and Single Nozzle Sparger.

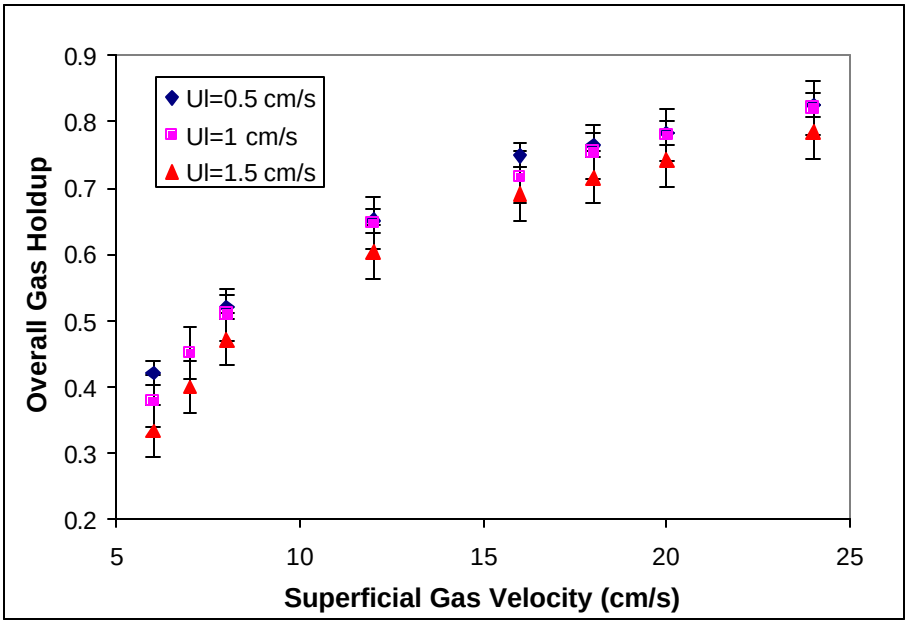

Figure 4.11 Overall Gas Holdup versus Superficial Gas Velocity in Multistage Bubble Column with Tray Type #1 (d_o=1.74 cm, 10.2% O.A.). Air-Surfactant System and Single Nozzle Sparger.

4.1.4 Effect of the Liquid Phase Physical Properties

The effect of the liquid phase has been analyzed in the previous sections. In fact, we have seen that the coalescing/non-coalescing nature of the liquid phase and its surface tension largely affect the column's hydrodynamic behavior. In this work, it is remarkable to see that overall gas holdups as high as 90% can be reached when an aqueous solution of an anionic surfactant (sodium dodecyl sulfate) and butanol is used. Figures 4-12 to 4.13 show the comparison of the results obtained with the air-water and the air-surfactant systems in the single stage and multistage bubble columns.

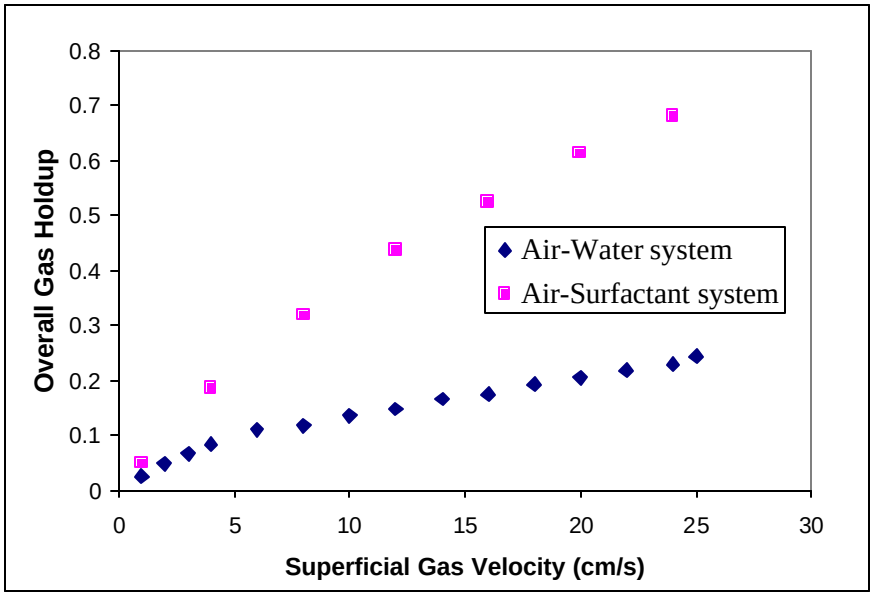

Figure 4.12 Comparison of the Overall Gas Holdup obtained in the Single Stage Bubble Column between the Air-Water and the Air-Surfactant Systems at U_l=0.5 cm/s. Single Nozzle Sparger.

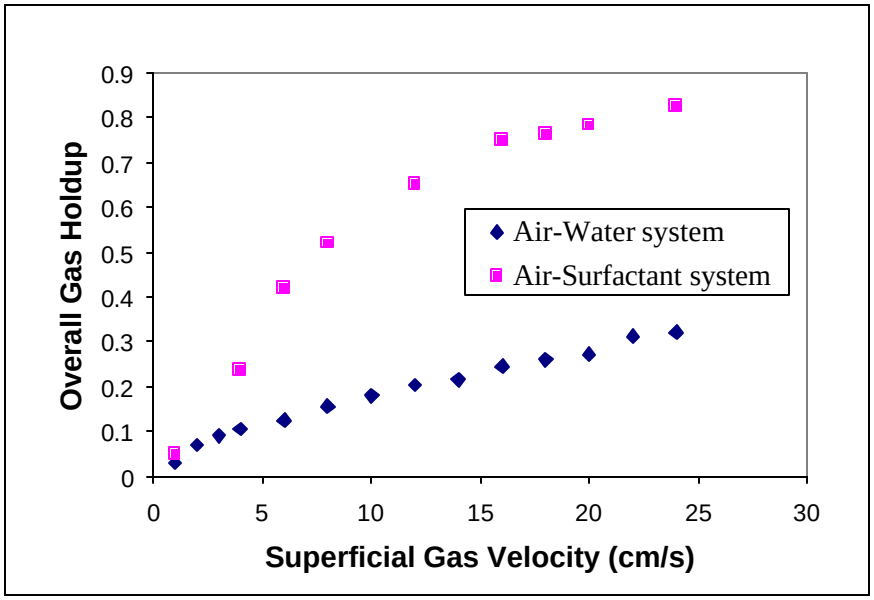

Figure 4.13 Comparison of the Overall Gas Holdup obtained in the Multistage Bubble Column with Tray Type #1 (d_o=1.74 cm, 10.2% O.A.) between the Air-Water and the Air-Surfactant Systems at U_l=0.5 cm/s. Single Nozzle Sparger.

4.1.5 Effect of the Gas Sparger

Figures 4.14, 4.15 and 4.16 show the overall gas holdup measured in the single stage column and in the multistage bubble column with tray types #1 and #2 for both single nozzle sparger (9.5 mm diameter) and perforated plate sparger (0.4 mm tray hole diameter, 163 holes and 0.07% O.A.). A significant increase in the overall gas holdup can be observed when the perforated plate sparger is used in the single stage column (Figure 4.14). The plot shows that the difference between the two spargers is maximum in the range of superficial gas velocities between 5 and 15 cm/s, and that at larger values the gas holdup curves for the two spargers seem to approach each other. In contrast, for the column with trays the effect of the gas sparger becomes less important (Figures 4.15, and 4.16).

The perforated plate sparger generates bubbles of smaller diameter than the single nozzle sparger, which are homogeneously distributed throughout the inlet cross sectional plane of the column. On the contrary, the single nozzle sparger introduces the gas as a jet stream at a single location point. Therefore, the former sparger distributes the gas much more efficiently than the latter. In the single stage bubble column, where there is no gas redistribution along the column, the sparger type is an important parameter of design in the low and middle range of superficial gas velocities.

The efficiency of the gas redistribution in the trayed bubble column is mainly related to diameter of the holes of the trays and the coalescing properties of the G-L system used, since they control the average bubble size in the column. Thus, as we can see in Figure 4.16, the overall gas holdup obtained in the trayed bubble column with tray type #2 (5.2% O.A., d_o=0.6 cm) becomes almost independent of the sparger type used. Furthermore, Figure 4.15 shows that when the trays of the largest hole diameter and open area are used (tray type #1, d_o=1.74 cm, 10.2% O.A.), then the perforated tray sparger gives overall gas holdups slightly larger than the single nozzle sparger.

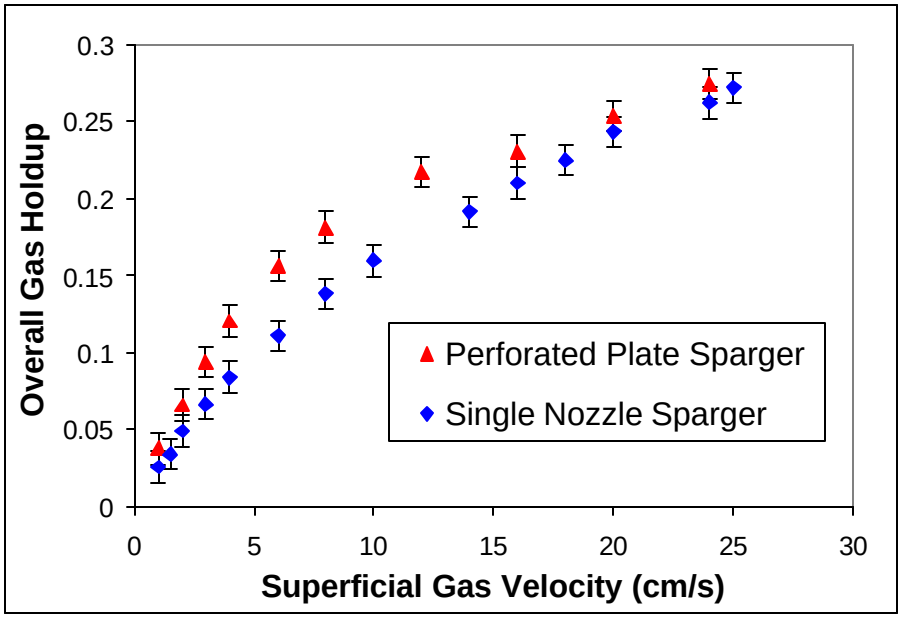

Figure 4.14 Overall Gas Holdup versus Superficial Gas Velocity in Single Stage Bubble with Single Nozzle and Perforated Tray (0.04 cm hole diameter, 0.07% O.A.) Spargers at U_l=0.5 cm/s. Air-Water System.

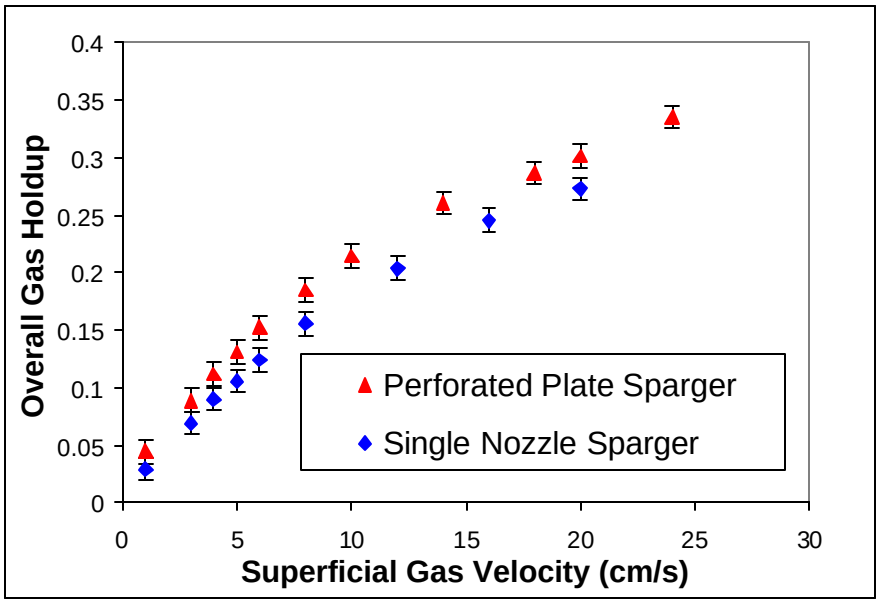

Figure 4.15 Overall Gas Holdup versus Superficial Gas Velocity in Multistage Bubble Column (Tray Type #1; 10.2% O.A., d_o=1.74 cm) with Single Nozzle and Perforated Tray (0.04 cm hole diameter, 0.07% O.A.) Spargers at U_l=0.5 cm/s. Air-Water System.

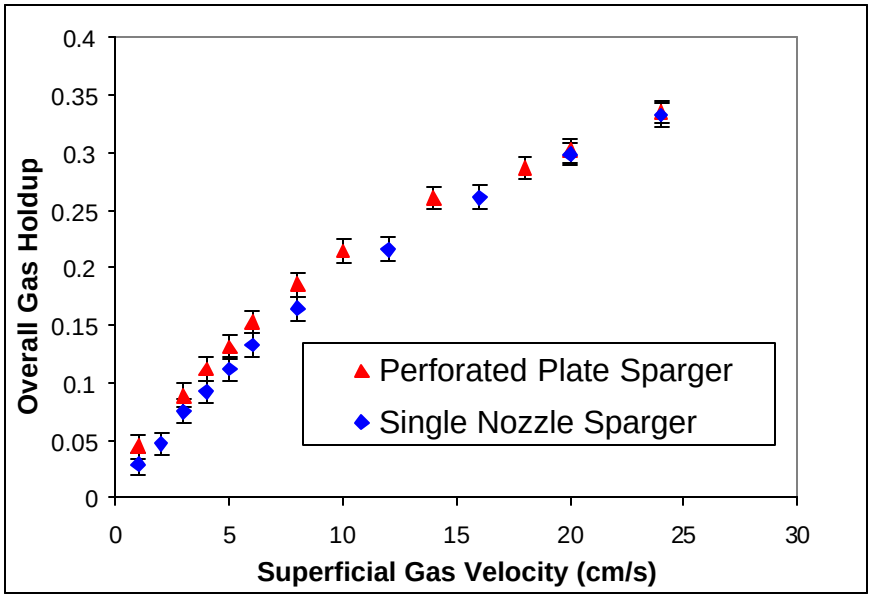

Figure 4.16 Overall Gas Holdup versus Superficial Gas Velocity in Multistage Bubble Column (Tray Type #2; 5.2% O.A., d_o=0.6 cm) with Single Nozzle and Perforated Tray Spargers (0.04 cm hole diameter, 0.07 % O.A.) at U_l=0.5 cm/s. Air-Water System.

4.2 Comparison of the Experimental Overall Gas Holdup with the Predictions of Published Correlations

In Figure 4.17, the overall gas holdups obtained in this work are plotted versus the gas holdups predicted by four published correlations developed for upflow co-current trayed bubble columns.

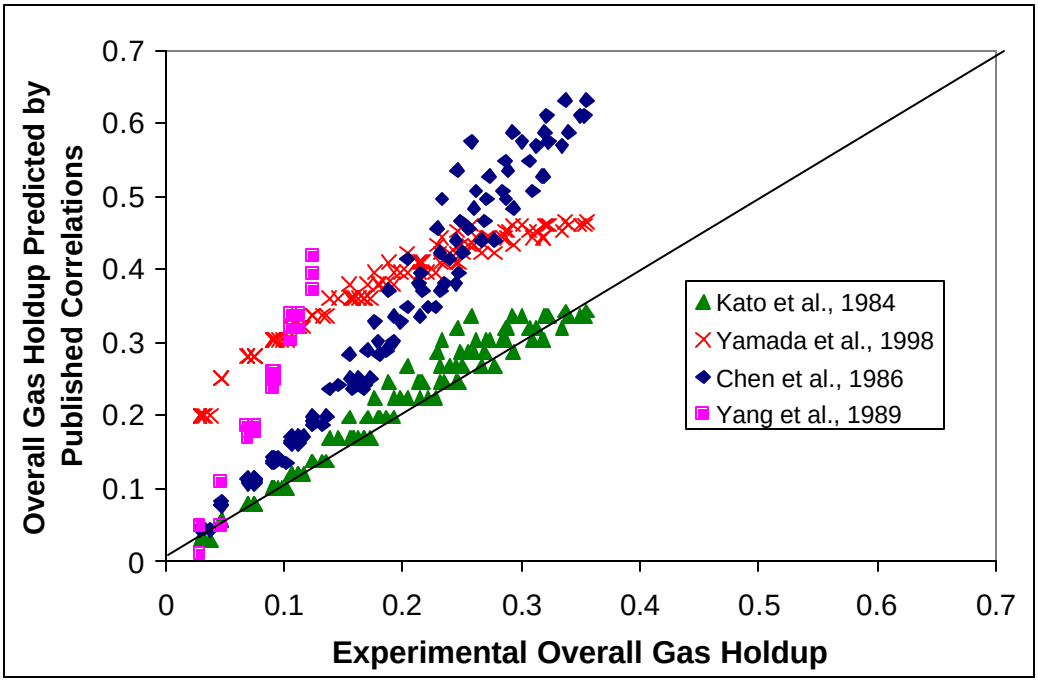

Figure 4.17 Experimental Overall Gas Holdups Measured in Multistage Bubble Column versus Overall Gas Holdups Predicted by Published Correlations for Co-current Upflow Trayed Bubble Columns. Air-Water System.

Table 4.1 Published Correlations for Upflow Co-current Trayed Bubble Columns

Reference	Correlation	Mean Relative Error (%)
Kato et al., 1984	$\varepsilon_g = \frac{U_g}{30+3.3U_g^{0.8}}$	9.1
Chen et al., 1986	$\varepsilon_g = 0.0448\,Ug^{0.81}U_l^{-0.055}$	66
Yang et al., 1989	$V_S = 0.115e_g^{-0.182}$ $V_S = \frac{U_g}{e_g} - \frac{U_l}{1-e_g}$ V_s=Slip Velocity (=) m/s	153
Yamada et al., 1998	$\varepsilon_g = \frac{U_g}{0.01+1.6\,U_g^{0.8}}$	160

Only the correlation by *Kato et al., 1984* is able to reasonably predict the experimental gas holdup data within a 10% mean relative error accuracy, whereas the other three largely overestimate the measured gas holdup (Table 4.1). The configuration and geometry of the trayed bubble column and the range of the chosen superficial gas and liquid velocities (U_g =1.5-13 cm/s, U_l =0.1-1.0 cm/s) used by *Kato et al., 1984* are very similar to the values selected in this work. The column was sectionalized into 4 and 8 stages by perforated trays of hole diameter and open area equal to d_o=0.65-1.20 cm and O.A.=6-28.9%, respectively. The holes in the tray were arranged following an equilateral triangular pitch design very similar to the trays of this work (Figure 3.2). The authors found that the overall gas holdup was sensitive only to the variation in the velocity of the gas phase, and that neither the different types of trays studied, nor the properties of the phases, or the tray spacing produced any effect on the overall gas holdup.

Chen et al., 1986 used perforated plates of Karr design (*Karr, 1959*), made of thick Teflon sheet drilled with 1.27 cm diameter holes and 53% of open area, to sectionalize a three meters long bubble column into 85 stages. The authors correlated the overall gas

holdup with the superficial gas and liquid velocities. However, the exponent of the latter term is so small that it barely affects the gas holdup. It can be seen in Figure 4.17 that in the low superficial gas velocity range, the correlation slightly overpredicts the experimental overall gas holdup obtained in this work. Nevertheless, the comparison worsens at larger gas velocities.

Yang et al., 1989 used the concept of slip velocity to correlate ϵ_g with U_g and U_l in a co-current trayed bubble column of 38 stages. The trays were built using sheets of stainless steel 6-mesh with a total open area of 64%. The correlation fails to predict both the trend and the values of the experimental gas holdups measured in this work.

Yamada et al., 1998 fitted their experimental gas holdup data with the same type of empirical expression that *Kato et al., 1984* used. The authors used a very small column (H_c=22.5 cm, D_c=2 cm), which was partitioned into 3, 5, 9, and 15 stages by plates made of stainless steel screen (d_o=0.12 cm and 73% O.A.). As shown in Figure 4.17, the correlation overpredicts the experimental data with a mean relative error larger than 160%.

As presented in Table 2.1, *Vinaya, 1994* reported the gas holdup to be a function of various operating and design variables. Therefore, in spite of the fact that the correlation of *Kato et al., 1984* predicted the experimental data obtained in this work fairly well, there is a need to develop an empirical correlation that in addition to the superficial gas velocity, also incorporates the effect of column dimensions, liquid velocity, and liquid physical properties.

4.3 Empirical Expression for the Overall Gas Holdup

In Section 4.1, we have seen that the overall gas holdup is a strong function of the superficial gas velocity and the physical properties of the liquid phase used. Also, the presence of the trays increases the volumetric gas fraction over the values found in single

stage bubble column at the same operating conditions. In fact, the tray hole diameter plays a more important role than the open area when trays of different dimensions were compared. The results obtained using two different gas spargers (a single nozzle and a perforated plate) showed that for the trayed column the effect of the gas sparger is not very significant due to the bubble size adjustment in each of the stages.

The following set of variables is considered to contain the key factors for the estimation of the overall gas holdup in upflow co-current trayed bubble columns:

$$\varepsilon_g = f\left(U_g,\ U_l, g,\ d_o,\ O.A., \rho_l, \mu_l, \sigma_l\right) \tag{4.1}$$

Some authors such as *Lucke et al., 1977* and *Vinaya, 1995* claimed that overall gas holdup increases with a reduction in tray spacing in coalescence liquid systems. *Vinaya, 1995* reported that the experimentally measured overall gas holdup scales with a power of –0.26 with tray spacing ($\varepsilon_g \ \alpha \ H_s^{-0.26}$) in a counter-current trayed bubble column. However, all the authors listed in Table 4.1 studied the effect of tray spacing in upf.low co-current trayed bubble columns and they found no significant effect.

By performing dimensionless analysis on the factors listed in Equation 4.1, the overall gas holdup can be written as a function of the following dimensionless groups:

$$\varepsilon_g = f\left(Fr_g, Fr_l, Mo, O.A.\right) \tag{4.2}$$

These dimensionless groups appearing in Equation 4.2 are defined as follows:

$$Fr_g = \left[\frac{U_g}{\sqrt{g\, d_o}}\right],\ Fr_l = \left[\frac{U_l}{\sqrt{g\, d_o}}\right],\ Mo = \left[\frac{m_l^4\, g}{r_l\, s_l^3}\right],\ O.A. = \text{Tray Open Area}$$

Fr_g, and Fr_l are the gas and liquid Froude numbers, respectively; Mo is the Morton number.

Further, it can be assumed that the following power law relationship holds:

$$\varepsilon_g = k\,Fr_g^{a}\;Fr_l^{b}\,Mo^{c}\,O.A.^{d} \tag{4.3}$$

The finding of the coefficients k, a, b, c, and d constitutes a multi-linear regression analysis problem, which can be solved by the least squares method. This procedure is based on the minimization of the following objective function:

$$\Phi(p_j) = \frac{\left[\sum_{i=1}^{n}\left(\log(\varepsilon_g^{pred}(p_j)) - \log(\varepsilon_{g,i}^{exp})\right)^2\right]^{1/2}}{n_{total} - 5}$$

$$\frac{\partial(\Phi(p_j))}{\partial p_j} = 0 \;\Rightarrow\; p_j \tag{4.4}$$

Where e_g^{pred} and e_g^{exp} are respectively the predicted and experimental overall gas holdups; p_j=k, a, b, c, and d; and n_{total} is the total number of data points.

The Statistical Toolbox from Matlab^{TM} 4.2 (The Math Works Inc.) was used to estimate the value of the coefficients that minimize the least squares function $\Phi(p_j)$.

As pointed out in Section 4.1.1, the dependency of the gas holdup with the superficial gas velocity is strongly influenced by the operating hydrodynamic regime. Thus, in order to capture this flow regime dependency properly, different expressions should be developed for the Bubbly and Churn Turbulent Regimes.

In order to find the coefficients of Equation 4.3, it is desirable to use not only the experimental data obtained in the work, but also data reported in the published literature. However, the literature survey conducted in Section 2.3 showed that the experimental gas holdup data available for trayed bubble columns is very limited and scattered. In fact, in the co-current arrangement only the four papers reported in Table 4.1 were found. In this sense, more experimental work is needed in order to gather the required experimental gas holdup database necessary to develop a more general correlation to predict the overall gas holdup for a wider range of conditions with a higher degree of confidence. Thereby, at this stage only the experimental data obtained in this work in the multistage bubble column will be inputted into Equation 4.4 to obtain the corresponding coefficients *k, a, b, c,* and *d* of Equation 4.3.

Below, Equation 4.3 can be rewritten into Equations 4.5 and 4.6 for the Bubbly and Turbulent flow Regimes, respectively.

Bubbly Flow Regime:

$$\varepsilon_g = \exp(9.306)\left[\frac{U_g}{\sqrt{g\,d_o}}\right]^{0.95}\left[\frac{U_l}{\sqrt{g\,d_o}}\right]^{-0.17}\left[\frac{\mu_l^4 g}{\rho_l \sigma_l^3}\right]^{0.29} O.A.^{0.242} \qquad (4.5)$$

k=exp(9.306), a=0.95 ± 0.067, b=-0.17 ± 0.09, c=0.39 ± 0.04, d=0.29 ± 0.15

The ranges over which the dimensionless numbers were varied are: Fr_g=0.02-0.33, Fr_l=0.06-0.12, Mo=2.63 10^{-11}-2.50 10^{-10}, O.A.=0.0552-0.102

Turbulent Flow Regime:

$$\varepsilon_g = \exp(10.541)\left[\frac{U_g}{\sqrt{g\,d_o}}\right]^{0.62}\left[\frac{U_l}{\sqrt{g\,d_o}}\right]^{-0.14}\left[\frac{\mu_l^4 g}{\rho_l \sigma_l^3}\right]^{0.48} O.A.^{0.12} \qquad (4.6)$$

k=exp(10.541), a=0.62 ± 0.05, b=-0.14 ± 0.05, c=0.48 ± 0.02, d=0.12 ± 0.08

The ranges over which the dimensionless numbers were varied are: Fr_g=0.04-1.03, Fr_l=0.06-0.12, Mo=2.63 10^{-11}-2.50 10^{-10}, O.A.=0.052-0.102:

Figures 4.18 and 4.19 show the experimental overall gas holdups versus the predicted values in the Bubbly and Turbulent flow regimes. We can see that Equations 4.5 and 4.6 do a better job predicting the experimental gas holdup at low values (data obtained with the air-water system), than at higher values (air-surfactant system). This is due to the larger variability present in the measurement of the overall gas holdup in the foamy air-liquid surfactant system. An estimation of the overall goodness of the predictions is given by the Mean Relative Error (MRE), which is defined as follows:

$$\text{MRE} = \frac{1}{\#\text{of Data Points}} \frac{\left|\varepsilon_g^{pred} - \varepsilon_g^{exp}\right|}{\varepsilon_g^{exp}} \text{x}100 \qquad (4.7)$$

The MRE between experiments and Equations 4.5 and 4.6 are 16.8% and 8%, respectively.

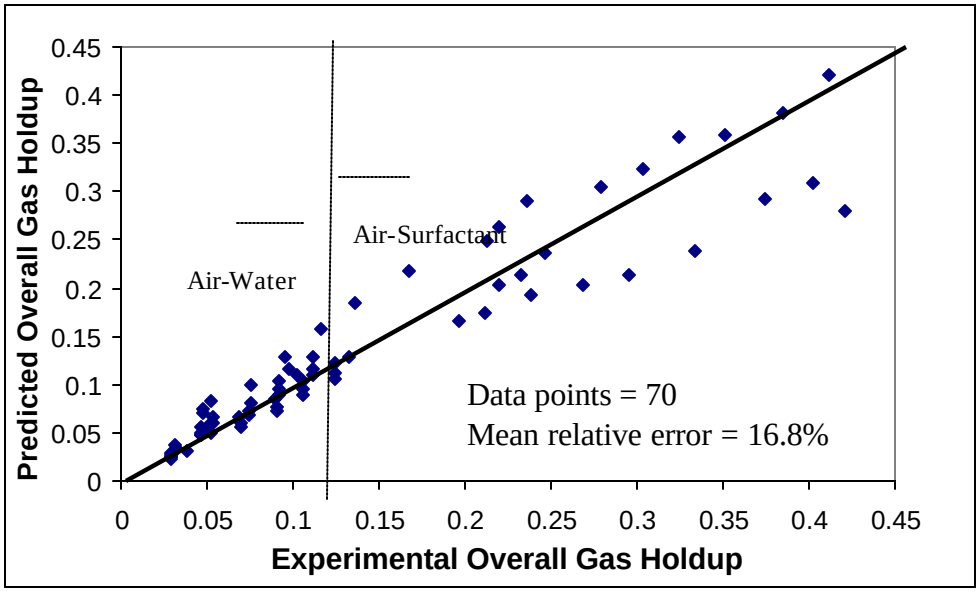

Figure 4.18 Experimental versus Predicted Overall Gas Holdup in the Bubbly Flow Regime.

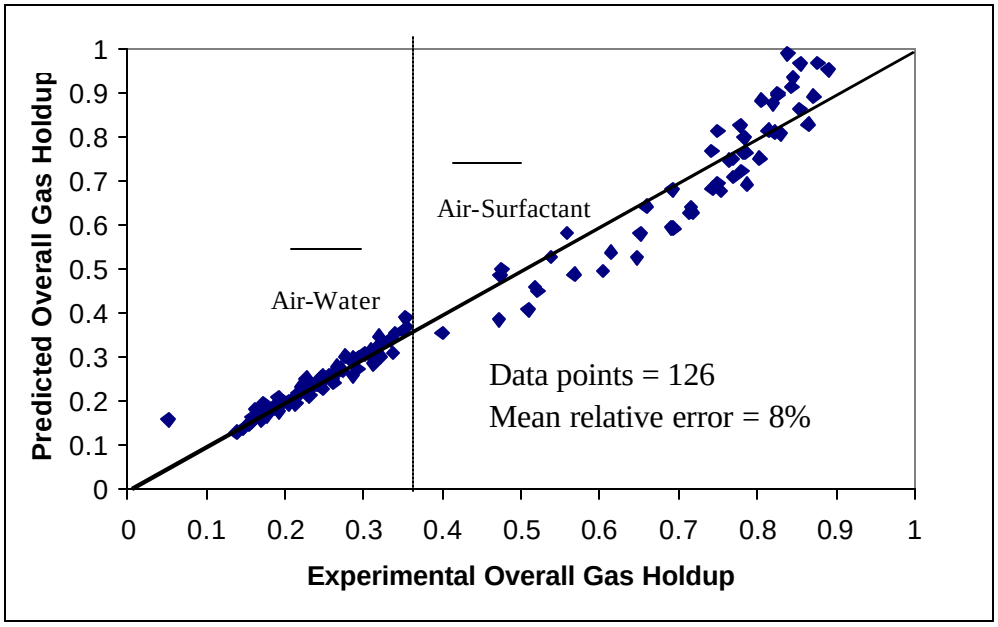

Figure 4.19 Experimental versus Predicted Overall Gas Holdup in the Turbulent Flow Regime.

The relative effect of the different variables studied on the overall gas holdup can be inferred from the power of the dimensionless numbers in Equations 4.5 and 4.6. Below, the effect of the different studied factors on the overall gas holdup is classified in order of importance from more to less important:

Bubble Regime: $U_g > \sigma_l > d_o > O.A > U_l$

Turbulent Regime: $\sigma_l > U_g > d_o > U_l > O.A.$

In general, we can see that superficial gas velocity and surface tension of the liquid phase have the most important effects, whereas tray open area and superficial liquid velocity are less important. It should be noticed that the overall gas holdup is more sensitive to the superficial gas velocity in the Bubbly Regime ($\varepsilon_g \alpha U_g^{0.95}$) than in the Churn-Turbulent Regime ($\varepsilon_g \alpha U_g^{0.62}$). Conversely, the effect of the surface tension of the liquid phase becomes more important in the Churn-Turbulent Regime ($\varepsilon_g \alpha \sigma_l^{-1.44}$) than in the Bubbly Regime ($\varepsilon_g \alpha \sigma_l^{-0.87}$).

4.4 Axial Gas Holdup Profile

The gas holdup has been simultaneously determined at four axial locations inside the column by the Pressure Drop Measurement Technique (Section 3.4). The measured gas volumetric fraction in each of the sampling regions is the time average value (averaged over the sampling period) corresponding to the space bounded by the planes of the pressure drop probes. The gas holdup and the pressure drop between the sides of the pressure transducer's diaphragm are related by Equation 3.5.

$$\varepsilon_{gas} = \frac{\Delta P_{Transducer}}{\rho_{liquid}\, g\, h} \tag{3.5}$$

Where h is equal to 20.3 cm for all the axial locations. The pressure drop signals were sampled at 100 Hz and the time average value was taken. Figure 4.20 shows a typical pressure time series signal measured in the trayed bubble column.

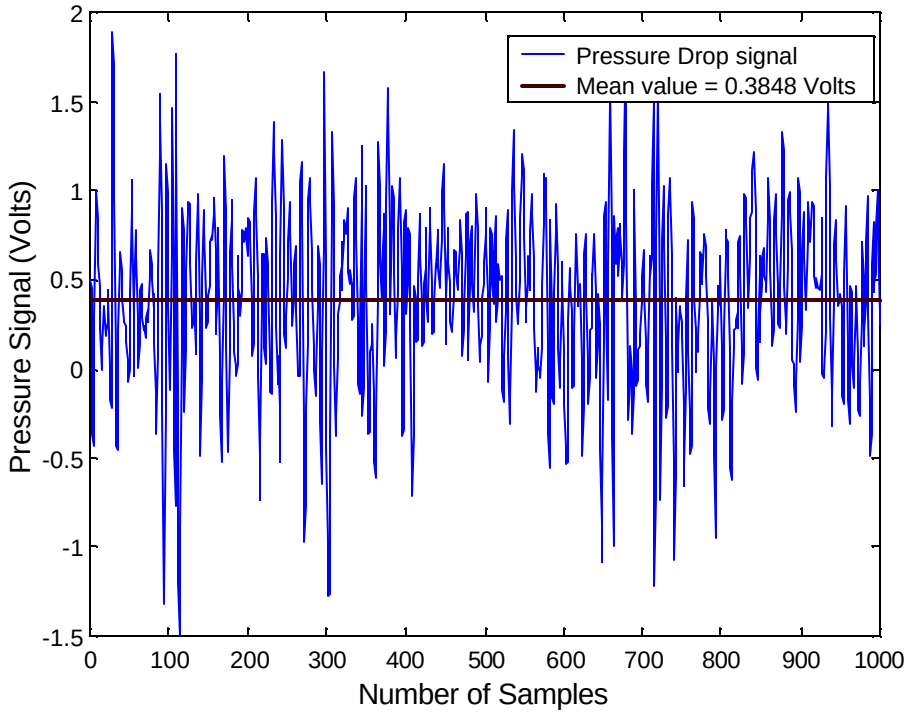

Figure 4.20 Typical Pressure Drop Signal in Trayed Bubble Column.

As explained earlier, the intent of this work was to cover a large range of experimental conditions. However, several problems appeared during the execution of the experimental program, which subsequently reduced the amount of available data. The intense foaming occurring in the column made the collection of accurate pressure drop readings impossible when the air-surfactant system was used. Thus, it was decided to run experiments only with the air-water system to avoid the interference of the foam.

Moreover, no experiments could be run with tray type #3, since the tray was not available at that time, and later experimentation was unfeasible due to the time constraint. However, it will be shown later that the results obtained with only two types of trays are enough to explain the effect of tray geometry on the staged gas holdup. Table A.1.3, in Appendix A.1 lists all the experimental data.

In the following subsections, the effects of superficial gas and liquid velocities, gas sparger design, and trays are discussed based on the experimental observations.

4.4.1 Effect of the Gas Sparger

The effect of the gas distributor is studied via comparison of the gas holdup profiles obtained with a single nozzle sparger (9.5 mm inlet diameter) and a perforated plate sparger (0.4 mm tray hole diameter, 168 holes, and an open area of 0.04%).

Previously, in Section 4.1.5, it was learned that in the single stage bubble column higher overall gas holdups are achieved when the perforated tray sparger is used. Further, the effect of the gas sparger is less important in trayed bubble columns because of the gas redistribution generated by the trays in each of the stages. The axial gas holdup profiles presented in Figures 4.21 and 4.22 reconfirm the previous conclusions. They show the experimental data measured in the single stage and in the multistage bubble columns (with tray type #2) for both types of spargers at superficial gas velocities of 4 and 12 cm/s; and superficial liquid velocity of 0.5 cm/s. It can be seen that in the column without

trays significantly higher gas holdups are achieved at all the axial locations when the perforated tray sparger is used as compared to the single nozzle sparger. The bubbles generated by the perforated plate sparger are generally of smaller diameter, and better distributed through the inlet cross section than the bubbles generated by the single nozzle sparger. *Joshi et al., 1998* distinguished between the average bubble size generated at the sparger (primary bubble size, d_{BP}), which depends on the liquid phase physical properties, the sparger geometry; and the equilibrium average bubble size in the bulk (secondary bubble size, d_{BS}). The latter is set by the balance between the breaking forces (viscous and turbulent sheer stresses) and the surface forces. The primary bubble size decreases with an increase in the rate of energy dissipated by the gas phase in the sparger. A perforated plate with small tray hole diameter dissipates more energy per unit volume than a single nozzle sparger. As a result, the former produces bubbles of smaller average diameter than the latter.

In addition, the coalescence/non-coalescence nature of the liquid phase is very closely related to the effect of the sparger type. In a coalescing system, such as air-water, the average bubble size changes in a very short distance from the sparger (height of the sparger region) from the primary to the secondary or equilibrium average bubble size. In the sparger region, the gas holdup increases along the column if d_{BP} is larger than d_{BS} and it decreases if d_{BP} is smaller than d_{BS}. However, in a non-coalescent system, the primary bubble size is preserved longer along the column provided it is smaller than the secondary bubble size. For this reason, the effect of the gas sparger would be more relevant in non-coalescent systems, whereas it would not be as important in coalescent systems.

As it was mentioned earlier, in the trayed column the situation is quite different. In this case, the redistribution of the gas phase in each of the trays helps to control the bubble size and therefore the effect of the sparger is only noticeable in the first stage of the column. As can be seen in Figure 4.22, the gas holdups measured in the second and higher stages for both types of spargers overlap with each other. Also, the axial gas

holdup profiles at locations above the first stage are smoother than in the single stage column due to the lack of the internal gas phase redistribution by the trays in the latter column.

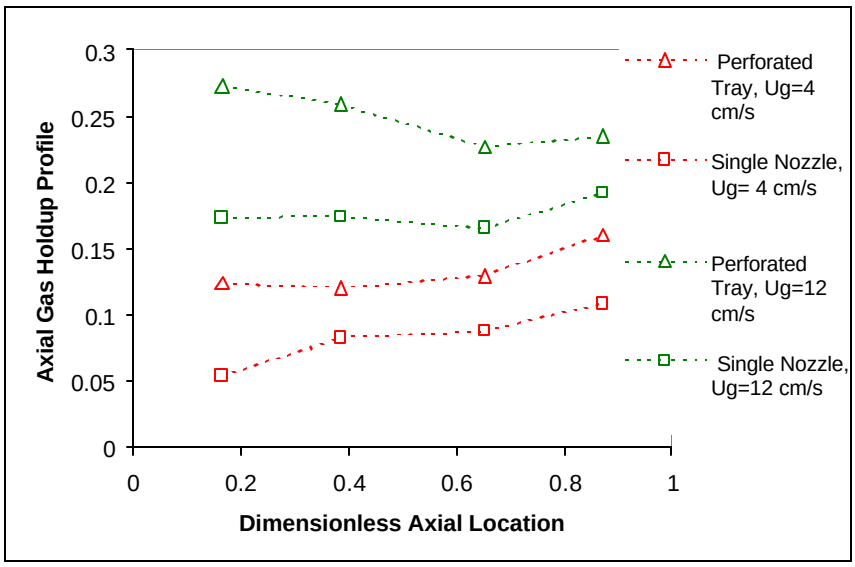

Figure 4.21 Effect of the Gas Sparger on the Axial Gas Holdup Profile in Bubble Column without Trays at U_g= 4, and 12 cm/s; and U_l=0.5 cm/s. Air-Water System.

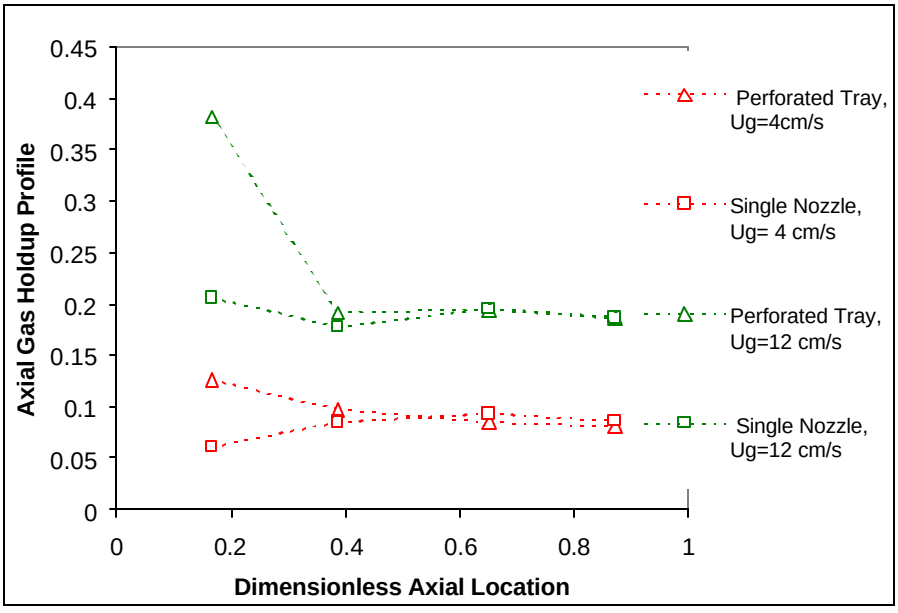

Figure 4.22 Effect of the Gas Sparger on the Axial Gas Holdup Profile in Trayed Bubble Column with Tray Type #2 (d_o=0.6 cm, and 5.2% O.A.) at U_g= 4, and 12 cm/s; and U_l=0.5 cm/s. Air-Water System.

4.4.2 Effect of the Superficial Gas and Liquid Velocities

Figures 4.23 and 4.24 show the axial gas holdup profile in the single stage bubble column at a range of superficial gas velocities (U_g=1-12 cm/s) with the single nozzle and perforated plate spargers, respectively. There is a slight increase in the gas holdup with axial direction. The change is more noticeable in the lower part of the column than at higher axial locations due to the effect of the gas sparger as discussed earlier.

In the multistage bubble column (Figures 4.25 and 4.26), the trays help to flatten the gas holdup profile by redistributing the gas in each of the stages. Thus, the profile can be considered to be almost flat at axial locations situated above the influence of the sparger region. As explained in Section 4.4.1, there is an important effect of the sparger type in the sense that the single nozzle sparger seems to introduce in the column bubbles of larger diameter than the equilibrium bubble size. Therefore, the gas holdup increases in the first stage until the bubbles reach the equilibrium bubble diameter. On the other hand, the opposite occurs with the perforated plate sparger since now the introduced bubbles present smaller sizes than the equilibrium diameter. In fact, it can be seen in Figure 4.26 that with the latter sparger as the gas velocity is increased the difference between the gas holdup measured in the first and higher stages also increases.

Figure 4.27 shows the effect of superficial liquid velocity on the axial gas holdup profile in the single stage bubble column with the single nozzle sparger. Similarly, to the overall gas holdup (Section 4.1), there is a small increase in the gas holdup as the liquid velocity is decreased. Further, the effect of the liquid velocity on the axial gas holdup profile is very mild, and as it can be seen in the figure, the curves for different U_l and same U_g stay almost parallel to each other.

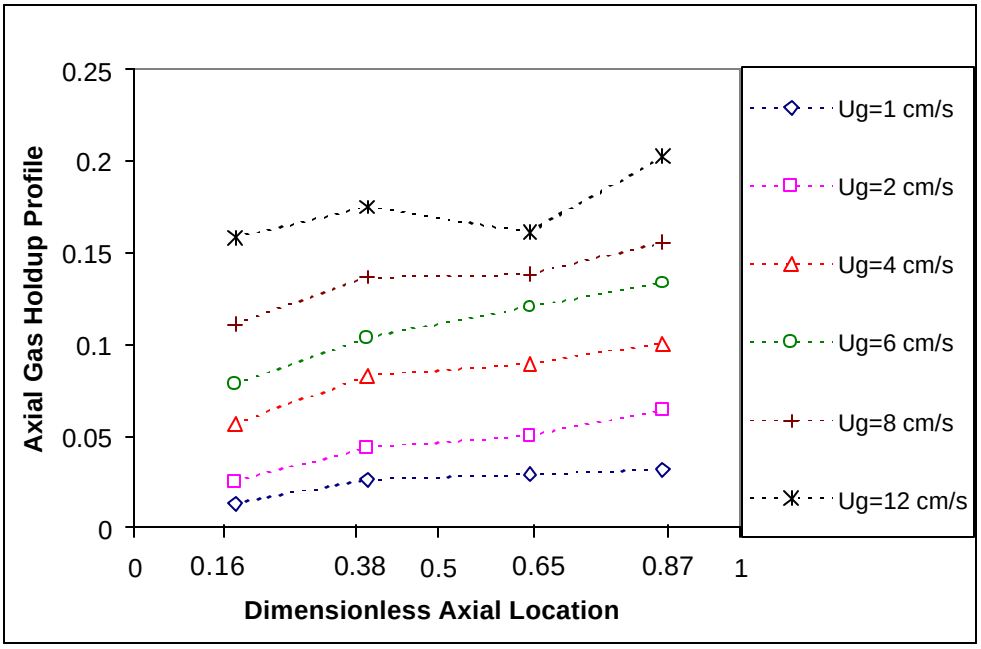

Figure 4.23 Effect of the Superficial Gas Velocity on the Axial Gas Holdup Profile in Bubble Column without Trays at U_l=1 cm/s. Air-Water System and Single Nozzle Sparger.

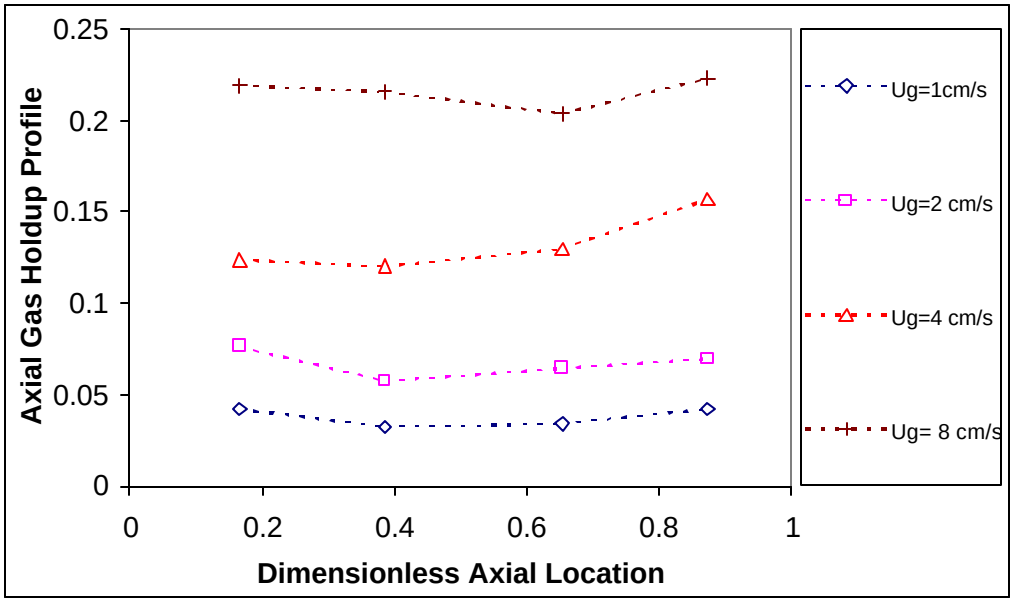

Figure 4.24 Effect of the Superficial Gas Velocity on the Axial Gas Holdup Profile in Bubble Column without Trays at U_l=0.5 cm/s. Air-Water System and Perforated Tray Sparger.

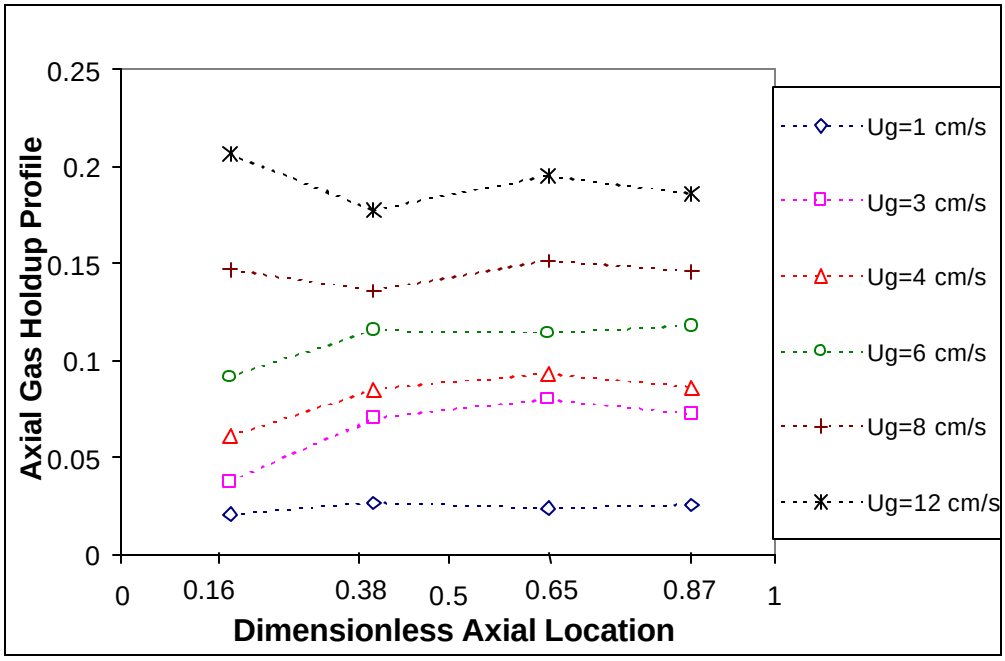

Figure 4.25 Effect of the Superficial Gas Velocity on the Axial Gas Holdup Prof .ile in Trayed Bubble Column with Tray Type #2 (d_o=0.6 cm, and 5.2% O.A.) at U_l=1 cm/s. Air-Water System and Single Nozzle Sparger.

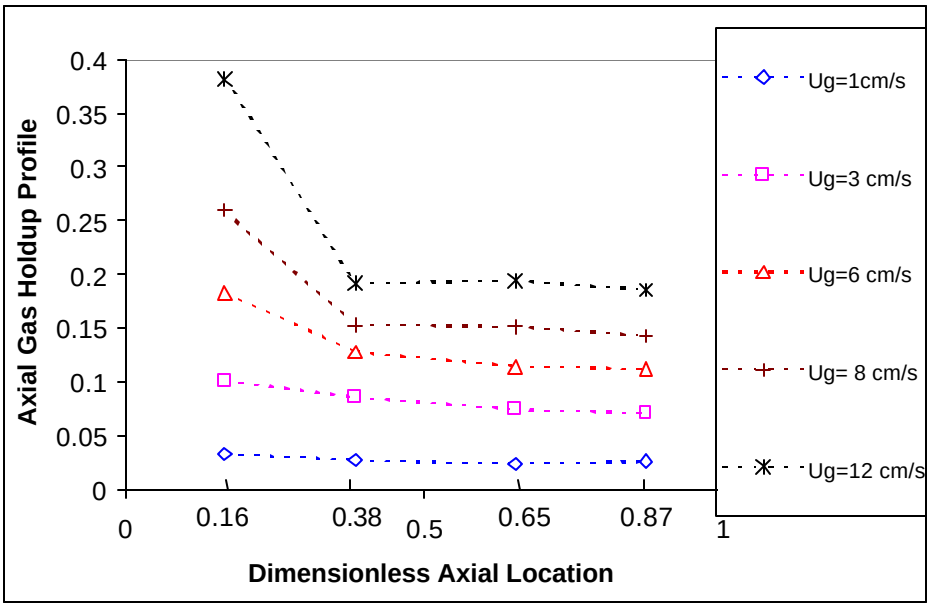

Figure 4.26 Effect of the Superficial Gas Velocity on the Axial Gas Holdup Profile in Trayed Bubble Column with Tray Type #2 (d_o=0.6 cm and 5.2% O.A.) at U_l=0.5 cm/s. Air-Water System and Perforated Tray Sparger.

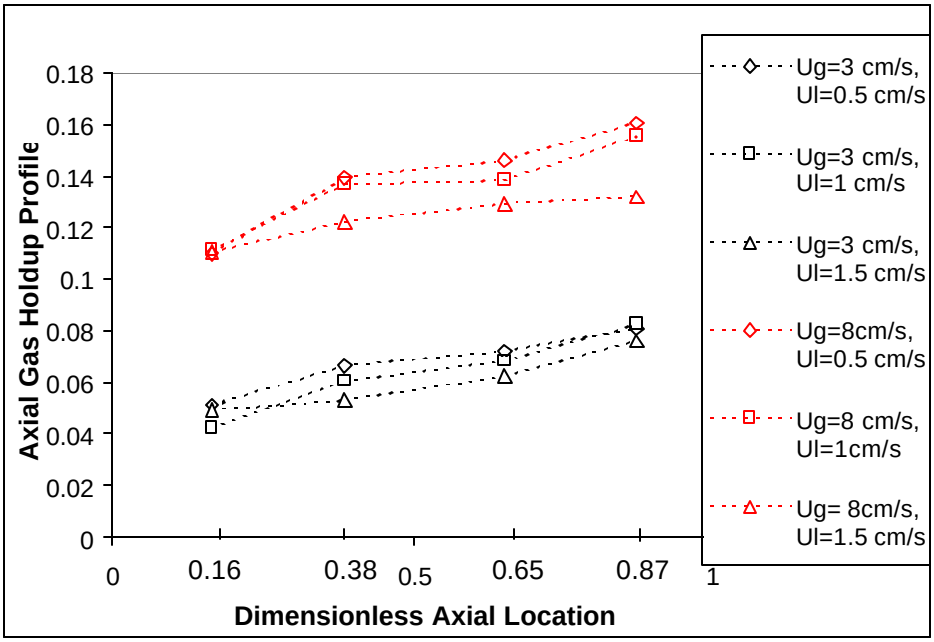

Figure 4.27 Effect of the Superficial Liquid Velocity (U_l=0.5, 1, and 1.5 cm/s) on the Gas Holdup Profile in Single Stage Bubble Column at U_g= 3, and 8 cm/s. Air-Water System and Single Nozzle Sparger.

4.4.3 Effect of the Tray Geometry

In previous sections, it has been extensively stressed how the trays redistribute the gas phase and help to control the bubble size in the trayed column. As a result, an almost flat axial gas holdup profile can be seen at locations situated above the sparger. A steeper profile, however, is established in the column when the trays are removed.

In Figure 4.28, the profiles for the single stage and multistage columns (with tray types # 1, and #2) are plotted at the following experimental conditions (U_g=4 and 18 cm/s at U_l=1 cm/s). We can see that at U_g=4 cm/s, the presence of trays does not affect much the stage gas holdups measured in the column. This is consistent with the findings reported in Section 4.1.1, that the trays have no effect on the overall gas holdup in the Bubbly Regime. On the other hand, at U_g=18 cm/s larger gas holdups are found with tray type #2 (d_o=0.6 cm, 5.2% O.A.) than with tray type #1 (d_o=1.74 cm, 10.2% O.A.). This is

mainly due to the smaller open areas and hole diameters of tray type #2, which dissipate energy more effectively and subsequently enhance the formation of smaller bubbles. However, the gas holdups measured in the single stage column are of the same order or even higher than the holdup values yielded by the trayed bubble column column. This observation contradicts the results reported in Section 4.1.2 where the overall gas holdup is significantly increased by the presence of trays in the Churn Turbulent Regime. It should be noted that the pressure drop sampling regions are located within the stages and not in between the trays (Figure 3.6). In fact, the observed accumulation of gas underneath the trays creates an unequal distribution of gas holdup between the bulk of the stage and the region right below the tray. On the contrary, in the column without trays, there is a more homogenous axial gas holdup distribution along the sections of the column corresponding to the different stages formed by the trays in the trayed bubble column. As a consequence, the stage gas holdup measured in the trayed bubble column is under estimated by the pressure drop method because it does not account for the fraction of gas located under the tray.

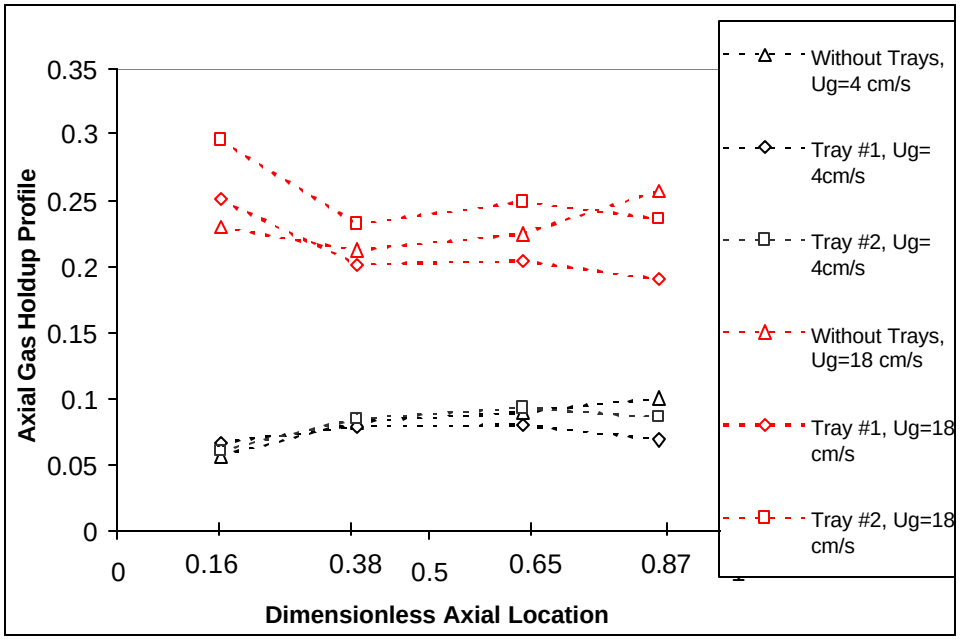

Figure 4.28 Effect of the Trays on the Gas Holdup Profile in Trayed Bubble Column with Tray Types #1 (d_o=1.74 cm and 10.2% O.A.) and Type #2 (d_o=0.6 cm, and 5.2% O.A.) at U_g= 4, and 18 cm/s; and U_l= 1cm/s. Air-Water System and Single Nozzle Sparger.

4.5 Overall Gas Holdup: Gas Disengagement versus Pressure Drop Methods

It is possible to estimate the overall gas holdup by integrating the gas holdup profiles obtained from the pressure drop measurements along the column, and compare them with the values obtained from the gas disengagement experiments.

The estimation of the local or staged gas holdup at a given axial location by the Pressure Drop Method (Equation 3.5) is based on the assumption that its value is constant within the measured region. However, in order to estimate the overall gas holdup through integration of the gas holdup profile along the column height, a continuous rather than a discrete profile is needed. We can assign the gas holdup value estimated for each of the measured regions to its middle point, which is also the middle of the stage, since the two

pressure probes are equidistant from the upper and bottom trays of the stage. Further, we can use natural cubic splines to interpolate piecewise polynomials through the four available data points. The overall gas holdup is calculated by analytical integration of the interpolating polynomials over the height of the column covered by the pressure drop measurement locations as follows:

$$e_g = \frac{\int_a^b e_g(z)\,dz}{(b-a)} \tag{4.8}$$

It should be noted that the sparger and the disengagement regions are not accounted for in this estimation of the overall gas holdup, since there are no pressure drop measurements in those regions. In fact, the limits of integration *a*, and *b* in Equation 4.8 correspond to points located above the sparger and below the disengagement region, respectively. In the multistage column, the contribution coming from the pressure drop across the trays is not considered either since the actual pressure drop measurements are located within the column stages and not in between them. As it was mentioned in Section 4.4.3, the unequal distribution of gas holdup between the bulk of the stage and the region right underneath the trays, translates into the underprediction of the gas holdup in the trayed bubble column. Therefore, some degree of discrepancy is expected between the two techniques being compared.

In Figures 4.29 and 4.30, the overall gas holdup as estimated by the Gas Disengagement and Pressure Drop Techniques are plotted together versus the superficial gas velocity for the single stage and multistage bubble columns (tray type #2), respectively. In both figures, the perforated tray sparger was used as gas distributor.

In the single stage column, it can be seen that in the range of low superficial gas velocities (U_g=1-6 cm/s) the overall gas holdups estimated by the two methods overlap each other. As the gas velocity is increased above 6 cm/s, the Pressure Drop Technique

gives slightly higher gas holdups than the gas disengagement. However, if U_g is further increased, the gas holdup measurements given by the compared methods converge to each other at velocities larger than 16 cm/s. The mean relative error over the whole range of superficial gas velocities tested is equal to 7.5%, which is within the experimental error of the Gas Disengagement Method.

Figure 4.30 shows the comparison between the two techniques in the multistage bubble column with tray type #2. In this case, it can be seen that the Pressure Drop Technique underpredicts the overall gas holdup measured by the Gas Disengagement Method. This observation is consistent with the fact that the formation of cushions of gas underneath the trays sets a large pressure drop across the trays, which is not taken into consideration in the estimation of the overall gas holdup from the integration of the gas holdup axial profile. The mean relative error over the whole range of superficial gas velocities studied is equal to 19%.

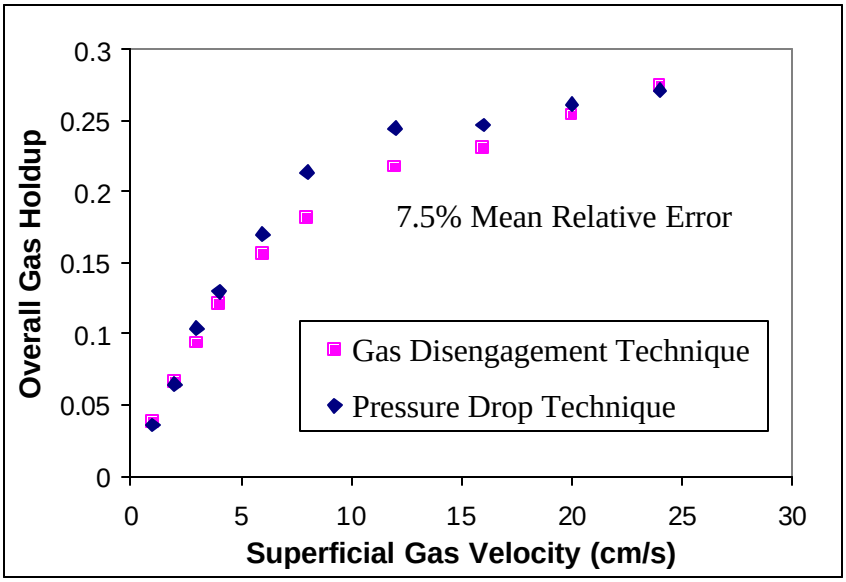

Figure 4.29 Comparison of the Overall Gas Holdup obtained by the Gas Disengagement and Pressure Drop Techniques in Single Stage Bubble Column with the Perforated Plate Sparger at U_l=0.5 cm/s. Air-Water System.

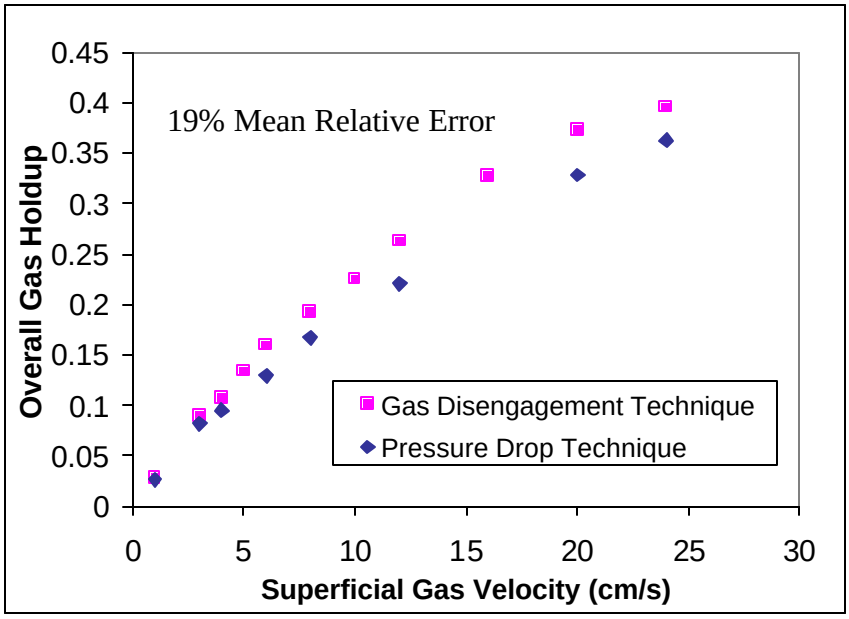

Figure 4.30 Comparison of the Overall Gas Holdup Obtained by the Gas Disengagement and Pressure Drop Techniques in the Trayed Bubble Column with Tray Type #2 (d_o=0.6 cm, 5.2% O.A.) at U_l=0.5 cm/s. Perforated Plate Sparger. Air-Water System.

4.6 Pressure Drop across the Trays

The pressure drop across the tray has been simultaneously measured at three different axial locations along the trayed bubble column with differential pressure transducers. Recalling Equation 3.6, one can express the pressure drop across the tray as the sum of a hydrostatic term due to the weight of the G-L mixture between the pressure probes and a dissipation term.

$$\Delta P_{dissipated} = \Delta P_{Transducer} - \rho_{gas}\, g\, h\, \bar{\varepsilon}_{gas} \qquad (3.6)$$

Here $\bar{e}_{gas}$ is the spatial ensemble average gas holdup corresponding to the 3-D region bounded by the cross sectional planes of the pressure drop probes. It has been observed that at the range of medium-high superficial gas velocities, the dispersed phase tends to accumulate right below the trays forming a cushion of gas. This accumulation

sets a positive hydrostatic pressure drop across the trays, which in turn drives the inter-stage liquid phase backmixing. Extremely high gas holdup gradients are formed in between the trays. As a result, in Equation 3.6 the hydrostatic and dissipation terms cannot be easily decoupled.

In Equation 3.6, the hydrostatic term corresponds to the pressure due to the weight of a column of water whose height is equal to $h(1-\bar{e}_{gas})$. On the other hand, the dissipation term accounts for the extent of energy dissipated by the G-L system as it crosses the tray. Both terms are complex functions of the operating conditions (gas and liquid superficial velocities), and of the trays geometry.

Figure 4.31 shows that no statistically significant differences were observed among the pressure drops measured at the three chosen axial sampling locations. This was confirmed for all the experimental conditions tested. The arithmetic mean of the three measurements will be considered to be the measured pressure drop across the trays for a given set of operating conditions and tray type. It should be pointed out that in this work only the experiments for the air-water system and the single nozzle sparger have been conducted. All the experimental data have been included in Table A.1.5 of Appendix A.1.

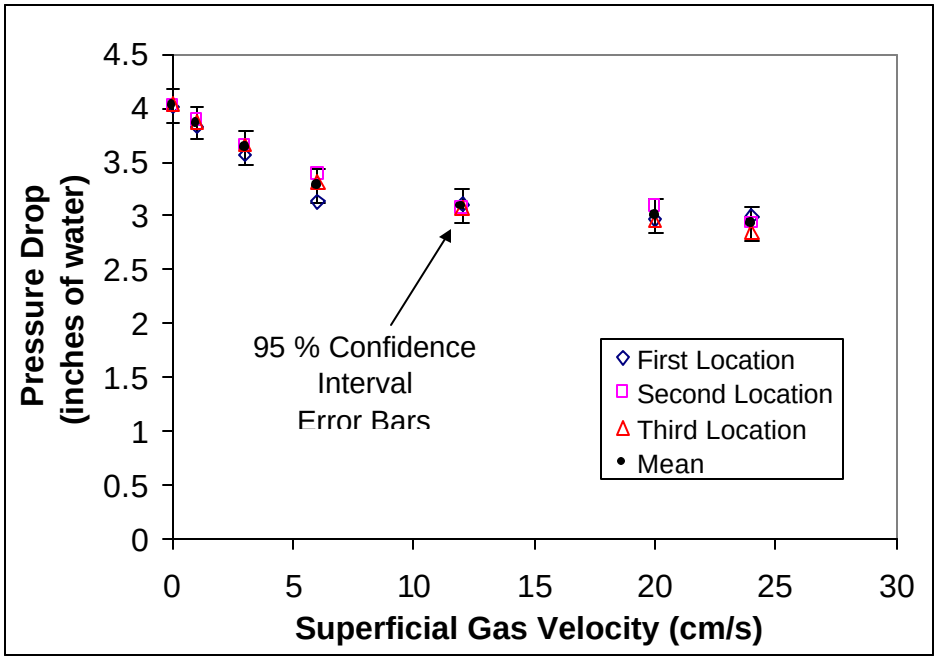

Figure 4.31 Effect of Tray Location on the Pressure Drop across the Tray in Trayed Bubble Column with Tray Type #2 at U_l=0.5 cm/s. Single Nozzle Sparger and Air-Water System.

4.6.1 Effect of the Superficial Gas and Liquid Velocities

An increase in the superficial velocity of the gas phase has two opposite effects on the pressure drop across the trays. The hydrostatic pressure decreases due to the reduction in the density of the gas-liquid mixture, since there is less liquid between the pressure probes. At the same time, the dissipation in the trays due to turbulence is increased.

Figures 4.32-4.35 show that in the range of low gas velocities the hydrostatic term is the predominant term in Equation 3.6 due to the linear decrease in the density of the gas-liquid phase. This is related to the almost linear increase of the gas holdup with U_g in the Bubbly Regime. However, at higher superficial gas velocity, the increasing influence of the dissipation term, added to the slower increase of the gas holdup with U_g in the Churn-Turbulent Regime slows down the decrease of the total pressure drop across the

trays with U_g. At a sufficiently large gas velocity both terms balance and a constant pressure drop is reached.

Also, one can see in Figure 4.32 that at the same superficial gas velocity the larger the superficial liquid velocity, the more energy of the flowing phases is dissipated in the trays. In order to isolate the effect of the superficial liquid velocity, the pressure drop across the trays was measured in single flow conditions (U_g=0 cm/s; Figures 4.32, 4.34 and 4.35). The figures show that at U_l=0.5 cm/s, the pressure drop across the trays is almost exclusively due to the hydrostatic component, since the pressure drop measured is equal to the pressure of a column of water 4 inches (10.16 cm) tall. This is the exact distance between the pressure drop probes in the column. On the contrary, at U_l=1.5 cm/s the measured pressure drop is slightly larger than 4 inches of water (e.g. 0.2 inches (0.52 cm) of water in the column with tray type #2). This proves that dissipation across the tray due to the liquid passage does occur. However, it is at least one order of magnitude smaller than the hydrostatic term.

4.6.2 Effect of the Tray Geometry

The pressure drop across the tray yielded by trays of the same open area (10.2% O.A.) but different hole diameters (d_o=1.74 cm versus d_o=0.6 cm) is plotted in Figure 4.33 at U_l=1.5 cm/s. Although, one would expect to see higher pressure drop across the trays with a decrease in the hole diameter due to the increase in the resistance to the flow of the phases, the opposite is observed. The reason is that the tray with the smallest hole diameter gives a higher overall gas holdup, and thus the amount of liquid present in between the probes is lesser. Therefore, the contribution to the total pressure drop coming from the hydrostatic component offsets the increase in the dissipation term when the tray with the smallest hole diameter is used.

A different conclusion can be reached when trays of the same tray hole diameter (d_o=0.6 cm) but different open areas (10.2% versus 5.2%) are compared. In this case, the

extent of the total pressure drop accounted by the hydrostatic term is somewhat similar in both trays, since the effect of the open area on the overall gas holdup is not as important as the tray hole diameter (see Section 4.1.2). As shown in Figures 4.33 and 4.35 for U_l=1.5 cm/s, it can be seen that tray type #2 (d_o=0.6 cm, 5.2% O.A.) introduces a larger pressure drop than tray type #3 (d_o=0.6 cm, 10.2% O.A.) since the former has a smaller open area, and therefore more energy has to be dissipated for the phases to travel across the trays. Moreover, the effect of increasing the superficial liquid velocity (from 0.5 cm/s to 1.5 cm/s) is to add more pressure drop across the trays and therefore, to enhance even more the differences between the two trays (Figures 4.34 and 4.35).

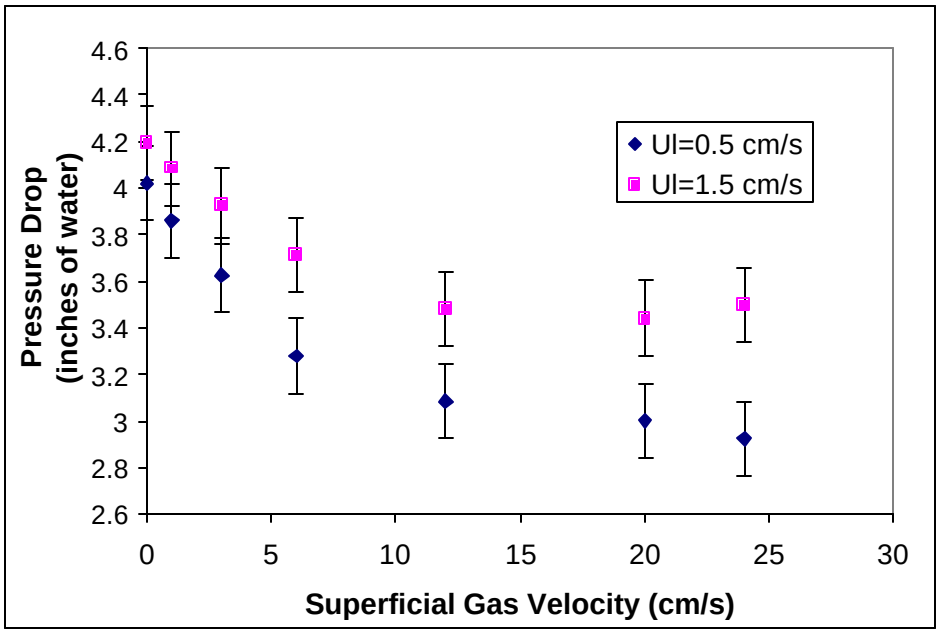

Figure 4.32 Pressure Drop across the Trays versus Superficial Gas Velocity at U_l=0.5 cm/s and U_l=1.5 cm/s in Multistage Column with Tray Type #2 (d_o=0.6 cm, 5.2% O.A.). Single Nozzle Sparger, and Air-Water System.

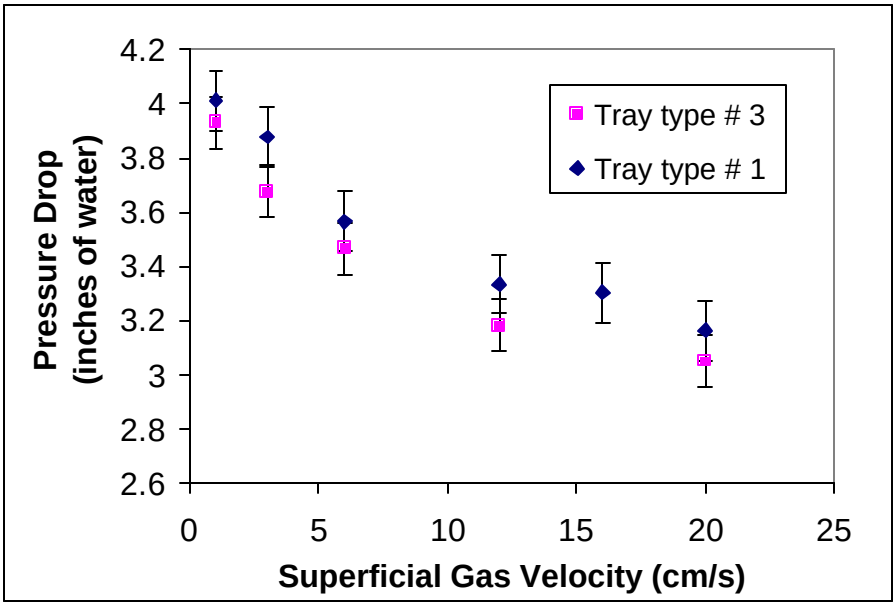

Figure 4.33 Pressure Drop across the Trays versus Superficial Gas Velocity at U_l=1.5 cm/s in Multistage Column with Tray Type #1 (d_o=1.74 cm, 10.2% O.A.), and Tray Type #3 (d_o=0.6 cm, 10.2% O.A.). Single Nozzle Sparger and Air-Water System.

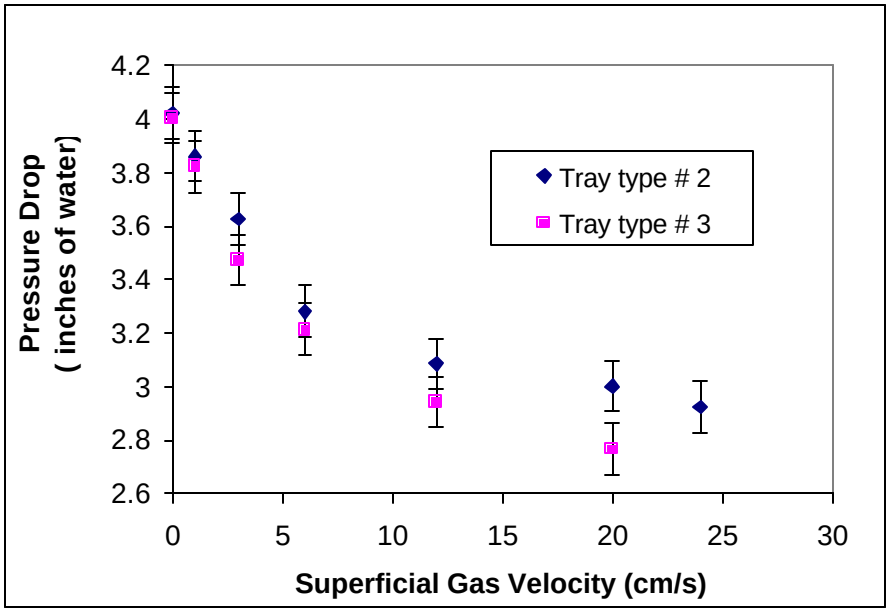

Figure 4.34 Pressure Drop across the Trays versus Superficial Gas Velocity at U_l=0.5 cm/s in Multistage Column with Tray Type #2 (d_o=0.6 cm, 5.2% O.A.) and Tray Type #3 (d_o=0.6 cm, 10.2% O.A.). Single Nozzle Sparger and Air-Water System.

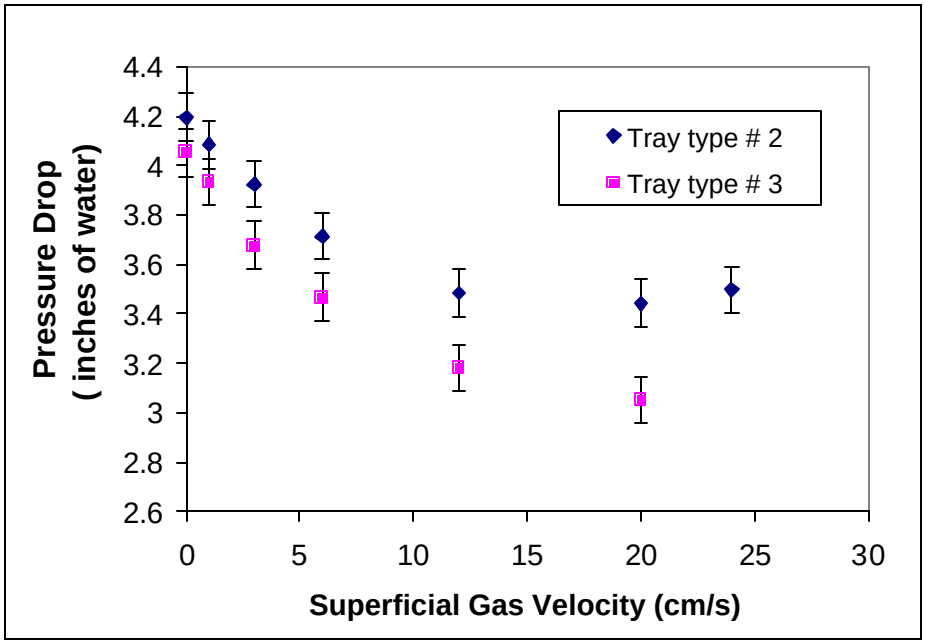

Figure 4.35 Pressure Drop across the Trays versus Superficial Gas Velocity at U_L=1.5 cm/s in Multistage Column with Tray Type #2 (d_o=0.6 cm, 5.2% O.A.) and Tray Type #3 (d_o=0.6 cm, 10.2% O.A.). Single Nozzle Sparger and Air-Water System.

Chapter 5 Overall Liquid Phase Mixing: Introduction, Objectives and Literature Review

5.1 Introduction and Motivation

Dudukovic et al., 1999; Joshi et al., 1998; and many others have reported the existence of a parabolic radial gas holdup profile in the operation of conventional bubble columns in the Churn Turbulent flow regime. This causes a difference in the density of the gas-liquid dispersion in the radial direction, with its maximum at the wall and its minimum at the center of the column. As a result, an intense axial liquid recirculation sets in the column. The liquid in the bottom is sucked towards the central part of the column, from where it travels upwards until it reaches the upper part of the column. In order to satisfy the momentum and mass balance equations, part of the liquid has to recirculate back to the bottom of the column through its outer part. As the bubbles of gas enter the column, the ascending liquid drives them towards the center and hence the radial gas holdup profile can be maintained in the column.

This intense mixing is advantageous in processes that require good mass and heat transfer capabilities. In isothermal multiphase reaction systems, however, the backmixing can be a clear disadvantage due to the dilution effect, which decreases the reaction driving force, and hence reactor volumetric productivity and reactants conversion.

The sectionalization of conventional bubble columns, for instance, by perforated trays (Trayed Bubble Columns), has been demonstrated to be an efficient way to break the liquid phase macrocirculation pattern by creating independent well mixed stages in between the trays, and therefore approaching plug flow efficiency *(Patil et al., 1984; Joshi et al., 1979;* and *Schugerl et al., 1977*).

As it was described in the first part of this work, several industrial processes such as the Visbreaking operation of petroleum residues (*Palaskar et al., 2000; and Dassori, 1999*) and the Fischer-Tropsch synthesis of paraffins from syngas (*Maretto et al., 2000*) have all benefited from the utilization of trayed bubble columns.

As opposed to single stage bubble columns, whose mixing characteristics have been extensively studied and reported in the scientific literature, only few authors have conducted experimental or fundamental research on this topic with trayed bubble columns (*Palaskar et al., 2000; Dudukovic et al., 1999; Vinaya 1995; Blass et al., 1977*; and some others).

The design of the trays, the flow phases arrangement, the gas and liquid superficial velocities, and the gas sparger type are among the most important parameters of design and scale-up that affect the extent of liquid axial backmixing in trayed bubble columns.

Many of the studies reported in the literature make use of simple and conventional liquid mixing model approaches to interpret the obtained experimental data and to quantify the effect of the different studied parameters. The Axial Dispersion Model (ADM) has been traditionally used to describe and quantify the extent of liquid backmixing in different reactor and contacting systems, because of its simple mathematical formulation and existence of single model parameter, which can readily be extracted from experiments (*Palaskar et al., 2000; and Magnussen et al., 1978*). However, multistage bubble columns are examples of contactors in which the flow of the phases seems to be more accurately represented by stagewise models such as the N-CSTR with Backmixing Model *(Kastánec et al., 1993*) and the Dispersion-Backflow Model (*Sekizawa et al., 1975*). In these models, the non-idealities of the liquid flow can be described by the total number of stages and the flowrates of the streams that connect the stages.

In spite of the effort done by the authors cited above, it is clear that a more exhaustive investigation of the effect of the controlling factors on the extent of the liquid phase backmixing is necessary to facilitate the design and operation of industrial scale upward co-current trayed bubble columns.

5.2 Objectives

The goal of this part of the study is to acquire experimental and fundamental knowledge about the effect of the design of the perforated trays and the operating conditions on the overall liquid phase mixing in trayed bubble columns.

The approach followed to achieve the above objective can be summarized as follows:

1. Review literature to identify the current models available for the description of the overall liquid phase mixing in trayed bubble columns, as well as empirical correlations to estimate their model parameters.

2. Conduct tracer mixing experiments in a bench scale co-current trayed bubble column set-up.

3. Evaluate existing models to describe the overall liquid phase mixing in trayed bubble columns, determine their needed parameters by non-linear fitting of the experimental data to the solution of the model equations.

4. Evaluate the effect of tray design and operating conditions on the extent of the overall liquid phase backmixing based upon the value of the fitted model parameters.

5. Develop mathematical expression(s) to estimate the model parameter(s) as function of the perforated tray design and operating conditions.

5.3 Literature Review

As mentioned in the introduction section, the amount of the available literature regarding the liquid phase axial backmixing in trayed bubble columns is limited. With the exception of *Vinaya, 1994*, most of the authors (see Tables 5.2, and 5.3) focused only on the effect of operating conditions (superficial gas and liquid velocities) and paid little attention to the design parameters of the trays (hole diameter, open area, hole distribution, stage height, and others). *Vinaya, 1994* reported empirical correlations for the estimation of the Peclet number. These correlations were developed based on experimental data collected in a counter-current trayed bubble column. However, such type of work has not been reported in co-current trayed columns yet.

In order to review the existing liquid backmixing literature for TBC, it is very convenient to group the published work based on the models that the authors used to interpret their experimental data. This is because the extent of liquid backmixing can be quantified by the value of the parameters of the models used. Usually, the accuracy of the model interpretation of the mixing phenomena is based upon the number of parameters that it contains. Therefore, a balance between an adequate physical realization of the reactor system and a simple experimental verification must be sought when assessing the validity of a model. Simplified models can serve the purpose of providing us with a reasonable insight into the flow description without having to invest too much time and effort during the process.

We can classify the available models into the following three main groups: discrete models, continuous models, and a combination of both. When we write the steady state mass conservation equations for the first type, simple mathematical algebraic equations

result. On the other hand, continuous models yield sets of ordinary or partial differential equations.

5.3.1 Continuous Models: The Axial Dispersion Model (ADM)

One of the most well known continuous models is the Axial Dispersion Model (ADM). The model is the simplest mathematical description of a flow system in which both convection and diffusion are the governing transport mechanisms. The diffusion term is modeled as a Fickian type process in which both microscopic diffusion (molecular), and macroscopic diffusion (caused by turbulent transport) are lumped into a single parameter model, known as axial dispersion coefficient (D_L). As for the convective transport term, the ADM assumes that any species in the system travels at the mean flow velocity. In a non-reactive gas-liquid system, the model equation for the liquid phase can be written as a parabolic partial differential equation *(Myers,* 1986), where ε_g is the system's overall gas holdup and the – and + signs in front of the convective term refers to whether the gas and liquid phases flow co-currently or counter-currently, respectively.

$$\underbrace{\frac{\partial C}{\partial t}}_{\text{Transient Term}} = \underbrace{\mp \frac{U_l}{(1-\varepsilon_g)} \frac{\partial C}{\partial z}}_{\text{Convection Term}} + \underbrace{D_L \frac{\partial^2 C}{\partial z^2}}_{\text{Diffusion Term}} \tag{5.1}$$

The model can also be written in a dimensionless form as follows:

$$\frac{\partial C^*}{\partial q} = \mp \frac{\partial C^*}{\partial Z} + \frac{1}{Pe} \frac{\partial^2 C^*}{\partial Z^2} \tag{5.2}$$

Where,

$$C^* = \frac{C}{C_o} \quad \theta = \frac{t\, U_l}{(1-\varepsilon_g) L} \quad Z = \frac{z}{L} \quad Pe = \frac{U_l L}{D_L (1-\varepsilon_g)} \tag{5.3}$$

The dimensionless parameter, Peclet number, quantifies the extent of the liquid phase axial backmixing. The ADM model has been widely applied. Sometimes, it is applied without any theoretical justification due to the convenience of being able to describe with only one parameter the whole spectrum of backmixing, from plug flow (no backmixing, Pe=infinity) to perfect mixing (Pe=0). The model has an added mathematical complexity coming from the parabolic nature of its equations. The solutions to parabolic partial differential equations predict an instantaneous response, felt everywhere in the domain, to a perturbation introduced into the system. This fact goes against real physical systems in which all the disturbances have a finite speed of propagation. In order to provide proper closure to the problem, one needs to define the boundary conditions at the entrance and exit of the domain. The boundary conditions of the axial dispersion model can be classified according to whether diffusion is allowed in and out of the reactor boundaries (open) or not (closed). Hence, we can define any of the four different possible combinations: open-open, closed-closed, open-closed, and closed-open. Their mathematical representation is given elsewhere (*Fan et al., 1975*). *Kastánec et al., 1993* pointed out that the choice of proper boundary conditions should be based upon the type of reactor to be modeled and the geometry of its inlets and outlets. The most popular boundary conditions used in the modeling of industrial reactor systems are the closed-closed type. *Danckwerts, 1953* claimed that the assumption of not allowing any material inside the system to leave its boundaries through diffusion is a good approximation in most of the real reactors due to the small diameter of their inlet and outlet pipes as compared to the reactor dimensions. In fact, the closed-closed boundary conditions are also named after him as Danckwerts Boundary Conditions.

Levenspiel, 1962 and others have evaluated the transient model response to an ideal pulse input (δ−Dirac function). Thus, for the open-open and semi open systems, there are exact time domain analytical solutions for the species concentration (Equations 5.4 and 5.5, respectively), whereas for the closed-closed systems only an approximate numerical solution is possible. The Method of Moments (*Nauman et al., 1983*) allows for a straightforward evaluation of the response curve moments (Table 5.1).

$$C = \frac{1}{2\sqrt{\pi\theta / Pe}} \exp\left[-\frac{(1-\theta)^2}{4\theta / Pe} \right] \tag{5.4}$$

$$C = \frac{1}{2\sqrt{\pi\theta^3 / Pe}} \exp\left[-\frac{(1-\theta)^2}{4\theta / Pe} \right] \tag{5.5}$$

Table 5.1 First and Second Dimensionless Moments for the ADM with Different Types of Boundary Conditions *(Thyn et al., 2000*).

Boundary Type	**First Moment,** q	**Second Moment,** s^2_q
Open-Open	1+2/Pe	$2/Pe+8/Pe^2$
Closed-Closed	1	$2/Pe+2/Pe^2$ [1-exp (-Pe)]
Semi-Open	1+1/Pe	$2/Pe+3/Pe^2$

The number of empirical correlations developed for the axial dispersion coefficient in conventional bubble columns is very large *(Myers, 1996).* This is in part due to the belief that a 1-D diffusive model can explain the fluid mixing of any given system without considering the particularities of the system mixing mechanism.

Table 5.2 provides a summary of the papers reviewed in this work, where the ADM has been used to explain the liquid mixing in trayed bubble columns. The main conclusions can be summarized as follows:

1. In general all the authors have agreed upon the effect of tray open area, tray hole diameter, tray spacing, and column diameter on the axial dispersion coefficient. The Axial Dispersion Coefficient (D_L) always increases with tray open area, tray hole diameter, tray spacing, and column diameter. It has unanimously been observed that

there is no further reduction in the overall liquid backmixing when the diameter of the holes in the perforated trays is kept smaller than 5 mm.

2. Some discrepancies appear regarding the effect of the superficial gas velocity on the extent of liquid phase backmixing. In fact, it has been reported that there is no dependency in the counter-current flow arrangement (*Vinaya et al., 1995*). Nevertheless, in co-current columns *Ichikawa et al., 1967* have reported a slight increase in the dispersion coefficient when U_g is smaller than 7 cm/s, point after which D_L rapidly increases until it reaches a maximum at 18 cm/s. However, most of the investigators did not find the maximum reported by *Ichikawa et al., 1967* but instead found a monotonic increase ($D_L \alpha U_g^e$, e=0.12-0.5), where the value of the exponent e is mainly a function of the operating regime.

3. *Ichikawa et al., 1967* and *Chen et al., 1989* could not find any effect of the superficial liquid velocity on D_L, whereas other authors such as *Schugerl et al., 1977; Vinaya, 1995*; and *Palaskar et al., 2000* described a significant superficial liquid velocity effect ($D_L \alpha U_l^{0.45-0.85}$). *Palaskar et al., 2000* reported that the superficial liquid velocity independence observed by the first group of investigators was due to the fact that the order of magnitude of the generated liquid circulation velocity was much higher than the liquid superficial velocity. This masked the effect of the increase in the superficial liquid velocity.

Table 5.3 Summary of the Available Published Work for Trayed Bubble Columns using the N-CSTR in Series Model

Reference	Arrangement	Apparatus and Conditions	Correlation(s)	Findings
Vinaya, 1995	Counter-current with downcomers	Hc=180,100 m; Dc=9.8, 15.4 cm Perforated trays d_o=3; 5, 10, 12 mm; O.A.=9.5, 10, 38.7, 52 %; H_S=5, 85 cm U_g=1.2-11 cm/s U_l=0-2.12 cm/s	Bubbly Regime $\frac{N_{eff}}{N} = 1.48\, U_l^{-0.66} OA^{1.21} d_0^{0.31} H_S^{-0.4}$ Turbulent Regime $\frac{N_{eff}}{N} = 0.103\, U_l^{-0.66} OA^{0.54} H_S^{-0.4}$	
Blass et al., 1977	Co-current	Hc=325 cm; Dc=14 cm; 4 perforated trays d_o=2, 4 mm; O.A.=1.1-36% H_s=53, 70 cm U_g=1.5-45 cm/s U_l=0.05-1 cm/s	$\frac{N_{eff}}{N} = 1.061\,(m/s)^{-0.19}\left(\frac{\overline{U}_g\ O.A.}{U_{ld}^2}\right)^{-0.19}$ $\frac{N_{eff}}{N} \leq 1$ $1.3\,(s/m) < \frac{U_g \varphi}{U_{ld}^2} \leq 10^3\,(s/m)$ $4.4\% < O.A. \leq 36\%$	- $N=N_{eff}$, if O.A. < 5 %, otherwise N_{eff}/N decreases with larger U_g, and smaller U_l - No significant effect of tray hole diameter - Formation of gas cushion underneath the trays, which increases with U_g.
Kitai et al., 1969	Co-current	Dc=7-14.5 cm; O.A.=2.4-9.8% 3 and 5 perforated trays d_o=2, 3, 5, 10 mm; H_s=20 cm U_g=1.83, 3.88, 4.15 cm/s U_l=0.05 cm/s		- Backmixing is a strong function of d_o. For d_o< 2 mm, complete column sectionalization - For d_o > 2 mm, only minor effect on liquid backmixing as U_g is increased. - No effect of tray spacing.

Table 5.2 Summary of the Available Published Work for Trayed Bubble Columns using the ADM (Continued)

Reference	Arrangement	Apparatus and Conditions	Correlation(s)	Findings
Chen et al., 1989	Co-current	Hc=120 cm Dc=5, 7.5, 15 cm 37 wire screen trays O.A.=64 %, H_S=5 cm U_g=0.2-8 cm/s U_l=0-3 cm/s	$D_L=0.0094\ U_g^{0.5}$	-D_L is independent of U_l. -D_L in TBC is three orders of magnitude smaller than in conventional BC -Each of the sections formed between trays behaves hydrodynamically in the same manner as a single BC
Houzelot et al., 1983	Co-current with baffles	Hc=400 cm; Dc=5 cm 4- 8 stages D_{baffle}=0.2 Dc	$D_L/ D_{L,o}$ = 0.25 for 4 stages $D_L/ D_{L,o}$ = 0.18 for 8 stages $D_L =0.054\ U_g^{0.47}$	
Magnussen et al., 1978	Counter-current without downcomers	H_c=400 cm, Dc=4,100 cm 2-16 sieve trays O.A.=20 %, d_o=1 cm	Plot of (Pe/Pe_o) versus number of trays, N_P For Dc=1m, Np=9 => N_S=8 (Pe/Pe_o)=8	-D_L decreases with an increase in number of trays -The effect of backmixing suppression due to the trays is stronger in columns with larger diameters

Table 5.2 Summary of the Available Published Work for Trayed Bubble Columns using the ADM (Continued)

Reference	Arrangement	Apparatus and Conditions	Correlation(s)	Findings
Ichikawa et al., 1967	Counter-current without downcomers	Hc=140, 188, 274 cm Dc=4.7, 9, 13.7, 19.8 cm Perforated trays d_o=1.5-20 mm, O.A.=10-43.45 %	$D_L=a\,(P/Dc)^{0.8}\,S^k\,Dc^{1.2}\,U_g^{\,b}$ $k=0.967\,U_g^{\,0.16}$ For U_g=1.4-7.1 cm/s a=1.9, and b=0.615 For U_g=7-18 cm/s a=0.64, and b=1.2	Effect on D_L of: -U_l, Negligible -U_g, Slight increase for values < 7.1 cm/s, else very sensitive, maximum at U_g=17.9 cm/s -d_o, No effect for >5 mm, large decrease when d_o=2.5 mm -O.A., $D_L \alpha$ O.A.^{k} -Dc, Increase -P, P α $(P/Dc)^{0.8}$

5.3.2 Discrete Models

Kastánec et al., 1992 divided the discrete models into two main groups according to the extent of the liquid backmixing of the unit to be modeled: single-stage combined models, and multistage (cascade) models.

A. Single Stage Models

In these types of models, the flow non-idealities are accounted for by combining the ideal models (CSTR, PFR, and others) with the following elements: recycle, bypass, cross-flow streams, and stagnant volumes. Many different combinations are possible and the real reactor configuration should lead the model development strategy. For instance, the model described by *Cholette and Cloutie, 1959* can be used to describe the backmixing of the single stages in sectionalized bubble column reactors. This model introduces a bypass stream and a dead volume to the perfectly mixed tank in order to simulate channeling and stagnancy, respectively, in the system.

B. Multistage Models

The axial mixing in real reactors is represented by a combination of individual interconnected stages of equal or different volumes. The connection between stages depends on the real reactor flow configuration. In addition to the main flow stream, we could have bypass, recycle streams and/or dead volumes to simulate the flow non-idealities. The applicability of these schemes ranges from the perfectly mixed to the plug flow situations. In the most general multistage models, single stages are considered to be perfectly mixed, although further non-idealities can be introduced to explain deviations from complete mixing behavior. For instance, in the Multistage Dispersion Model described by *Nishiwaki and Kato, 1972*, the Axial Dispersion Model expresses the longitudinal mixing of the liquid in each of the stages. Hence, in addition to the total number of tanks and the backmixing flow between them, the Peclet number associated

with each of the individual stages needs to be defined as well. The number of plausible model combinations is unlimited. However, one should always keep in mind that the advantages of any model are measured not only by how accurately it can describe the reactor behavior, but also by how specifically the model parameters can be experimentally estimated. Thus, the utilization of models containing more than two parameters should be avoided unless it is strictly necessary. The following is a survey of some of the multistage models that can be used to describe the overall liquid phase mixing in sectionalized bubble columns.

B.1 The N-CSTR in Series Model

This is the simplest stagewise model. It consists of a series of N equal and completely mixed stages interconnected by the unidirectional main flow stream. Since all the tanks have the same volume, the average residence time in each of them is equal to the total average residence time divided by the number of tanks.

The expressions for the model dimensional and dimensionless exit age density functions (Equations 5.6 and 5.7, respectively), as well as the dimensionless variance (Equation 5.8) are found in most of the classic chemical reaction engineering textbooks (*Levenspiel, 1962*).

$$E(t) = \left(\frac{N}{\bar{t}}\right)^N \frac{t^{N-1}}{(N-1)!} e^{-N t/\bar{t}} \tag{5.6}$$

$$E_D(\theta) = \frac{N^N}{(N-1)!}\, \theta^{N-1}\, e^{-N\theta}, \quad \theta = \frac{t}{\bar{t}} \tag{5.7}$$

$$\sigma_D^2 = \frac{1}{N} \qquad 0 < \sigma_D^2 \leq 1 \tag{5.8}$$

The model allows for straightforward parameter estimation. The total number of tanks is the inverse of the experimental dimensionless variance s_D^2. Equations 5.6 and 5.7 are only defined for integer values of *N*, and hence intermediate degrees of backmixing between two given integer number of tanks are not permitted. One can overcome this situation upon the realization that *G(N)=(N-1)!*, where Γ is the gamma function (Equation 5.9). Thus, Equation 5.7 can be rewritten into Equation 5.10, which is also defined for non-integer and greater than zero values of *N*. The above extension of the N-CSTR in series model for non-integer values of *N* is called the Gamma Function Model *Buffham and Gibilaro, 1968.*

$$\Gamma(N) = \int_0^\infty \theta^{N-1} e^{-\theta} d\theta, \quad N > 0 \tag{5.9}$$

$$E(\theta) = \frac{N^N}{\Gamma(N)}\ \theta^{N-1}\, e^{-N\theta} \tag{5.10}$$

In fact, this modification of the tanks in series model allows for a dimensionless variance in the range [0, infinite]. However when formulated in such a way, the model loses its physical interpretation and *N* becomes just a fitting parameter.

Some authors have used the model to evaluate the overall axial liquid backmixing in co-current trayed bubble columns (Table 5.3). When the number of physical stages differs from the calculated number, as estimated from the model, the ratio of the real to the effective (estimated) number of stages has been introduced to quantify the disagreement. *Blass et al., 1977* used this approach to correlate this ratio with the reactor's operating conditions and the tray open area. They found that complete sectionalization, that is $N=N_{eff}$, always holds when the tray open area is less than 4.4% in all the interval of superficial gas and liquid velocities. Moreover, when they increased the tray open area above 4.4% and up to 36%, then they observed that by increasing the gas

velocity and reducing the liquid velocity, the relation N_{eff}/N decreased. It was postulated that the backmixing of liquid from stage to stage, and not an insufficient mixing within the stage, was the responsible. The reason they offered to explain this phenomenon was that the formation of cushions of gas underneath the trays sets a positive pressure gradient above the trays that causes liquid to drop back to the lower stage. However if the superficial gas velocity is too high, then the upward momentum of gas will eventually stop the liquid backflow through the orifices. Nevertheless, they never experimentally verified this upper limit.

Table 5.3 Summary of the Available Published Work for Trayed Bubble Columns using the N-CSTR in Series Model

Reference	Arrangement	Apparatus and Conditions	Correlation(s)	Findings
Vinaya, 1995	Counter-current with downcomers	Hc=180,100 m; Dc=9.8, 15.4 cm Perforated trays d_o=3; 5, 10, 12 mm; O.A.=9.5, 10, 38.7, 52 %; H_S=5, 85 cm U_g=1.2-11 cm/s U_l=0-2.12 cm/s	Bubbly Regime $\frac{N_{eff}}{N} = 1.48\, U_l^{-0.66} OA^{1.21} d_0^{0.31} H_S^{-0.4}$ Turbulent Regime $\frac{N_{eff}}{N} = 0.103\, U_l^{-0.66} OA^{0.54} H_S^{-0.4}$	
Blass et al., 1977	Co-current	Hc=325 cm; Dc=14 cm; 4 perforated trays d_o=2, 4 mm; O.A.=1.1-36% H_s=53, 70 cm U_g=1.5-45 cm/s U_l=0.05-1 cm/s	$\frac{N_{eff}}{N} = 1.061\,(m/s)^{-0.19}\left(\frac{\overline{U}_g\ O.A.}{U_{ld}^2}\right)^{-0.19}$ $\frac{N_{eff}}{N} \leq 1$ $1.3\,(s/m) < \frac{U_g \varphi}{U_{ld}^2} \leq 10^{3}\,(s/m)$ $4.4\% < O.A. \leq 36\%$	- $N=N_{eff}$, if O.A. < 5 %, otherwise N_{eff}/N decreases with larger U_g, and smaller U_l - No significant effect of tray hole diameter - Formation of gas cushion underneath the trays, which increases with U_g.
Kitai et al., 1969	Co-current	Dc=7-14.5 cm; O.A.=2.4-9.8% 3 and 5 perforated trays d_o=2, 3, 5, 10 mm; H_s=20 cm U_g=1.83, 3.88, 4.15 cm/s U_l=0.05 cm/s		- Backmixing is a strong function of d_o. For d_o< 2 mm, complete column sectionalization - For d_o > 2 mm, only minor effect on liquid backmixing as U_g is increased. - No effect of tray spacing.

B.2 The N-CSTR in Series with Backmixing Model

Although the N-CSTR in Series Model can predict the spreading of a tracer's exit age density curve as the number of tanks increases, it explains liquid axial mixing in a very particular way. Since the tanks are perfectly mixed, there is an intense short-range mixing occurring when the liquid from one stage enters the next. Hence, no fraction of liquid that has moved to a position downstream of a given stage can ever come back. This is an unrealistic physical situation, especially when it is used to model trayed bubble columns with trays of large open areas and hole diameters. The model can be easily extended to account for liquid dropping back from downstream locations by introducing liquid backflow streams into the conventional N-CSTR in Series Model configuration (Figure 5.1). Thus, in addition to the total number of stages, *N*, a new model parameter named Backmixing Coefficient, *k*, is introduced. This parameter, which is defined as the ratio of the liquid backflow rate to the net liquid flow rate in the main direction of flow, can take values between zero (no liquid backflow) to infinite (batch liquid). Therefore, the model can describe the whole spectrum of axial mixing situations from plug flow (N=infinite, and k=0) to total mixed flow (k=infinite).

The model's system of ordinary differential equations (Equations 5.11 to 5.13) is easily derived from the material balance applied to an injected tracer in each of the stages. The tracer is injected as an ideal pulse (Dirac-δ function) at the inlet of the first stage. There are a total of N equations, each one corresponding to a single stage, and different types of equations for the inlet (first), outlet (last), and intermediate tanks (*Buffham, 1968*).

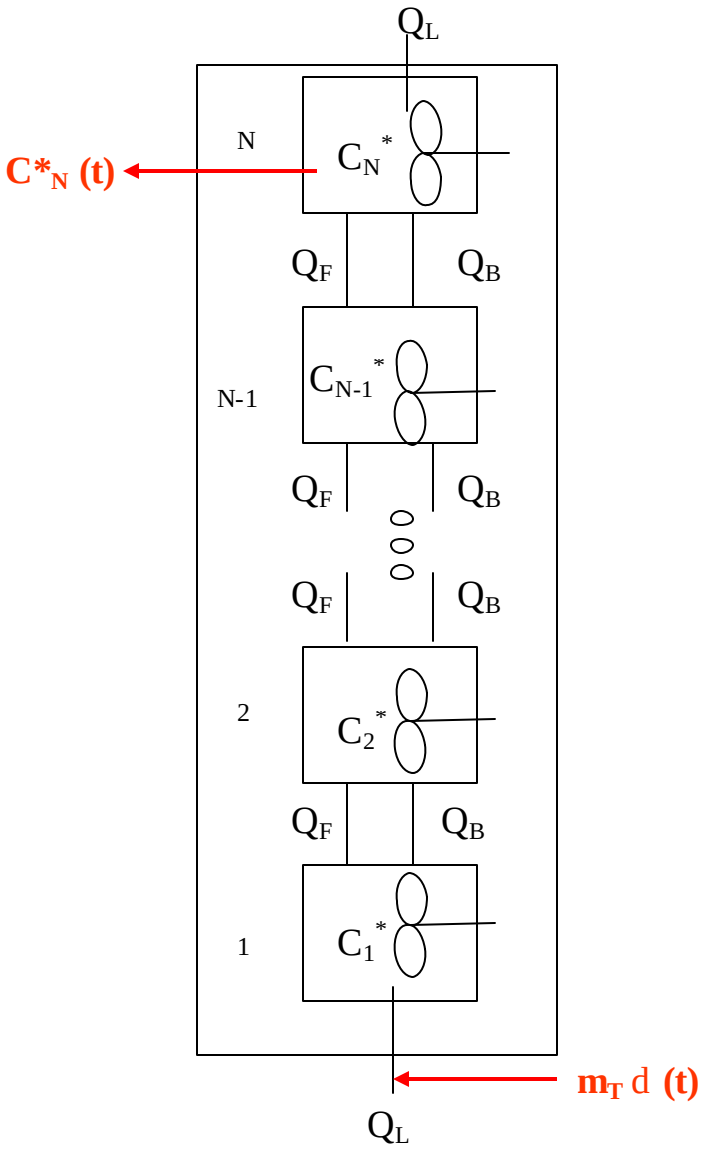

Figure 5.1 Schematic Diagram of the N-CSTR in Series with Backmixing Model.

$$\frac{dC_1^*}{dq} = k\,C_2^* - (1+k)\;C_1^* \qquad \text{First Tank} \qquad (5.11)$$

$$\frac{dC_i^*}{dq} = (1+k)\;C_{i-1}^* - (1+2\,k)\,C_i^* + k\,C_{i+1}^* \qquad \text{Intermediate Tank, i =2 to N-1} \qquad (5.12)$$

$$\frac{dC_N^*}{dq} = (1+k)\;C_{N-1}^* - (1+k)\;C_N^* \qquad \text{Last Tank} \qquad (5.13)$$

$$\theta = \frac{t}{\bar{t}} = \frac{L\,t}{V_i\,N} \quad C_i^* = \frac{C_i V_i\,N}{m_t} \quad k = \frac{Q_B}{Q_L}$$

Initial Conditions:

$$\text{At } \theta = 0 \quad C_1^* = N,\; C_2^* = C_3^* = ... = C_i^* = ... = C_N^* = 0$$

Although the above system of differential equations is linear in nature, its time domain analytical solution is quite involved. In fact, it is much easier to numerically solve the resultant system of equations for a given set of the model parameters *N*, and *k*.

The solution will give us the dimensionless transient concentrations of the tracer in each of the stages ($C_1^*, C_2^*, \ldots, C_{N-1}^*, C_N^*$). *Roemer and Durbin, 1967* transformed the equations into the Laplace domain, and by using the Method of the Moments they derived general expressions for the mean residence time q_n (Equation 5.14) and for the dimensionless variance $\sigma_{D,n}^2$ (Equation 5.15) in the n^{th} tank of the series of N tanks.

$$\theta_n = \frac{1}{N}\left[n + k - (1+k)\,p^{\gamma}\right] \qquad (5.14)$$

$$\sigma_{D,n}^2 = \left(\frac{1+k}{N^2}\right)\left[(n + k(1+p) + k(1+2\,p^N) - 4(\gamma+k)p^{\gamma} - (1+k)p^{2\gamma}\right] \qquad (5.15)$$

$$p = \frac{k}{(1+k)}$$

$$g = N - n + 1$$

The average residence time (Equation 5.16) and the dimensionless variance (Equation 5.17) at the last stage of the series can be written by substituting $n=N$, and $g=1$ into Equations 5.14 and 5.15.

$$\theta = 1 \tag{5.16}$$

$$s_D^2 = \frac{1+2k}{N} - \frac{2k(1+k)(1-p^N)}{N^2} \tag{5.17}$$

Kats et al., 1967 performed an extensive study of the liquid longitudinal mixing in a co-current sparged reactor sectionalized with sieve trays. The N-CSTR in Series with Backmixing model was used to interpret their experimental tracer experiments. The authors conducted their experiments in two multi-stage bubble columns of different heights and diameters with a large number of different tray configurations: Column #1 ($H_{c,1}$ =2.05 m; $D_{c,1}$=0.95 m; N=5 and 10; O.A.=2.2-26.5%;d_o=0.0015-0.008 m), and Column #2 ($H_{c,2}$ =6.00 m; $D_{c,2}$=0.40 m; N=10; O.A.=0.68%-6% ; d_o=0.0032-0.008 m)

Based on the velocity of the gas phase, the researchers distinguished four regions in which the nature of the longitudinal liquid mixing was found to be different. In the first region (U_g=0.0001–1 m/s), the liquid backmixing diminishes with increasing gas velocities. The diffusional nature of the mixing in this regime can explain the observations. The second region is characterized by the lack of influence of the superficial gas velocity on the liquid axial mixing as the stages can be considered perfectly mixed. They developed the following empirical relation for the backmixing coefficient in this region:

$$k = 7\,10^{3}\,U_{l,h}^{-1.2} d_0^{2.12}\,\delta^{0.31}\left(\frac{H_c}{D_c}\right)^{-0.43} \tag{5.18}$$

Here $U_{l,,h}$ is the liquid velocity in the tray holes; U_l is the superficial liquid velocity (based on the column cross section); d_o is the tray hole diameter; δ is the tray thickness; H_c is the column height; and Dc is the column diameter. In all the equations, the variables have to be used in S.I. units.

$U_{l,h}$ and U_l are related by the following equation:

$$U_{l,h} = \left(\frac{U_l}{3600\ O.A.}\right) \quad U_l\text{=0.00022-0.11 m/s} \tag{5.19}$$

The transition between regions 1 and 2 depends upon the superficial gas velocity based on the column cross sectional area. The third region starts at gas velocities W_o (based on the holes of the trays) between 3 and 10 m/s, conditions at which a sharp reduction in the liquid mixing as the gas velocity increases is observed. The following empirical correlation was proposed in this region:

$$k = 380\,U_{l,h}^{-0.93} d_o\,\delta^{0.64}\,H_c^{0.67}\log\left(\frac{\overline{W}_o}{W_o}\right) \tag{5.20}$$

$$\overline{W}_0 = 3.8\left(\frac{D_c}{d_o}\right)^{0.25} \quad U_l\text{=0.00022-0.00330 m/s} \tag{5.21}$$

By setting Equations 5.18 and 5.20 equal, the authors estimated the gas velocity at which the transition from region 2 to 3 occurs, W_0^T, as follows:

$$\log(W_0^T) = \log(\overline{W}_0) - 18.4 U_{l,h}^{-0.27} d_0^{1.12} d^{-0.33} h^{-1.1} D_c^{0.43} \tag{5.22}$$

Finally, the fourth region starts at gas velocities, W_o > 7-13 m/s. It is characterized by a total absence of backflow between stages (k=0). In this region, the N-CSTR in series model always predicts a total number of stages equal to the actual physical number in the column.

Schugerl et al., 1977 used the model to interpret their experimental results obtained in a 6-stage co-current trayed bubble column. In the range of the covered gas superficial velocities (U_g=1-10 cm/s), they found values for the backmixing coefficient *k* between 2 and 5.

B.3 Multistage with Partially Mixed Stages Models

Until this point, all the multistage models that have been described assume that the stages are perfectly mixed. However, this may not be the case in real reactor systems in which the geometry of the stages and/or trays can enhance the formation of fast liquid flowing regions or stagnancy. For instance, in counter-current columns with trays with downcomers, an important fraction of the liquid that enters the stage bypasses it through the downcomers. *Reháková et al., 1967* postulated that the N-CSTR with Backmixing Model can be modified in such a way that each of the tanks can be subdivided into a number of S perfectly mixed vessels with backmixing between them. In order to reduce the total number of parameters, they assumed that the number of vessels per stage and the backflow ratio between vessels *b* were the same for all the stages. It was also assumed that the total number of stages *N* is equal to N_t+1, where N_t is the total number of physical trays used. Hence, this new model has the following three parameters: number of vessels *S*, backflow ratio between stages *k*, and backflow ratio between vessels *b*. As a rule of thumb for parameter model evaluation from experimental data, they suggested to construct a chart from which the abscissa for the maximum point of the exit age distribution curve is given for different values of *S*, *b*, and *k*. By doing so, one can read the model parameters corresponding to a given experimental curve. The assumption of equal backflow ratio between vessels in a stage is more than questionable in real reactor

systems because of the unpredictable effect of the inlet and outlet stages that make the stages close to them behave differently than the rest. However, the main drawback of the model is the non-trivial model parameter identification, in which different combinations of the parameters may yield the same system's response.

Chiang et al., 1975 extended the Cholette-Cloutier model (*Cholette and Cloutier, 1959*) to multistage systems. In this model, in addition to the main flow stream that interconnects the single stages, there are bypass streams and a dead volume region in each of the stages. The dead volume region, which carries a fraction of the total volume of the stage, does not exchange any mass with the flowing liquid and it is therefore an unutilized part of the stage. The model formulated in this way contains three floating parameters, number of tanks, fraction of the total flow rate that it is bypassed, and fraction of the total stage volume that is occupied by the dead region. *Raghuraman et al., 1972* decided to extend the model by including an extra parameter to account for the exchange of mass between the active and dead regions. The new model parameter formulated in this way is defined as the fraction of the flow entering the stage that exchanges mass with the dead region. The authors used the model to successfully interpret the experimental residence time distribution of glass beads in a multistage fluidized bed.

5.3.3 Continuous and Discrete Combined Models: The Dispersion-Backflow Model (DBM)

DBM combines a continuous model (ADM) to describe the liquid axial dispersion within individual stages with a stagewise model (N-CSTR in Series with Backmixing). *Nishiwaki et al., 1972* have reported that this model is well suited for the description of the liquid mixing in co-current trayed bubble columns. The overall liquid dispersion is formulated as the summation of all the resistances to dispersion, both the ones due to the single stages ($Pe_{L,i}$) and those due to the backmixing between the trays ($Pe_{L,b}$). The following expression for the overall extent of liquid phase mixing can be written:

$$Pe_{L,o} = \sum_{i=1}^{N} Pe_{L,i} + Pe_{L,b} \tag{5.23}$$

$$Pe_{L,b} = \left(\frac{N}{2\,(N-1)^2} + \frac{k}{N} \right)^{-1} \tag{5.24}$$

Here $Pe_{L,o}=U_L\,L/D_{L,o}$ is the overall Peclet number for the multistage system, $Pe_{L,i}= U_L\,\Delta l_i/D_{L,i}$ is the Peclet number for the i^{th} stage, and $Pe_{L,b}$ quantifies the extent of backflow between trays. The relationship of equivalence between the N-CSTR in Series with Backmixing Model and the ADM is used to evaluate $Pe_{L,\,b}$ through Equation 5.24, which was derived by *Miyauchi, 1960.*

Sekizawa et al., 1975 used the DBM model to correlate their liquid mixing experimental data obtained in three different co-current trayed bubble columns. They used the Thermal Tracer Technique, where heat is supplied at a constant rate to the liquid at the top of the column by a heater. Once the steady state is reached, the axial temperature profile is measured by thermocouples. From the solution of the steady state heat transfer equation, both the backflow ratio and the thermal conductivity coefficient in each of the stages can be estimated. The values of the latter were found to agree well with the axial dispersion coefficients. The dimensions of the columns and the trays that they used in this work are as follows: H_c=1, and 1.2 m; D_c=0.05, 0.1, and 0.02 m; N=3, 5, 6, and 10; H_s =0.1, 0.2, and 0.4 m; O.A.=0.7-0.202; d_o=0.22-2.0 cm; and δ=0.003, 0.005, and 0.01 m.

The authors presented correlations for the axial dispersion coefficient within individual stages (Equation 5.25), as well as for the backmixing coefficient between stages (Equation 5.26).

$$\frac{D_{Li}}{D_L} = \frac{U_g^{0.1}}{(1+0.5(D_C/L_i)^{0.2})} \tag{5.25}$$

$$k = \frac{7.15\ U_g^{0.1}\ O.A.}{1+0.01\ (U_g/O.A.)}\left(\frac{1}{U_l} - \frac{0.552}{U_l^{0.85} O.A.^{0.2}}\right)\left(\frac{1.48}{\exp[(-1.5/d_o)(\mu_L^{0.5}+0.01\delta^{0.2}/d_0)]}\right) \tag{5.26}$$

Although, the DBM constitutes an improvement over the N-CSTR in Series with Backmixing Model, since it characterizes the extent of mixing inside the stages, the practical applicability of the model is more than questionable due to the large number of model parameters that have to be experimentally determined.

Chapter 6 Tracer Studies Experimental Setup

6.1 Tracer Experimental Setup

The same cold flow unit used for the overall gas hold up measurements has been used for the tracer experiments with minor modifications (Figure 6.1).

An external loop fabricated in PVC (3.8 cm I.D.) was attached to the top section of the column at the gas-liquid disengagement plane (Figure 6.2). Transparent PVC was chosen so that the level of the liquid inside of the straight section of the loop could always be monitored. The purpose of this loop is to have an enhanced liquid mixing device in which the liquid mixing cup concentration could be measured on-line by conductivity probes. It was designed to have enough clearance in its base where the probe could be placed, and also to minimize the liquid backpressure in the column. In fact, the latter could not be totally eliminated and as a result the total liquid-gas height was increased by a few centimeters as compared to the column without the loop. The end of the loop was connected to a transparent plastic hose that took the outlet water stream directly to the room sewer. The conductivity probe was mounted in the base of the loop through the T connector using teflon Swagelok ferrules with the purpose of being able to move the probe up and down to make sure that it was always inside the liquid stream (Figure 6.2).

In the lower part of the column, the liquid inlet piping was redesigned in such a way that it allowed for a fast drainage of the column. At the same time, several service ports were added for injection and detection purposes (Figure 6.3). The inlet conductivity probe, located 10 cm upstream from the column plenum, was mounted so that the tip of the probe remained in the center of the inlet pipe, 1.27 cm away from its wall. The injection port was located in the horizontal pipe, 84 cm upstream from the plenum. It

consisted of a T female connector, with a 0.95 cm Swagelok male adaptor screwed to it. A 1.27 cm in diameter septa plug was placed in between them in order to seal the connection. The special properties of this material allowed it to be perforated through with a sharp object and then sealed off as the object was removed. The tracer was introduced into the column by injection using a 10 ml glass syringe with a 5 cm long and 17 gauge needle. The large diameter of the needle was necessary for a fast evacuation of the liquid in the syringe.

The conductivity probes used in this work were obtained from Microelectrodes Inc. (MI-900 Series, dimensions: 0.635 cm x 30.5 cm). They consisted of two electrodes coated in black platinum, approximately 3 mm apart, and encased in plastic tubing. The probes were properly calibrated by measuring their response to solutions of tracer of known concentration (Appendix A.2). The signal from the electrodes was transmitted to conductance meters (YSI Model 35), which provided a reading in units of conductance ($ohms^{-1}$). The meters were interfaced to a Pentium computer through a Data Acquisition Board (AT-MIO-16E-10 from National Instruments Inc.). This configuration allowed for a reliable on-line measurement and recording of the conductivity probes signals at a sampling frequency of 10 Hz (Appendix A.3). This value is three to four orders of magnitude larger than the tracer wash-out curves at the experimental conditions covered in this work (10^{-3}-10^{-2} Hz).

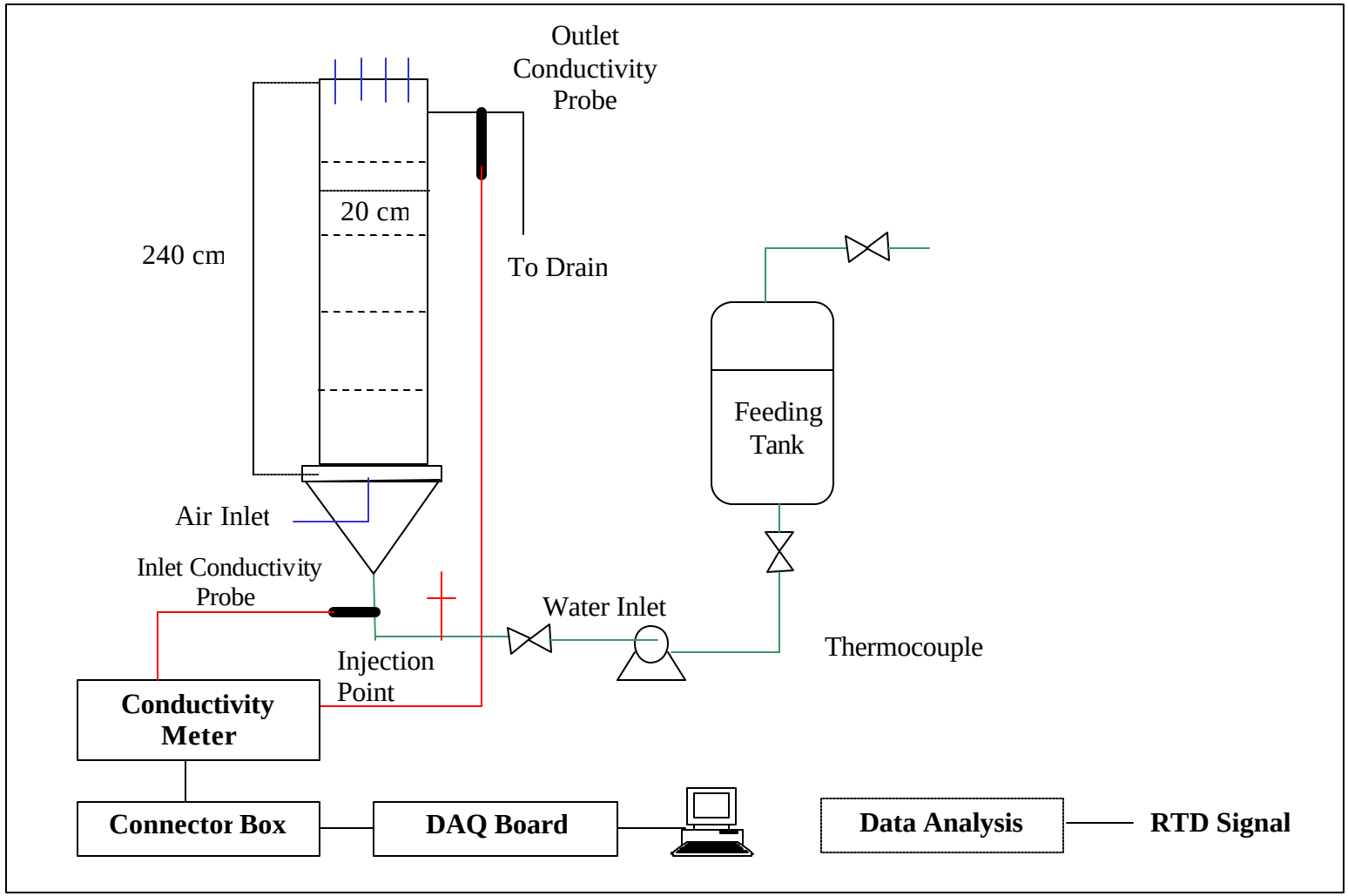

Figure 6.1 Schematic Diagram of the Trayed Bubble Column with the Tracer Experimental Setup.

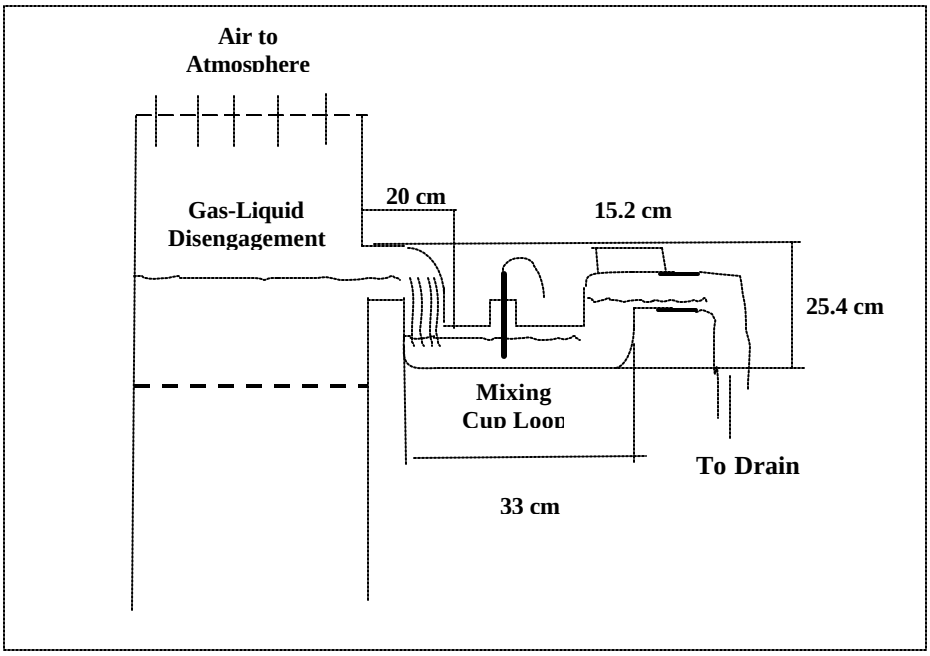

Figure 6.2 Schematic Diagram of the Mixing Cup Loop Located Downstream of the Column's Liquid Outlet.

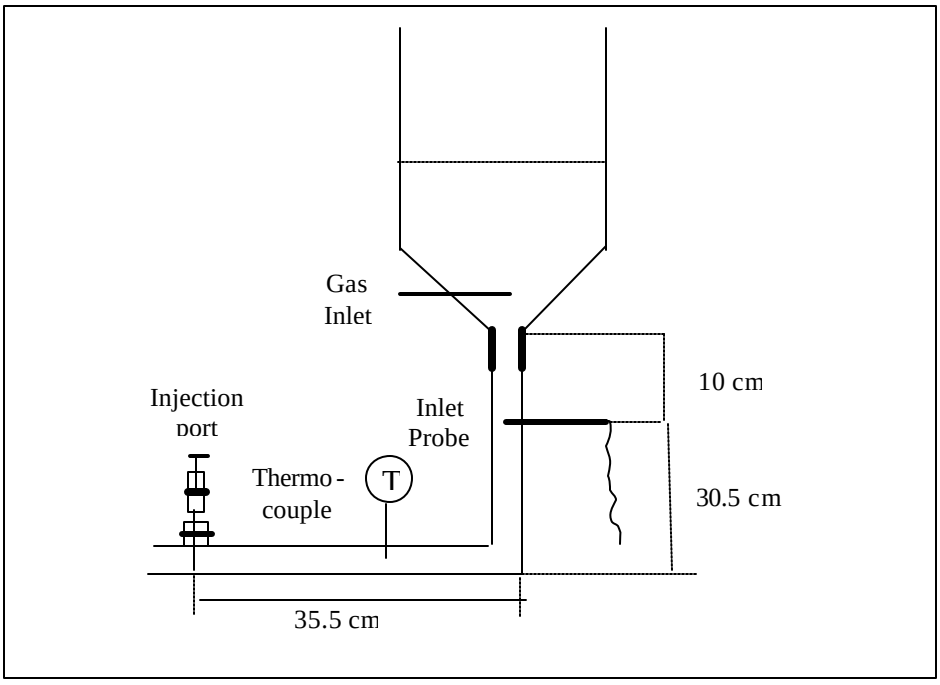

Figure 6.3 Schematic Diagram of the Injection System Located Upstream of the Column's Liquid Inlet.

6.2 Liquid Phase Tracer

The Conductivity Method has been applied to determine the Exit Age Density function of a pulse-injected liquid tracer. A suitable tracer has to have the following properties:

1. Be non-volatile and totally miscible with the liquid phase (water in this case).

2. The conductivity of the tracer in solution has to be well above of that of the solvent, so that the combined conductivity (tracer + solvent) can be readily distinguished from the background conductivity (solvent).

3. There should be a linear relationship between the tracer concentration and its corresponding conductivity in a wide range of concentrations. This is necessary to make sure that the tracer's mass balance is always satisfied.

Based on the above considerations Potassium Chloride (KCl) was chosen. When a molecule of KCl gets dissolved into a polar solvent such as water, it gets dissociated into its constitutive ions K^+ and Cl^-, therefore significantly increasing the liquid medium conductivity. The tracer has a large region of linearity between total amount of salt dissolved and medium conductivity achieved.

By trial and error, it was found that 10 ml of 0.2 gm KCl produces the best possible signal. As it was stated in Section 6.1, with the selected syringe the 10 ml can be injected into the system in less than a second.

6.3 Operating Conditions

Due to the time constrain of this research work, it was decided to focus only on the effect of the gas and liquid superficial velocities and the tray geometry; and leave the

study of the effect of other parameters such as the gas sparger and the liquid phase for future work. The air-water system and the single nozzle sparger were selected to run the column. In this way, the extensive experimental knowledge acquired in Part I using this system can be complemented with an improved understanding of the liquid mixing.

The following range of superficial gas and liquid velocities in the single stage and multistage bubble columns (with the three available tray designs) was attempted in this study to cover both the Bubbly and Churn-Turbulent flow regimes: Superficial Liquid Velocities, U_l= 0.5, 1.0, and 1.5 cm/s; Superficial Gas Velocities, U_g= 1, 4, 8, 12, 16, and 20 cm/s

In addition to those conditions, selective runs with no gas were executed as an exercise to see how the gas changes the mixing of the liquid as compared to the single-phase flow only.

However, several problems were encountered that made the collection of data at every single condition initially intended not viable. For instance, it was not possible to run the column at U_l=1.5 cm/s and at the highest gas flow rates (U_g >12 cm/s) since the backpressure created by the mixing cup loop was so intense that it in fact flooded the column.

Some experiments had to be discarded due to problems with the tracer injection, data acquisition system, and/or baseline-tail displacement. All these factors made the collection process very tedious and, thus only one run per set of experimental conditions was performed.

The lack of repetition at every single condition kept us from knowing about the associated experimental variability at that given condition. However, a very careful and meticulous procedure, described in Appendix A.4, was followed in order to minimize the human component of the experimental error. Moreover, the associated experimental

standard error was estimated by repeating the tracer injection experiments eight times at selected conditions (Appendix A.9). From these repeated experiments, the calculated standard deviations of the parameters that one is interested in (for instance, the first and second moments of the E-curve) were assumed to be the standard deviation associated at any other given set of experimental conditions.

Chapter 7 Data Analysis and Experimental Results

7.1 Theoretical Background

The response of a linear process y(t) to a stimulus function x(t) is determined by the structure of the flow in the system. The stimulus and its response are mutually related by the convolution integral:

$$y(t) = \int_0^t E(t-t)\,x(t)\,dt = \int_0^t E(t)\,x(t-t)\,dt \qquad (7.1)$$

Here E (τ) is the system's Probability Density Function (PDF), also known as Exit Age Density function, or E-curve. Since it is a probability density function, it can only take positive values between 0 and 1 and the area under it must be unity.

If the stimulus function is the impulse or δ−Dirac function, which is defined as δ (t-a)=0 for t≠a, and δ(t-a)=∞ for t=a, then by substituting it into the convolution integral (7.1) we can write:

$$y(t) = \int_0^t E(t)\,d(t-t)\,dt = E(t) \qquad (7.2)$$

Thus, the measured response to the introduced stimulus is directly the system's Exit Age Density Function *E (t).*

Certain considerations must be observed in order to assure that the experimental system's response can be interpreted in terms of the tracer's exit age density function:
1. The system is closed and thus transport in and out its boundaries is only by convection,

and no diffusion is allowed; 2. The mixing cup (flow averaged) concentration must be monitored at the exit.

The conductivity probes used in this work detect point measurements. Therefore, the following precautions have been taken to assure that the response registered by the probes can accurately represent the tracer's exit age density function:

1. The tracer was injected in less than a second at the center of the liquid inlet pipe, which is 2.54 cm in diameter. At the liquid flow rates selected in this work (2.25-7.5 GPM), the flow regime in the inlet pipe was turbulent (Re=71394-481910). This fact assured the validity of the assumption that the tracer was radially mixed before it entered the column. In fact, at the lowest superficial liquid velocity, and assuming that the injection time is around one second (Δt ~1 second), the length of the "cloud" of tracer was around $\Delta l = U_l \Delta t$ ~ 70 cm, which was approximately equal to the length of the pipes between the tracer injection location and the reactor inlet. Therefore, the tracer traveled for approximately one second as a plug of 70 cm of length before it entered the reactor. The quality of the approximation to an ideal input signal depends on the relative ratio of the injection time to the system mean residence time, $\Delta t / \bar{t}$. The smaller the ratio, the better the approximation. *Prenosil et al., 1968* claimed that for tracer experiments in bubble columns, as long as this value is smaller than 0.05 then the approximation to an ideal input signal is acceptable. As it is shown in Appendix A.5, the above criterion is always fulfilled in this work.

2. The Mixing Cup Loop installed after the column outlet enhanced the liquid mixing. Therefore, the conductivity probe approximately measured the mixing cup concentration at this location.

The impulse response *E(t)* is obtained upon the normalization of the tracer response *R(t).*

$$E(t) = \frac{C(t)}{\int_0^\infty C(t)\,dt} = \frac{R(t)}{\int_0^\infty R(t)\,dt} \tag{7.3}$$

We can use the second equality only when there is a linear relationship between the tracer concentration and the measured response signal.

The integral of the denominator in Equation 7.3 can be evaluated as follows:

$$\int_0^\infty C(t)\,dt = m_T / Q \tag{7.4}$$

Where Q is the carrier plus tracer flow rate, and m_T is the total mass of tracer introduced into the system.

Similarly, the principle of mass conservation requires the total area under the E-curve to be equal to one. Thus:

$$1 = \int_0^\infty E(t)\,dt = \frac{Q}{m_T}\int_0^\infty C(t)\,dt \tag{7.5}$$

$$m_T = Q\int_0^\infty C(t)\,dt \tag{7.6}$$

Equation 7.5 can be used to check the mass balance for a given tracer injection experiment.

The moments of the E-curve can be calculated as follows:

$$m_1 = \int_0^\infty t\,E(t)\,dt \tag{7.7}$$

$$m_2 = \int_0^\infty t^2\,E(t)\,dt \tag{7.8}$$

$$s^2 = \int_0^\infty (t - m_1)^2\,E(t)\,dt = m_2 - m_1^2 \tag{7.9}$$

For a system with closed boundaries, the first moment m_1 of the E-curve is equal to the mean residence time $\bar{t}$, defined as the column volume times liquid hold up divided by the liquid flow rate. The variance of the E-curve (7.8) measures the dispersion of the E-curve around the mean residence time.

It is very convenient to non-dimensionalize the E-curves by its residence time. Thus, we can write a Dimensionless Exit Age Density Function E_D, and a dimensionless variance s^2_D as follows:

$$\theta_i = \frac{t_i}{\bar{t}};\ E_D(\theta_i) = E(t_i)\bar{t} \tag{7.10}$$

$$\sigma_D^2 = \int_0^{\theta_{final}} E_D(\theta_i)\theta_i^{\,2} d\theta - 1 = \frac{\sigma^2}{\bar{t}^2} \tag{7.11}$$

The dimensionless variance quantifies the degree of the system's internal backmixing. For non-pathological flows, s^2_D varies between 0 (for plug flow) and 1 (for a perfectly mixed tank). Pathological flows, like bypass and stagnancy are present in systems whose s^2_D is greater than 1.

7.2 Data Analysis Procedure

The data analysis followed in this work can be summarized into the next steps:

1. From the tracer inlet response curve, the time elapsed between the initiation of the acquisition system and the detection of the tracer by the inlet probe is estimated.

2. The output tracer response is filtered using the filtering algorithm developed by *Gupta et al., 2000*. The tolerance and cutoff frequencies of the filter are chosen so that both the unbiased (white noise) and the biased (due to bubble passage) components of the

signal noise are removed without oversmoothing the signal. In general, a third order Butterworth filter with a cutoff frequency in the range of 0.02-0.1 Hz and tolerances no larger than 10^{-3} worked well (see Appendix A.6).

3. Over the resultant filtered signal, the time coordinate is rescaled so that the section of the base line prior to the injection is removed. If needed, the tail and the base line are leveled off by the Base Line Drift Technique illustrated in Appendix A.7.

4. The calibration curve is used to convert the outlet response curve from conductance units (volts) to concentration units (g KCl/ml).

5. The mass balance is checked by integrating the area under the curve, and by the subsequent use of Equation 7.5.

6. The E-curve is obtained upon the normalization of the concentration-time series by the integrated area under the curve. The first and second moments of the distribution are evaluated from Equations 7.6 and 7.7. The Exit Age Density Function is rescaled by the first moment (Equation 7.9) and the corresponding dimensionless variance is obtained (Equation 7.10).

In this form, the E-curve is expressed in dimensionless units and therefore it can be compared directly with the model curves for fitting purposes.

7.3 Experimental Response Curves

The objective of this section is to present some of the experimental tracer response curves obtained in this work and to qualitatively discuss the effect of tray geometry and operating conditions on the shape and magnitude of the response curves to assess the extent of the liquid axial backmixing in the column.

Figure 7.1 shows the tracer output response curves obtained in both trayed and single stage bubble columns at U_l= 1 cm/s and U_g = 1 cm/s. The reduction of the liquid mixing in the trayed bubble column as compared to the column without trays is clear from the figure. The experimental response signal for the column without trays is closer to that of a CSTR than the multistage column, since the former shows a wider distribution of residence times with the peak of the curve appearing earlier. However, as it can be seen from the plot, the effect of the different studied trays cannot be accurately evaluated without further quantitative analysis of the tracer response signals. Therefore, no conclusions can be drawn until the calculation and comparison of their respective first moments and variances are performed.

Figures 7.2 and 7.3 show the effect of variation of superficial liquid velocity (U_l= 0.5, 1, 1.5 cm/s) at constant superficial gas velocity (U_g = 8 cm/s) in the column with tray type #1 (d_o=1.74 cm, and 10.2 % O.A.) and without trays, respectively. The observed shift of the curves maximum towards the right, along with the increase in their width, as the superficial liquid velocity is reduced, is a clear indication of the growing importance of the diffusional effects over the convectional transport in the column. Note that in Figures 7.2 and 7.3, the E-curves have been left in their dimensional form since the normalization by their respective first moments would have packed them very close together, and it would have made the visual interpretation of the effect of the superficial liquid velocity more difficult.

In Figure 7.4, the effect of superficial gas velocity on the tracer response curve at U_l = 0.5 cm/s is shown. A clear trend can be recognized in the figure, in which the overall liquid mixing increases with an increase in the gas velocity. This trend is also a function of the superficial liquid velocity and it can be seen that at U_l=0.5 cm/s, the dependence of the liquid axial mixing on U_g is stronger than at U_l=1.5 cm/s. Further, in Figure 7.4 it is of special interest to compare the E-curves for the case in which no gas is passed through (U_g=0 cm/s) with the two-phase flow conditions. Even at gas velocities as low as 2 cm/s,

the presence of the gas is strongly felt and the liquid phase mixing is significantly increased.

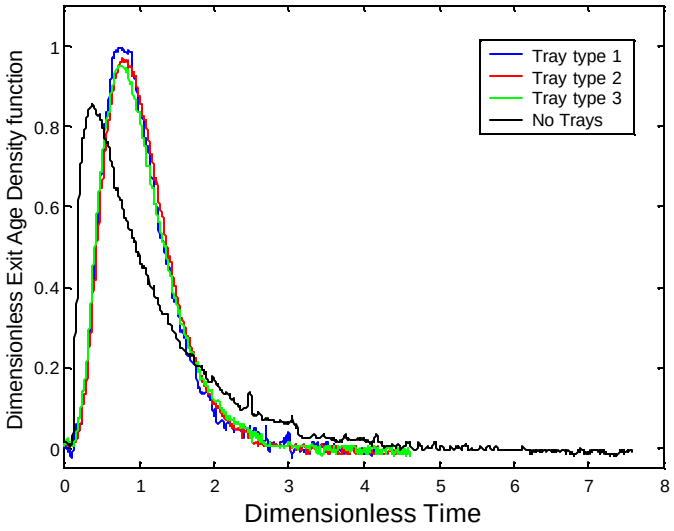

Figure 7.1 Effect of the Trays on the Experimental Dimensionless E-Curve in Trayed Bubble Column (with tray types #1, #2, and #3) and Bubble Column without Trays at U_l= 1 cm/s, and U_g = 1 cm/s.

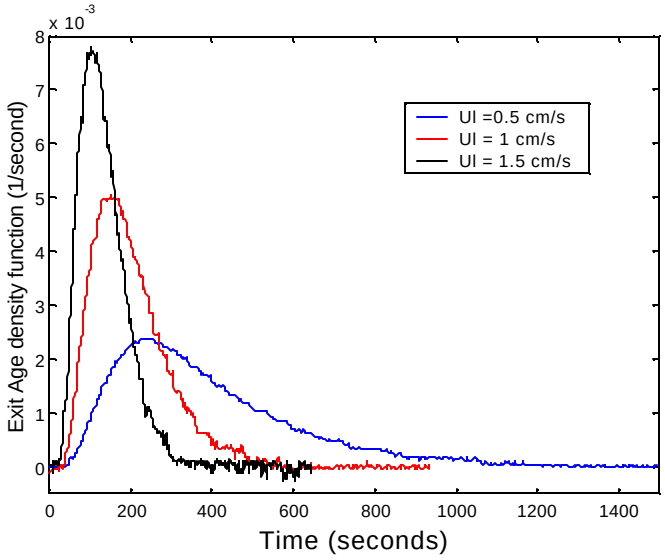

Figure 7.2 Effect of the Superficial Liquid Velocity (U_l=0.5, 1.0, and 1.5 cm/s) on the Experimental E-Curves in Trayed Bubble Column with Tray Type #1 (d_o=1.74 cm, 10.2% O.A.) at U_g=8 cm/s.

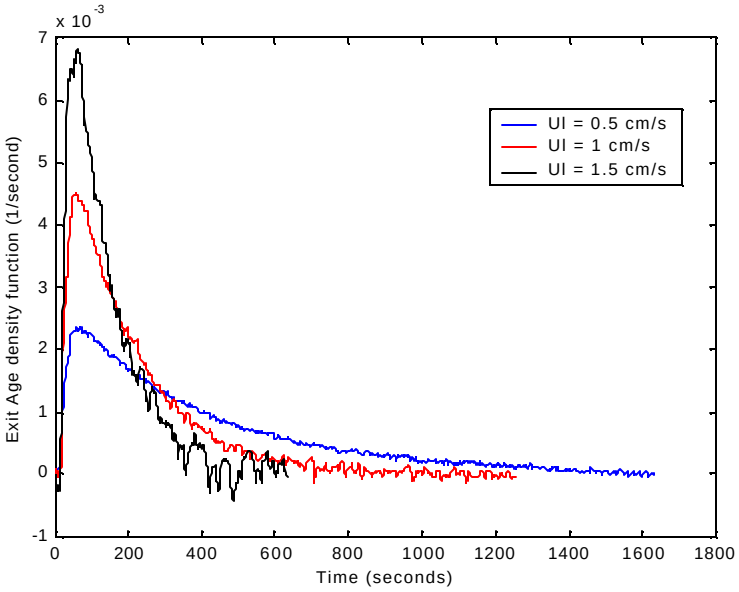

Figure 7.3 Effect of the Superficial Liquid Velocity (U_l=0.5, 1.0, and 1.5 cm/s) on the Experimental E-Curve in Bubble Column without Trays at U_g=8 cm/s.

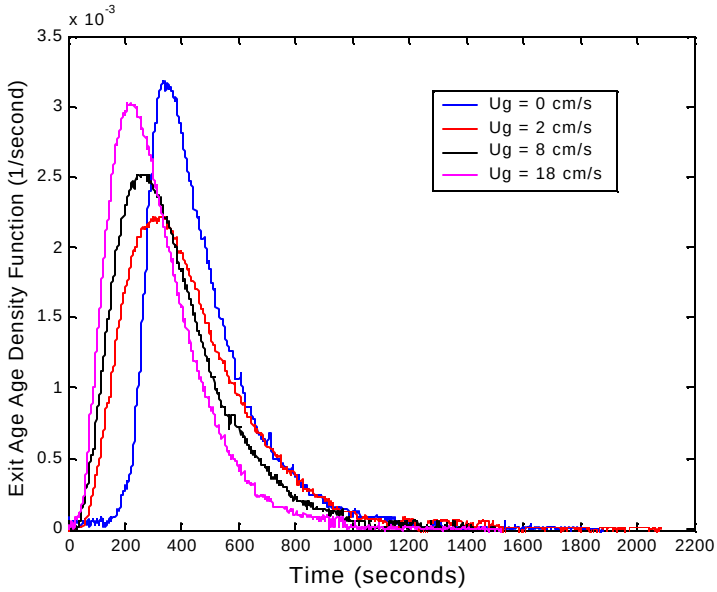

Figure 7.4 Effect of the Superficial Gas Velocity (U_g=0, 2, 8, and 18 cm/s) on the Dimensional E-Curve in Trayed Bubble Column with Tray Type #2 (d_o=0.6 cm, 5.2% O.A.) at U_l= 0.5 cm/s.

7.4 Analysis of the Experimental Results

Table A.10.1 in Appendix A.10 lists the results of the analysis of the experimental tracer response curves at every single condition tested in this work. The superficial gas velocity, the total mass of tracer detected (out of 2 grams of KCl injected), the first moment of the E-curve (mean residence time), the dimensional and the dimensionless variances about the mean, and the number of perfectly mixed tanks as predicted by the N-CSTR in series model ($N=1/\sigma^2_D$) constitute the column entries of Table A.7.1.

In Figure 7.5, we can see the comparison of the liquid residence time ($\bar{t} = V_c\varepsilon_l / Q_L$) and the first moment of the E-curve calculated from the experiments. In general, the first moments of the curve slightly overpredict (always by less than 10%) the liquid residence times.

Figures 7.6 and 7.7 show the experimental dimensionless variances versus the superficial gas velocity for all the conditions tested in this work. The width of the error bars displayed in the plots covers a 95% confidence interval around the mean value.

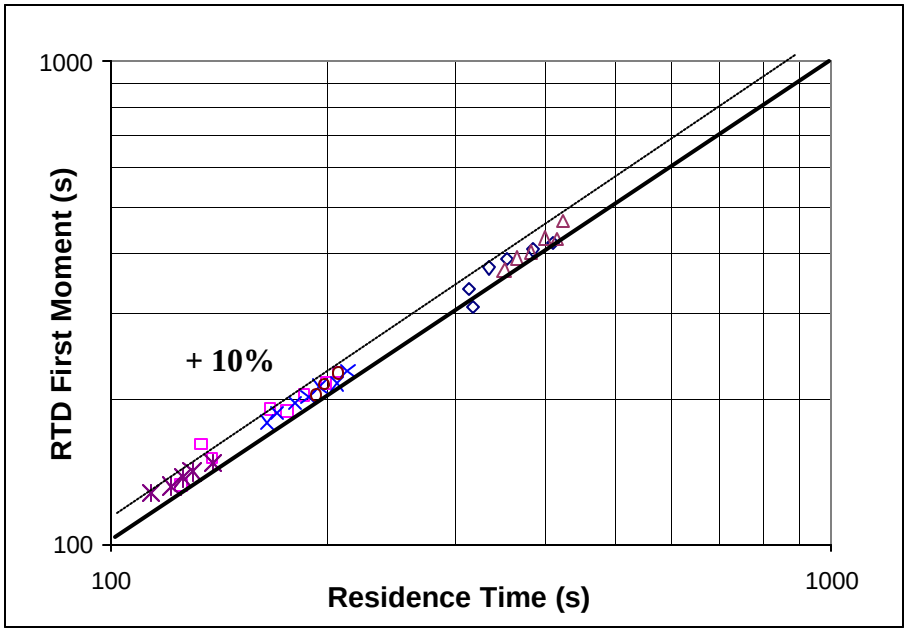

Figure 7.5 Comparison of the Liquid Residence Time and the First Moment of the E-Curves (Log-Log Scale).

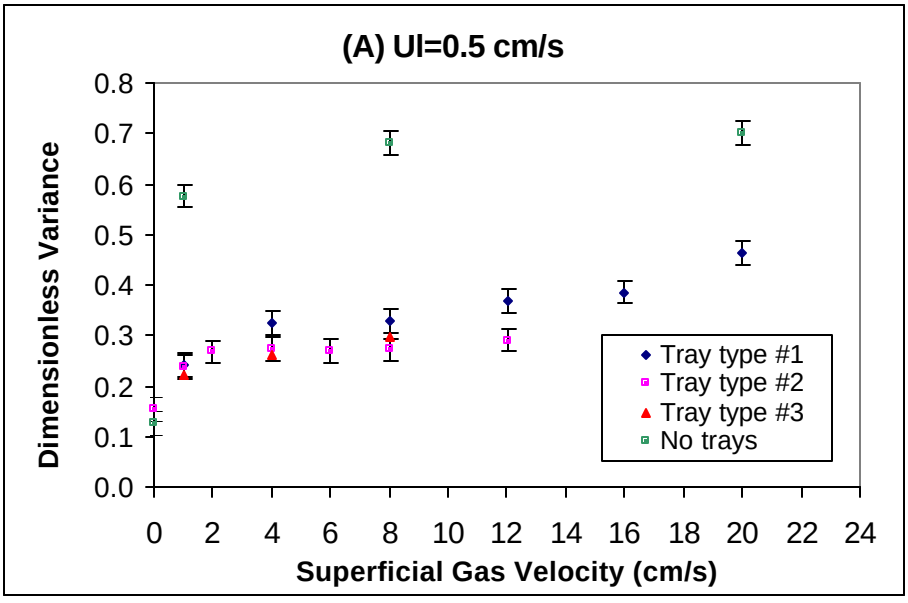

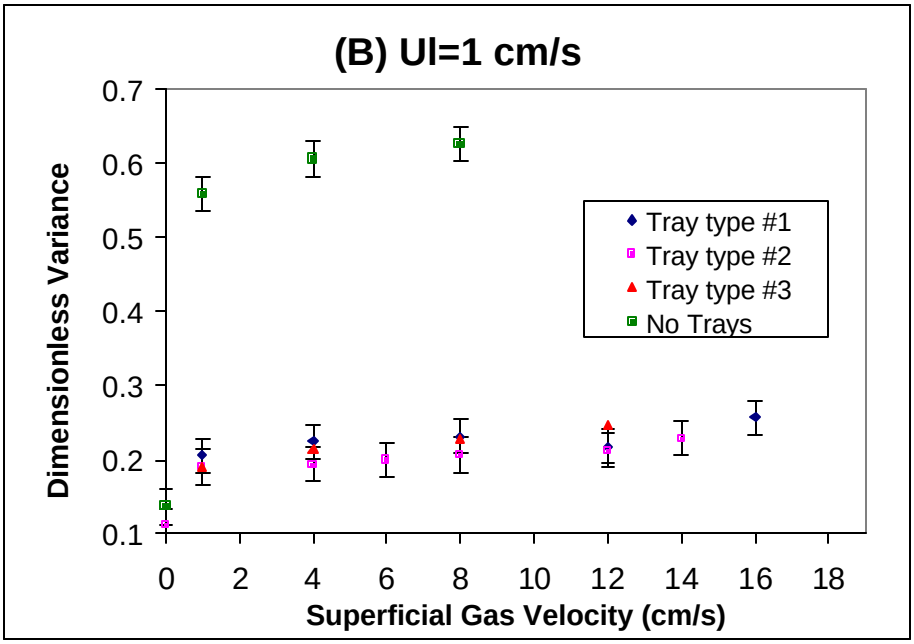

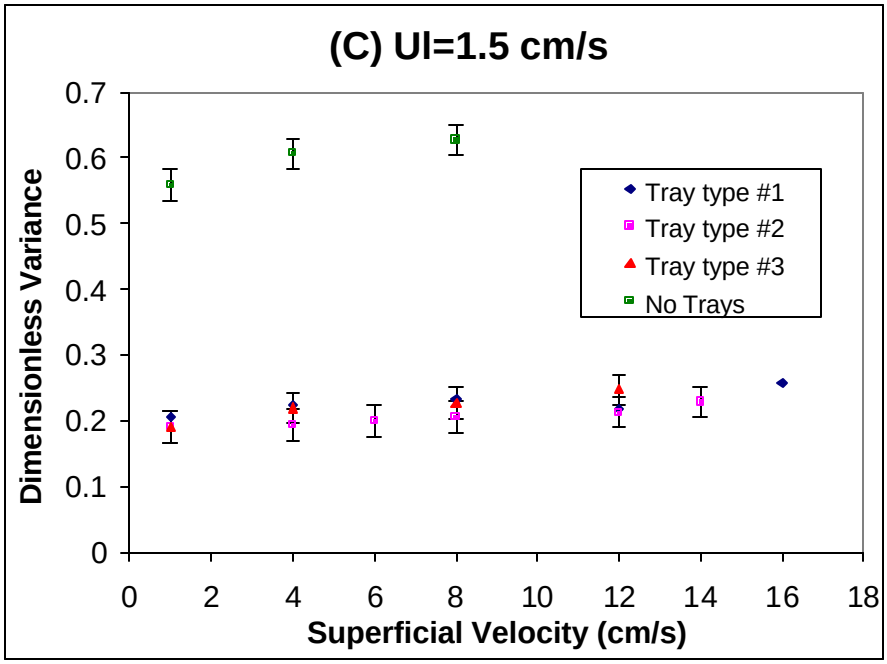

Figure 7.6 Experimental Dimensionless Variance versus Superficial Gas Velocity in Column without Trays and Trayed Column with Tray Types #1, #2, and #3 at (A) U_l=0.5 cm/s, (B) U_l=1 cm/s, and (C) U_l=1.5 cm/s.

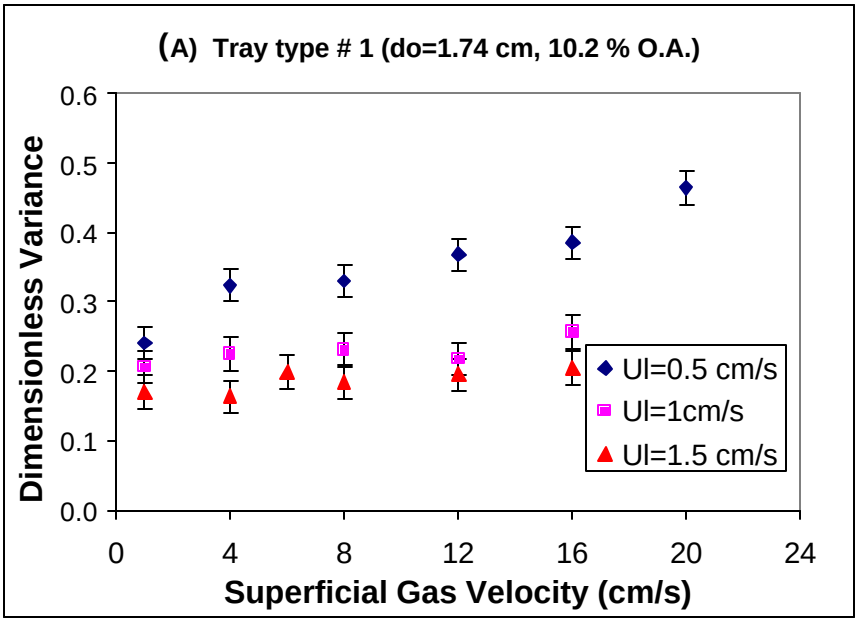
(A) Tray type # 1 (do=1.74 cm, 10.2 % O.A.)
Dimensionless Variance
0.6
0.5
0.4
0.3
0.2
0.1
0.0
0
4
8
12
16
20
24
Superficial Gas Velocity (cm/s)
Ul=0.5 cm/s
Ul=1cm/s
Ul=1.5 cm/s

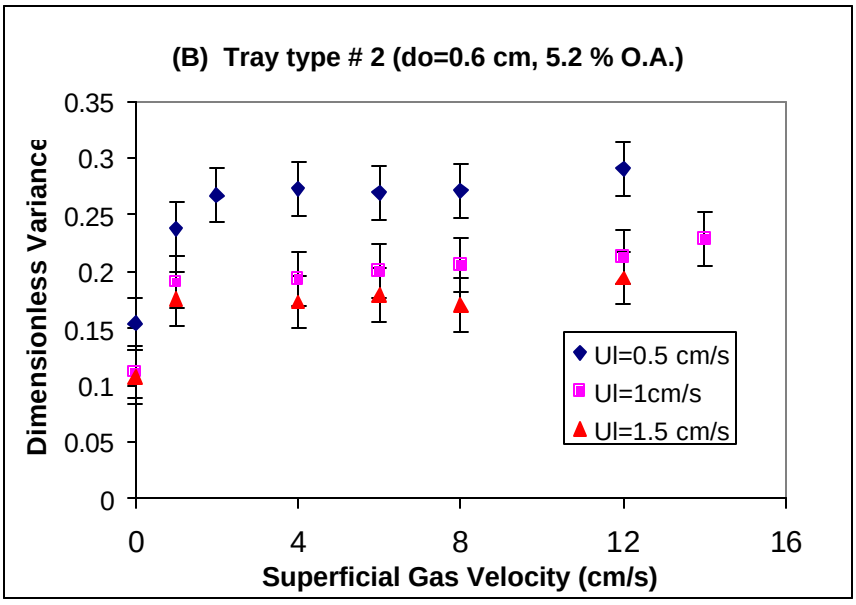
(B) Tray type # 2 (do=0.6 cm, 5.2 % O.A.)
Dimensionless Variance
0.35
0.3
0.25
0.2
0.15
0.1
0.05
0
0
4
8
12
16
Superficial Gas Velocity (cm/s)
Ul=0.5 cm/s
Ul=1cm/s
Ul=1.5 cm/s

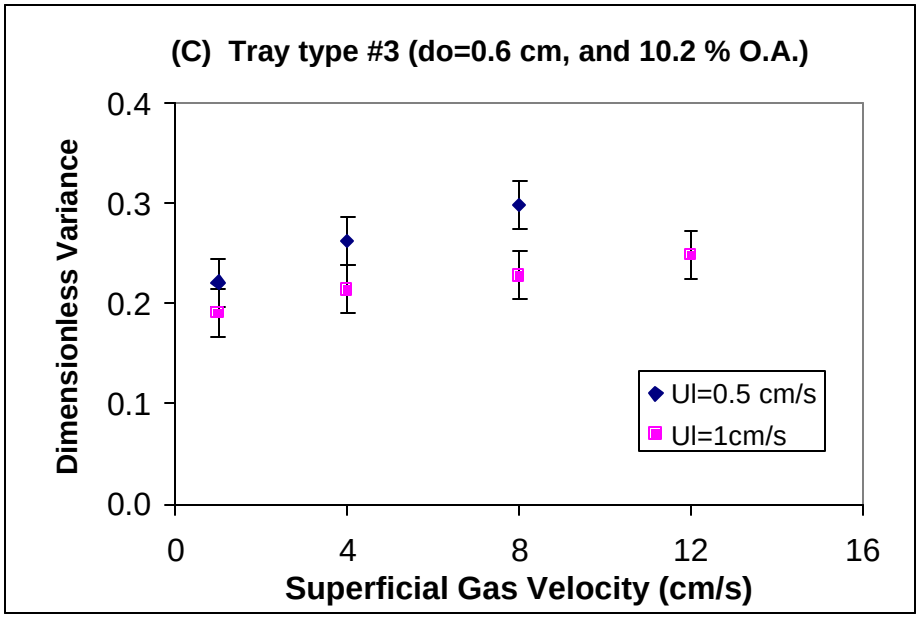

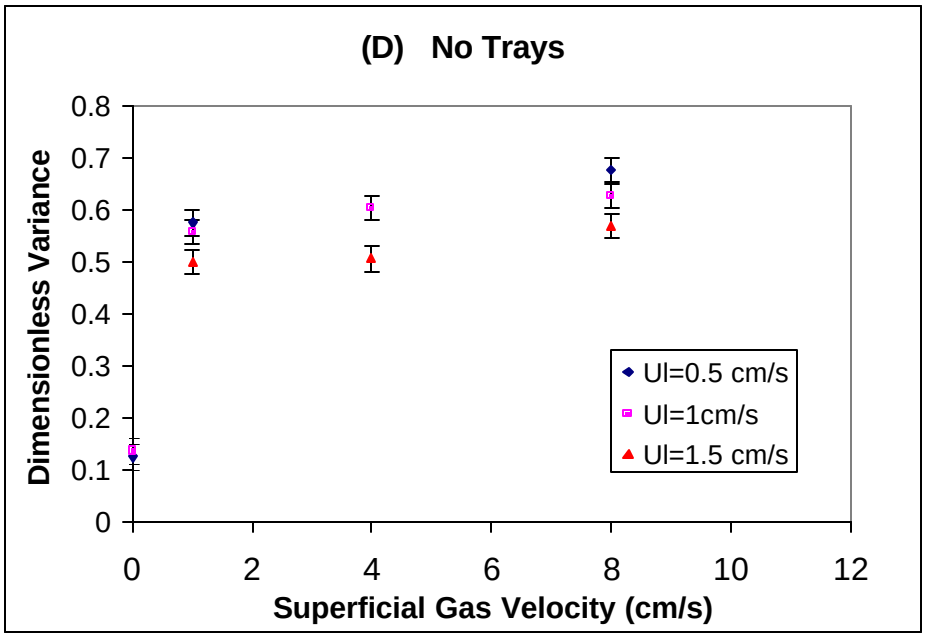

Figure 7.7 Experimental Dimensionless Variance versus Superficial Gas Velocity in Trayed Bubble Column with Tray Types #1 (A), #2 (B), #3 (C), and Column without Trays (D) at Superficial Liquid Velocities U_l=0.5, 1, and 1.5 cm/s.

It is important to realize that only a preliminary conclusion about the effect of the trays and operating conditions on the overall liquid mixing can be drawn from the variances estimated from the experimental E-curves. As a matter of fact, the estimation of the variances of the E-curves is subject to the inaccuracies inherent to the determination of the tail of the curves (Appendix A.7). It would be more adequate to rely on the comparison of the values of a given parameter estimated from a chosen model (e.g. Peclet number, or Backmixing Coefficient) rather than on the variance of the experimental E-curves. The estimation of the model parameter values is done by matching the experimental tracer response curves to the model E-curves. In the fitting process, the whole experimental E-curve is used and therefore the effect of the tail of the curve is not so critical since it is similarly weighted with the rest of the E-curve.

The following preliminary conclusions can be drawn from the analysis of the experimental curves, which is based on the values of the dimensionless variances:

1. The placement of perforated trays in a conventional bubble column significantly reduces the overall axial liquid phase backmixing (Figures 7.6 A-C). In fact, the experimentally measured dimensionless variances are almost three times larger in the column without trays.

2. As shown in Figures 7.6 A-C, the independent effects due to tray open area, and tray hole diameter cannot be in general statistically differentiated because the corresponding vertical error bars for the three types of trays tested overlap with each other. A most reliable analysis based on adequate model parameter identification should be attempted to clarify this issue.

3. From Figures 7.7 A-D, it is clear that as the superficial liquid velocity is increased, the liquid backmixing decreases. Assuming that the characteristic gas-liquid macro-circulation pattern, observed in conventional bubble columns, develops in each of the stages in the multistage column, *Joshi et al., 1998*

reported that with an increase in the superficial liquid velocity, the extent (magnitude and area) of the liquid downflow near the wall decreases. Therefore, with an increase in U_l, there is less axial mixing in the column and the overall liquid flow pattern is closer to plug flow.

4. An increase in the velocity of the gas phase promotes not only a higher liquid backmixing inside the stages, but also an increase in the inter-stage backmixing. In Figures 7.6 and 7.7, it can be seen that there is a slight increment in the variances of the curves in the low-medium range of superficial gas velocities, after which a constant value is reached. The effect of U_g is enhanced at low superficial liquid velocities as it can be seen, for instance, in Figure 7.7 A.

Chapter 8 Model Interpretation of the Experimental Results

8.1 Parameter Estimation Procedures

As already stated in the literature review (Section 5.3), a good starting strategy to choose the proper liquid mixing model should be based upon the agreement of the physical model conception with the real reactor arrangement. A proper model should offer a balance between an accurate physical realization of the real system with the minimum number of parameters for a straightforward and univocal interpretation of the experimental data. The model parameters are determined by finding the best fit of the model to the experimental data. If the model's transfer function can be written in a linear form, then the parameters can be estimated by a simple linear regression procedure (*Ostergaard, 1969*). Unfortunately, this is not the case for the Axial Dispersion Model, and the N-CSTR in Series with Backmixing Model, which are the models of choice to describe the liquid mixing in co-current trayed bubble column reactors. In this work, a non-linear regression approach in both time and Laplace domains has been followed (Appendixes A.8).

8.2 Parameter Estimation of the N-CSTR in Series with Backmixing Model

The description of the model has been extensively covered in the literature review section in Chapter 5. We can recall the model's system of ordinary differential equations and the corresponding initial conditions (Equations 5.11-5.13).

$$\frac{dC_1^*}{dq} = k\,C_2^* - (1+k)\;C_1^* \qquad \text{First Tank} \qquad (5.11)$$

$$\frac{dC_i^*}{dq} = (1+k)\;C_{i-1}^* - (1+2\,k)\,C_i^* + k\,C_{i+1}^* \qquad \text{Intermediate Tank, i =2 to N-1} \qquad (5.12)$$

$$\frac{dC_N^*}{dq} = (1+k)\ C_{N-1}^* - (1+k)\ C_N^* \qquad \text{Last Tank} \qquad (5.13)$$

$$q = \frac{t}{\bar{t}} = \frac{L\,t}{V_i\ N} \quad C_i^* = \frac{C_i V_i\ N}{m} \quad k = \frac{Q_{LB}}{Q_{LN}}$$

Initial Conditions:

$$At\ q = 0 \quad C_1^* = N, C_2^* = C_3^* = ... = C_i^* = ... = C_N^* = 0$$

The number of well-mixed tanks can take integer values between 2 and infinity (plug flow model), whereas the backmixing coefficient k can take any natural number between zero (no liquid backflow) and infinity (no net liquid flowrate in the column).

The dimensionless variance or the second moment around the mean residence time is given by Equation 5.17.

$$s^{\ 2}_{D,B} = \frac{1+2k}{N} - \frac{2k(1+k)(1-p^N)}{N^2} \qquad (5.17)$$

Here p is defined as follows:

$$p = \frac{k}{1+k}$$

Equations 5.11-5.13 form a simple linear eigenvalue problem, which can be solved by matrix inversion or by a Runge-Kutta scheme. The transient dimensionless concentration at a given tank in the series of tanks is equal to the model's Exit Age Density Function in that tank.

In order to determine the model parameters, a time domain-fitting scheme has been implemented based on the minimization of the objective function (Equation 8.1), which can be written as follows:

$$R_B^t(N,k) = \sqrt{\sum_{i=1}^{t_{total}} \frac{\left[E_E(\theta_i) - E_M(\theta_i, N, k)\right]^2}{t_{total} - 2}}$$

$$i = 1,\ldots,t_{total} \qquad t_{total} >> 2 \tag{8.1}$$

In this case the total number of model parameters is equal to two *(N, k)*, and t_{total} is equal to the total number of experimental sample points.

A least squares minimization code was written and executed in MATLAB^{TM} v. 4.3 (The Math Works Inc.). The program is initialized by inputting a given range of values for *N* and a starting guess value for *k*. The first step is to numerically solve the system of Equations 5.11-5.13, with *N* being equal to the first value of the chosen range and *k* being the starting guess value. In order to do that, a 4th order Runge-Kutta subroutine is called by the main program, the output of which is the model dimensionless residence time distribution curve $E_M(q)$ evaluated at the Nth tank. The residual function $R_B^t(N,k)$ is then calculated according to Equation 8.1 by substituting the estimated model $E_M(q)$ and experimental $E_E(q)$ transfer functions. The next step is to select a new value for *k*, based on the previous result, and to repeat the same procedure to find the corresponding R_B^t. This iterative process will end when the final residual value is smaller than a selected tolerance. The described procedure is repeated for the next value of *N* in the inputted range to find the new optimum *k* and the associated residual $R_B^t(N,k)$. The optimum *N* of the inputted range will be the one that yields the lowest residual value. With the purpose of speeding up the optimization process, it is convenient to set upper and lower bounds for *N* in order to reduce the length of the range of *N* fed to the algorithm. In general, the N-CSTR in series model can be very helpful in this matter since the total number of tanks predicted by this model, which is the inverse of the experimental dimensionless variance, is usually greater or equal than the total number of tanks calculated by the N-CSTR with Backmixing model. The procedure should also observe

the natural constraints of the problem that *N* and *k* are positive integer and positive real numbers, respectively. Table A.10.2 of Appendix A.10 displays the result of this parameter estimation exercise for the trayed column with the three different types of trays, and the column without trays. It can be observed that for the trayed bubble column, the total number of mixed tanks *N* varies between 4 and 7.

Conversely, one can keep *N* equal to the total number of physical stages in the column (*N=5*) and fit only the value of the backmixing coefficient *k*. In this case, the backmixing coefficient can be physically interpreted as the fraction of the total amount of liquid in the upward direction that backflows into each of the stages in the column. The objective function can be written as follows:

$$R_B^t(N=5,k)=\sqrt{\sum_{i=1}^{t_{total}}\frac{\left[E_E(\theta_i)-E_M(\theta_i,N=5,k)\right]^2}{t_{total}-1}}$$

$$i=1,\ldots,t_{total} \qquad (8.2)$$

$$t_{total}>>2$$

Table A.10.3 summarizes the results of the parameter estimation using this method. The residual of the time-domain fit R_B^t provides a quantitative measure of the agreement between model and experiments. Therefore, it can be used to assess the validity of a given model versus other proposed models.

Figures 8.1, 8.2 and 8.3 show the experimental E-curves and their corresponding model predictions (best fit) at selected operating conditions in the trayed bubble column. We can observe that the N-CSTR with Backmixing Model fits the experimental data satisfactorily. Furthermore, the model predictions obtained by means of fitting both parameters N and k is only slightly better than keeping N equal to the total number of physical stages in the column (N=5) and fit for k. The comparison of the dimensionless variances calculated from the experimental E-curve and from the fitted model E-curve

(N=5 and fitted k) can be seen in Figure 8.4. The disagreement between them is always within the ±5% interval range.

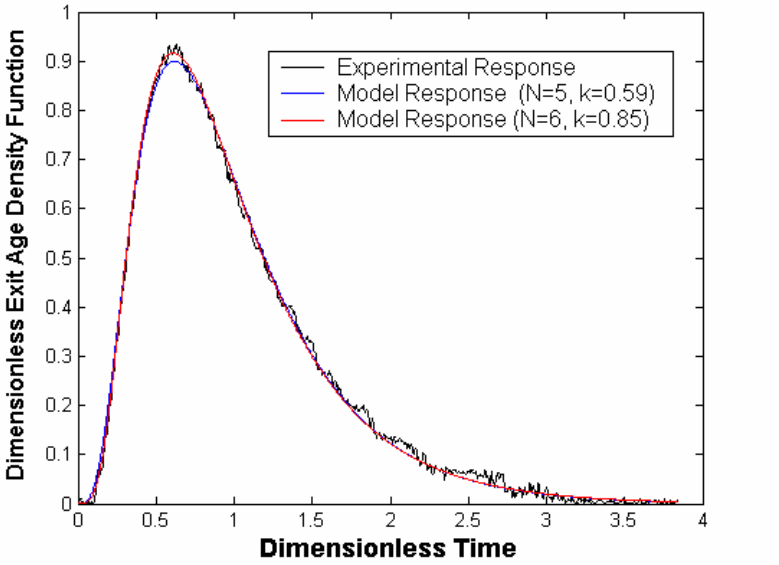

Figure 8.1 Comparison of the Experimental E-curve and the N-CSTR with Backmixing Model E-curves (Fitted N & k; N=5 and Fitted k) in Trayed Bubble Column with Tray Type #1 (d_o=1.74 cm, 10.2% O.A.) at U_l=0.5 cm/s and U_g=8 cm/s.

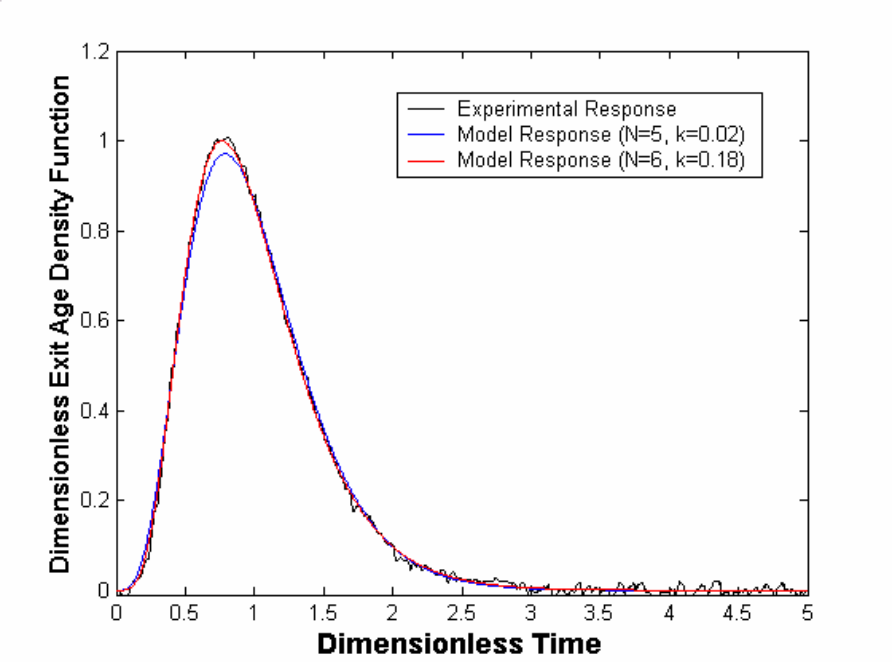

Figure 8.2 Comparison of the Experimental E-curve and the N-CSTR with Backmixing Model E-curves (Fitted N & k; N=5 and Fitted k) in Trayed Bubble Column with Tray Type #2 (d_o=0.6 cm, 5.2% O.A.) at U_l=1.0 cm/s and U_g=12 cm/s.

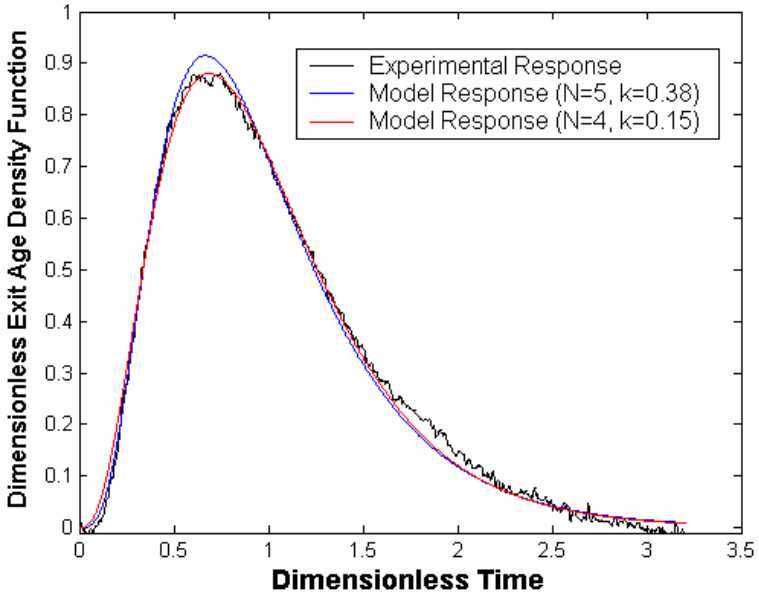

Figure 8.3 Comparison of the Experimental E-curve and the N-CSTR with Backmixing Model E-curves (Fitted N & k; N=5 and Fitted k) in Trayed Bubble Column with Tray Type #3 (d_o=0.6 cm, 10.2% O.A.) at U_l=0.5 cm/s and U_g=4 cm/s.

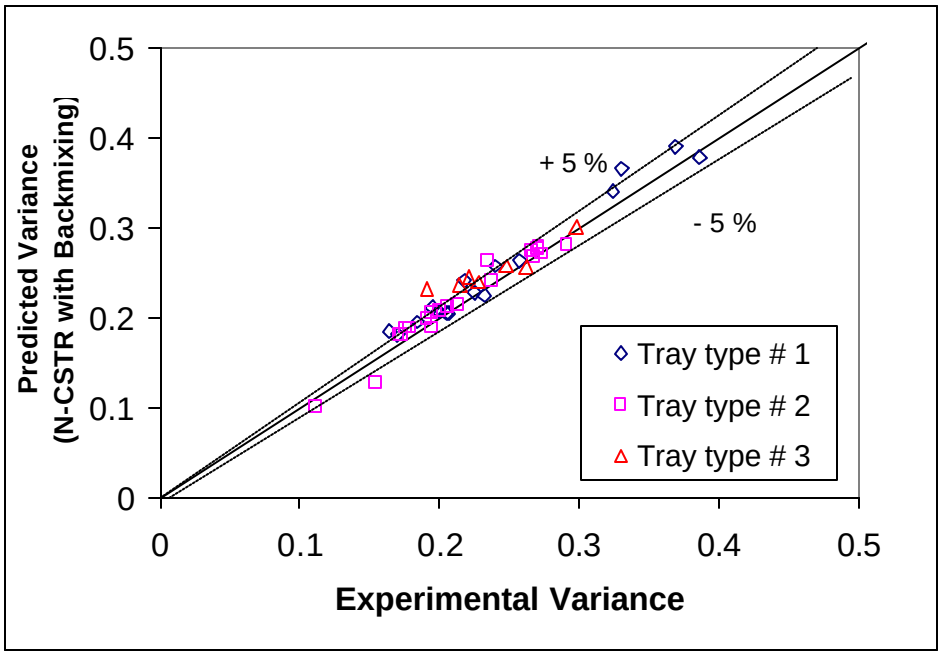

Figure 8.4 Comparison of the calculated Dimensionless Variance between the Experimental and the Model (N=5, fitted k) E-curves.

8.3 Parameter Estimation of the Axial Dispersion Model

The transient axial dispersion model equations with closed-closed boundary conditions for an ideal pulse injection of tracer at the reactor inlet, *Nauman et al., 1983*, are:

$$\frac{1}{Pe}\frac{\partial^2 \overline{C}(Z,\theta)}{\partial Z^2} - \frac{\partial \overline{C}(Z,\theta)}{\partial Z} = \frac{\partial \overline{C}(Z,\theta)}{\partial \theta} \tag{8.3}$$

$$-\frac{1}{Pe}\frac{\partial \overline{C}(Z,\theta)}{\partial Z} + \overline{C}(Z,\theta) = \delta(\theta) \quad \text{at } Z = 0 \tag{8.4}$$

$$\frac{\partial \overline{C}(Z,\theta)}{\partial Z} = 0 \qquad \text{at } Z = 1 \tag{8.5}$$

Brenner, 1962 presented the solution to the above Boundary Value Problem (Equation 8.6), which can be obtained through the inversion of the Laplace domain system's transfer function by the Residue Theorem.

$$\overline{C}(1,\theta) = e^{Pe/2}\sum_{n=0}^{\infty}\left[\frac{2w_n \sin(w_n)\left[Pe^2 + 4w_n^2\right]\exp\left[-\frac{Pe^2 + 4w_n^2\,\theta}{4Pe}\right]}{Pe\left[Pe^2 + 4w_n^2 + 4Pe\right]}\right] \tag{8.6}$$

Here, w_n are the positive roots of the following expression:

$$\tan(w_n) = \frac{4w_n Pe}{4w_n^2 - Pe^2} \tag{8.7}$$

The above series converges very slowly for small times, and hence it is not very convenient to be used for fitting purposes.

The Laplace domain fitting is much more appropriate since the model transfer function (Equation 8.8) can be easily obtained from the solution of Equations 8-3-8.5 in the Laplace domain (*Nauman et al., 1983*).

$$\overline{C}(1,s) = \overline{E}_M(1,s^*) = \frac{4a(s^*)\exp\left[\frac{Pe}{2}(1-a(s^*))\right]}{(1+a(s^*))^2 - (1-a(s^*))^2\exp\left[-Pe\,a(s^*)\right]} \tag{8.8}$$

$$a(s^*) = \sqrt{1+\frac{4s^*}{Pe}} \tag{8.9}$$

Applying the Method of Moments, described by *Nauman et al., 1983*, on the transfer function (Equation 8.8), the second moment or variance around the mean residence time at the exit can be easily derived:

$$\sigma^2_{D,\,ADM} = \frac{2}{Pe} - \frac{2}{Pe^2}(1 - e^{-Pe}) \tag{8.10}$$

The Laplace domain objective function for the Axial Dispersion Model with closed-closed boundary conditions $R^L_{ADM}(s^*_i, Pe)$ can be written as follows:

$$R^L_{ADM}(s^*_i, Pe) = \sqrt{\sum_{i=1}^{S_{total}} \frac{\left[\overline{E}_E(s^*_i) - \overline{E}_M(s^*_i, Pe)\right]^2}{t_{total} - 1}} \tag{8.11}$$

$i = 1,...,t_{total}$

Here t_{total} is the total number of experimental data points.

The experimental transfer function $\overline{E}_E(s*)$ can be numerically evaluated from Equation A.8.3 in Appendix A.8.

$$\overline{E}_E(s^*_j) = \sum_{i=0}^{t_{final}} \overline{E}_E(q_i)\ \exp(-s^*_j q_i)\,\Delta q_i \tag{A.8.3}$$

An optimization algorithm similar to the one described in the previous section has been implemented to estimate the model parameter (Peclet number) that minimizes the residual sum of squares function R^L_{ADM}. Table A.10.4 in Appendix A.10 shows the results for all the conditions covered in this work.

Figures 8.5 to 8.7 show the fitted model versus the experimental E-curves for the trayed column with the three different types of trays, and for the column without trays at selected operating conditions. In order to obtain the E-curves shown in the figures, the

transfer function of the model (Equation 8.8) was numerically inverted at the fitted Peclet number by the algorithm developed by *De Hoog et al., 1982*. By looking at the sample figures, it seems that the Axial Dispersion Model fails always to predict the maximum of the experimental E-curves. Figure 8.8 shows the model predicted versus the experimental dimensionless variances (Parity Plot). The ADM slightly over predicts the experimental dimensionless variance within the 10% error range.

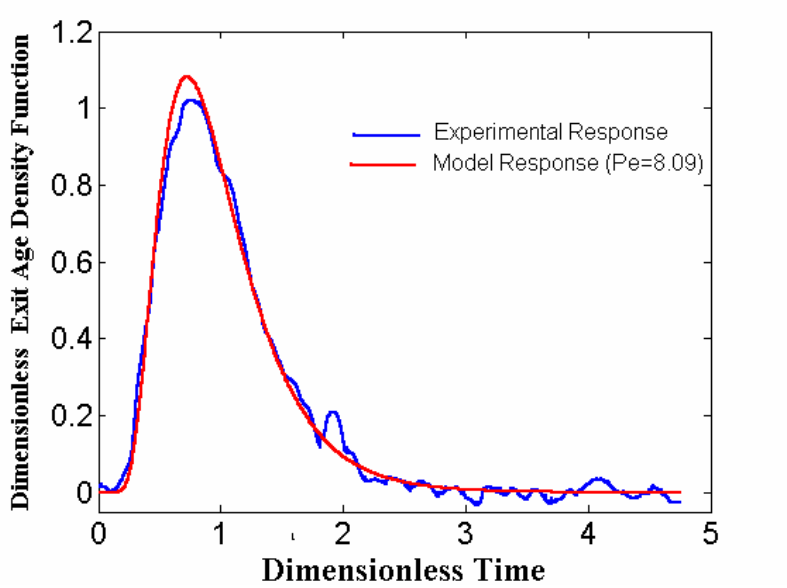

Figure 8.5 Comparison of Experimental and Axial Dispersion Model E-Curves in Trayed Bubble Column with Tray Type #1 (d_o=1.74 cm, 10.2% O.A.) at U_l=1.5 cm/s and U_g=12 cm/s.

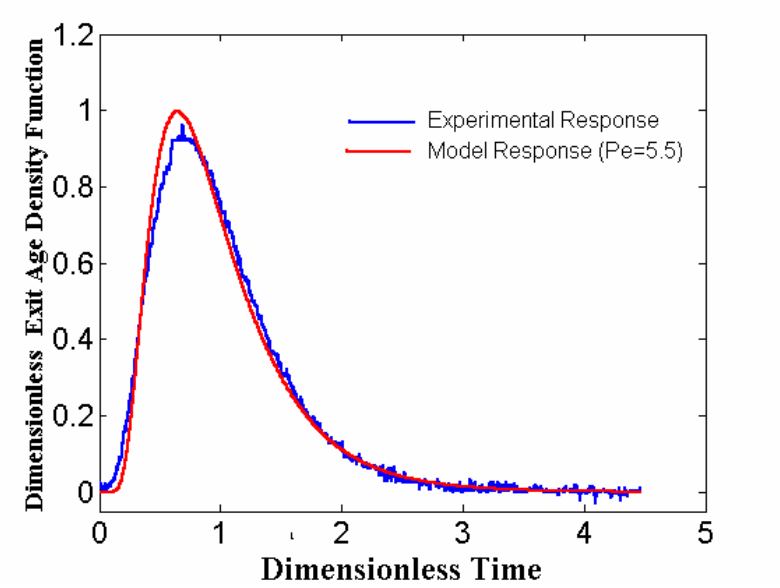

Figure 8.6 Comparison of Experimental and Axial Dispersion Model E-Curves in Trayed Bubble Column with Tray Type #2 (d_o=0.6 cm, 10.2% O.A.) at U_l=0.5 cm/s and U_g=4 cm/s.

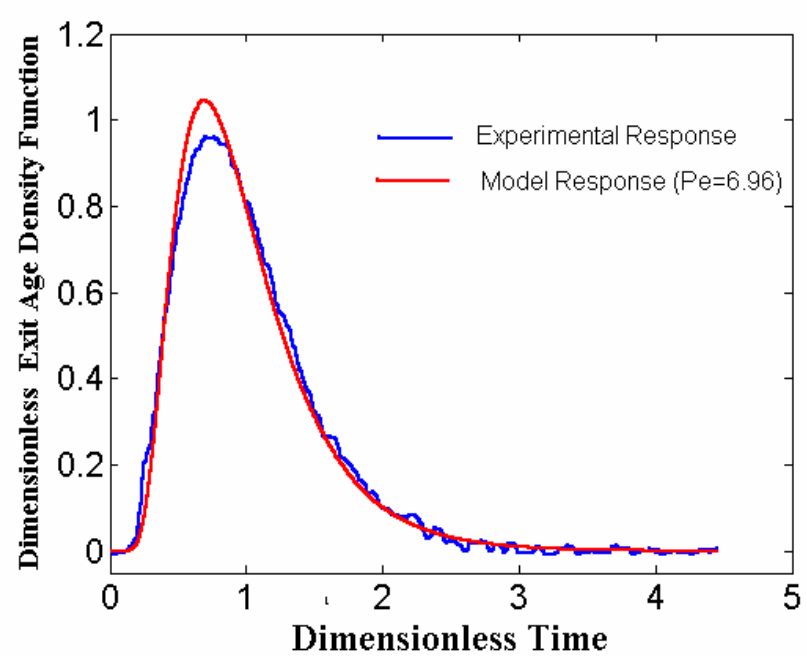

Figure 8.7 Comparison of Experimental and Axial Dispersion Model E-Curves in Trayed Bubble Column with Tray Type #3 (d_o=0.6 cm, 5.2% O.A.) at U_l=1 cm/s and U_g=4 cm/s.

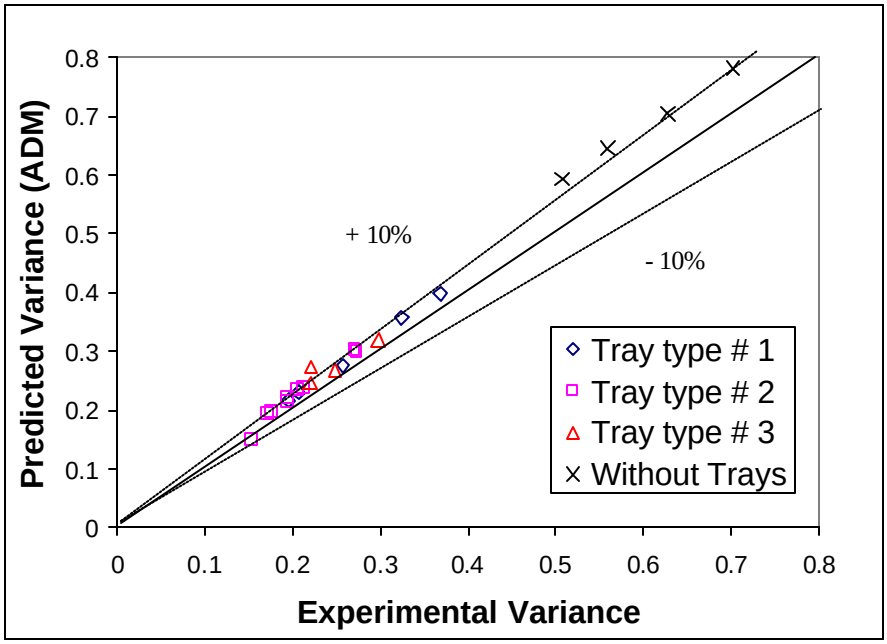

Figure 8.8 Model Predicted versus Experimental Dimensionless Variances.

8.4 Model Discrimination: ADM versus N-CSTR with Backmixing Model

The comparison of the values of the residuals of the fit can be used for proper model discrimination. As described in Section 8.2, the N-CSTR with Backmixing Model allowed us to fit the experimental results to the model in its natural time domain frame. Unfortunately, this was not possible for the Axial Dispersion Model, and the Laplace transformation technique was used instead (Section 8.3). For this reason, and in order for the comparison between the two models to be meaningful, the residuals of the fit have to be evaluated in the same frame of reference. We can compare the value of the residuals in the time domain or in the Laplace domain. Either way, if the residuals for one of the two models are statistically smaller than the other, then it can be concluded that this model fits the experimental data better than the other. In Appendix A.11, it has been demonstrated that the residuals of the N-CSTR with Backmixing model are in fact statistically smaller than the ADM when they are estimated and compared in the time domain.

The series of Figures 8.9-8.11 shows the graphical comparison of the two models to match the experimental E-curves at selected conditions. The ADM seems to always overpredict the maximum of the experimental response curve, whereas the N-CSTR with Backmixing Model nicely follows the experimental curve through the whole domain. As explained in Chapter 5, the N-CSTR with Backmixing model offers a more plausible description of the liquid phase macromixing mechanism inside the trayed bubble column than the ADM.

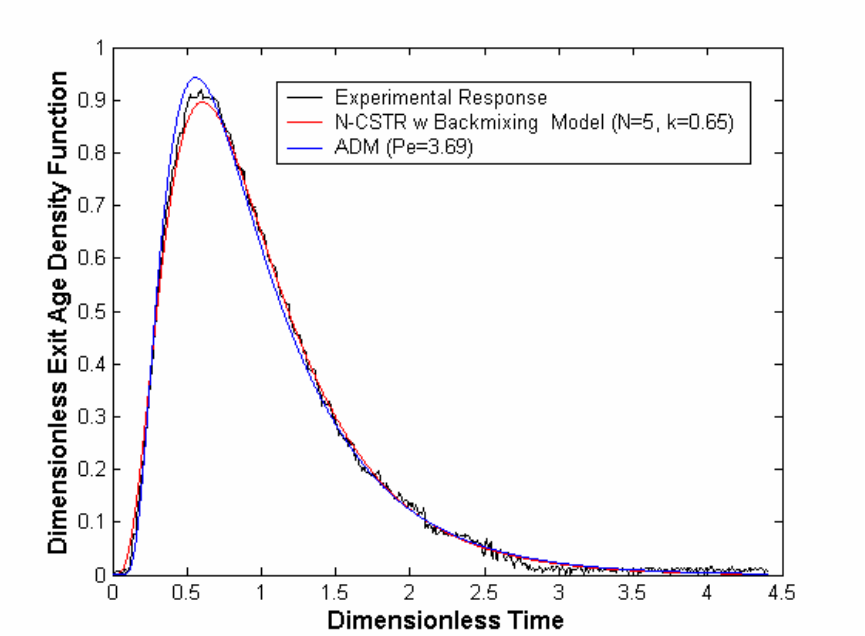

Figure 8.9 Comparison of the Experimental versus the ADM (Pe=3.69) and the N-CSTR with Backmixing Model (N=5, k=0.65) E-Curves in Trayed Bubble Column with Tray Type #1 (d_o=1.74 cm, 10.2% O.A.) at U_l=1 cm/s and U_g=16 cm/s.

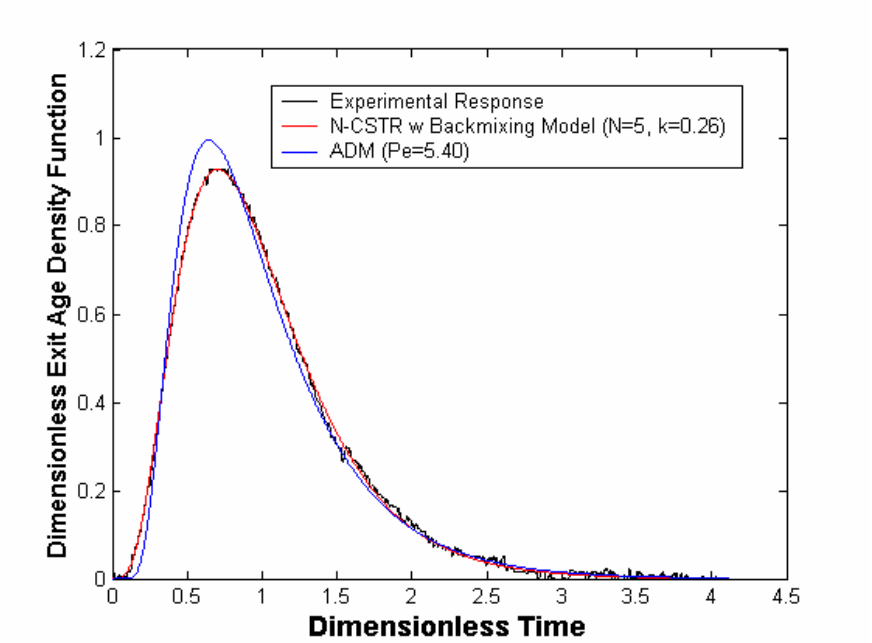

Figure 8.10 Comparison of the Experimental versus the ADM (Pe=5.40) and the N-CSTR with Backmixing Model (N=5, k=0.26) E-Curves in Trayed Bubble Column with Tray Type #2 (d_o=0.6 cm, 5.2% O.A.) at U_l=0.5 cm/s and U_g=8 cm/s.

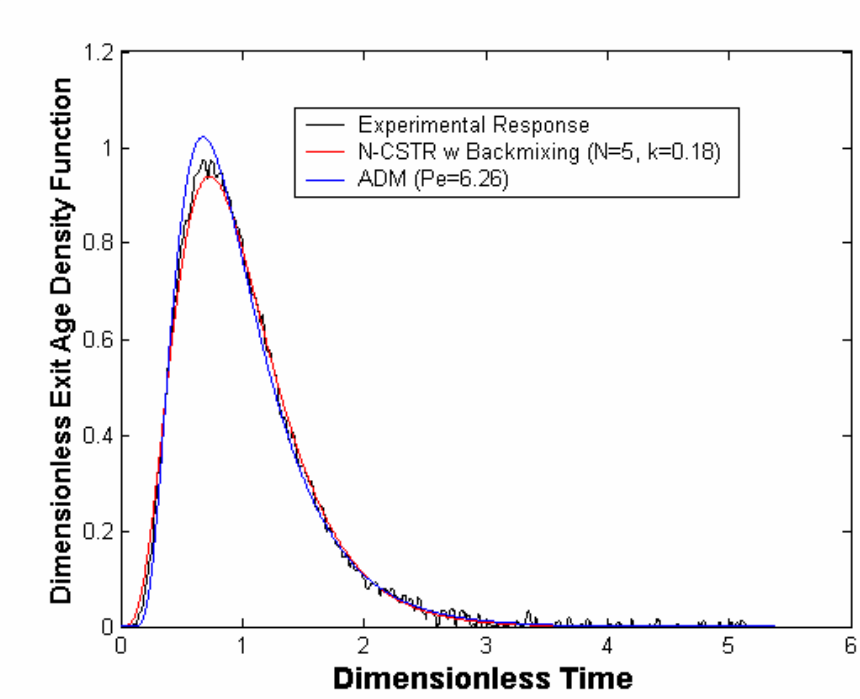

Figure 8.11 Comparison of the Experimental E-curve versus the ADM (Pe=6.26) and the N-CSTR with Backmixing Model (N=5, k=0.181) E-Curves in Trayed Bubble Column with Tray Type #3 (d_o=0.6 cm, 10.2% O.A.) at U_l=1.0 cm/s and U_g=12cm/s.

8.5 Effect of Operating Conditions and Tray Geometry on the Liquid Backmixing

In Appendix A.11, it was shown that the N-CSTR with Backmixing Model was able to match the experimental tracer response curves better than the ADM. The model has two adjustable parameters, *N and k*. A valid approach to quantify the degree of axial liquid backmixing is to assume *N* to be equal to the total number of physical stages in the column (number of trays plus one) and thus use the fitted backmixing coefficient *k* to estimate the amount of the net inlet liquid flow rate that it is backmixed in each of the stages. The N-CSTR with Backmixing Model, as formulated in Chapter 5, assumes that the backmixing coefficient is the same in all the stages of the column.

The effect of trays and operating conditions (superficial gas and liquid velocities) can be observed in Figures 8.12, and 8.13.

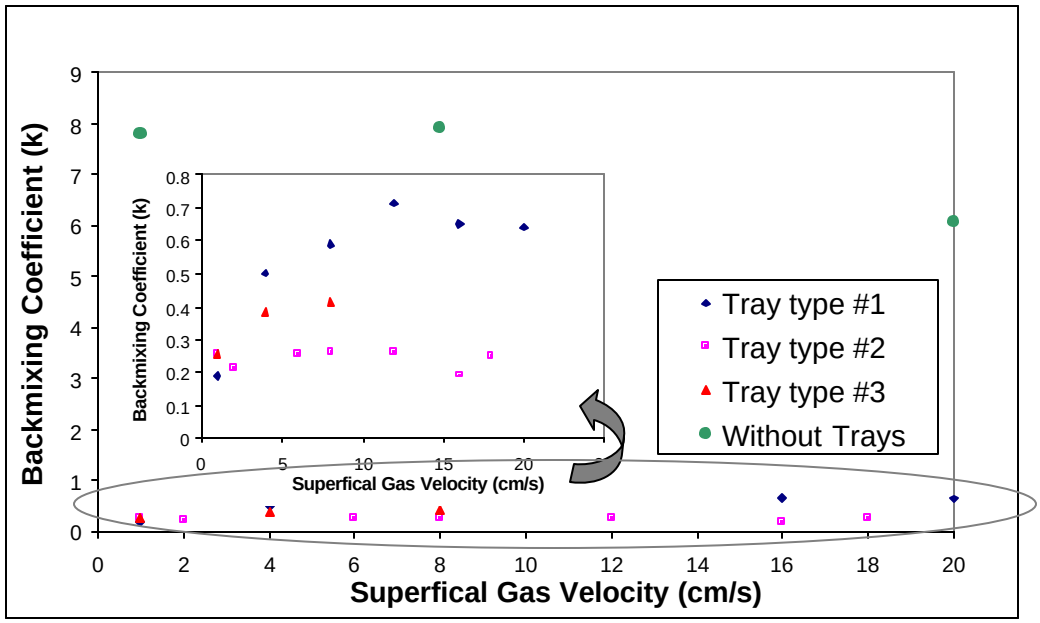

Figure 8.12 Effect of Tray Type on the Backmixing Coefficient *k* (N-CSTR with Backmixing Model) with N=5 in Trayed Bubble Column (Tray Types #1, #2, and #3) and in Column without Trays at U_l=0.5 cm/s.

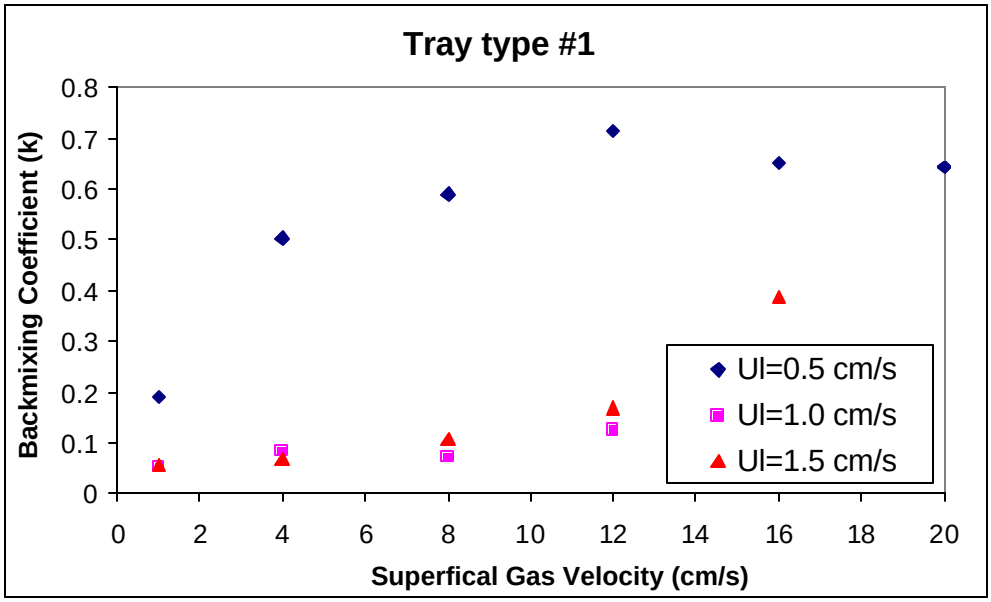

Figure 8.13 Effect of Superficial Liquid Velocity (U_l=0.5, 1.0, and 1.5 cm/s) on the Backmixing Coefficient *k* (N-CSTR with Backmixing Model) with N=5 in Trayed Bubble Column with Tray Type #1 (d_o=0.6 cm, 10.2% O.A.).

In Figure 8.12, the backmixing coefficient has been plotted versus superficial gas velocity in the trayed bubble column with the three types of trays tested in this work and in the column without trays. It should be pointed out that in order to obtain the values of *k* for the column without trays by means of matching the experimental E-curves with the N-CSTR with Backmixing Model, N was made equal to 5. This is necessary to make sure that the backmixing coefficient obtained in the trayed bubble column, where N=5 is the total number of physical stages, and in the column without trays are comparable. Table A.10.3, in Appendix A.10, lists the experimental data for all the conditions tested.

The effect of placing perforated trays inside the column, as compared to the column without trays, is to dramatically reduce the liquid phase backmixing in the axial direction (Figure 8.12). There is a 10 to 40-fold increase in the backmixing coefficient, depending on type of tray and superficial gas and liquid velocities. This observation can be explained by noting that in a bubble column without trays, the liquid phase axial dispersion is mainly caused by its characteristic G-L macrocirculation pattern, where the

gas bubbles rise up through the central part of the column creating a cross sectional density gradient, which enhances the liquid backmixing. The trays break this circulation pattern by redistributing the gas phase more evenly in each of the stages, which ultimately results in the reduction of the density gradient.

The tray open area provides the strongest effect of the tray on liquid phase backmixing. In Figures 8.12, it can be seen that for a 100% open area reduction from tray type #3 (d_o=0.6 cm, 10.2% O.A.) to tray type #2 (d_o=0.6 cm, 5.2% O.A.), there is a significant decrease in the backmixing coefficient. The effect of the tray open area in the liquid mixing seems related to the backmixing produced by liquid dropping back from the upper to the lower stages through the tray holes. As a result, the total amount of liquid that flows back from one stage to another seems to be proportional to the total tray open area. A decrease in the tray hole diameter also reduces the liquid backmixing, although the effect it is not as important as the open area. In fact, when the tray hole diameter is decreased from d_0=1.74 cm (with tray type #1) to d_0=0.6 cm (with tray type #3) at the same open area (10.2% O.A.), there is a reduction in liquid backmixing.

In Figure 8.13, the effect of superficial liquid velocity is displayed. It can be seen that an increase in liquid velocity significantly reduces liquid backmixing. This is because with a decrease in the mean liquid residence time, the gas-liquid convection in the upward direction rapidly becomes the leading transport mechanism over turbulent and molecular diffusion. The decrease in liquid backmixing with superficial liquid velocity is almost independent of tray type and superficial gas velocity (see also the numerical data listed in Table A.10.3).

The extent of liquid backmixing is affected by superficial gas velocity in the low range, whereas it becomes independent of it at higher values. The effect is strongly coupled with the superficial liquid velocity, and the tray geometry. From Figure 8.13, it can be observed that the lower the liquid velocity and the smaller the open area, the stronger the effect of U_g is on the extent of liquid backmixing. One hypothesis that can

explain this observation is that in the range of low gas velocities the stages are partly mixed, and as U_g is increased the growing degree of turbulence generated within the stage is responsible for the increase in its internal liquid recirculation. Also, the appearance of cushions of gas underneath the trays sets a large hydrostatic pressure gradient across the trays, which drives the backflow of liquid from the upper to lower stages. However, after a certain value in the gas velocity, the stages become perfectly mixed and the upward momentum of the gas and liquid phases prevent the inter stage backmixing. As a result, further increases on U_g have little effect on the overall liquid backmixing.

8.6 Comparison of the Backmixing Coefficient between Empirical Correlations and Fitted Values

We can compare the values of the backmixing coefficient found in this study with the values predicted by two published correlations, which were reported in Section 5.3, (*Kats et al., 1967*; and *Sekizawa et al., 1974*) to verify whether they can provide good estimations of *k*. Figures 8.14 and 8.15 show the corresponding parity plots for the two correlations. Further, Table 8.1 gives the mean relative error between fitted and predicted values of *k*.

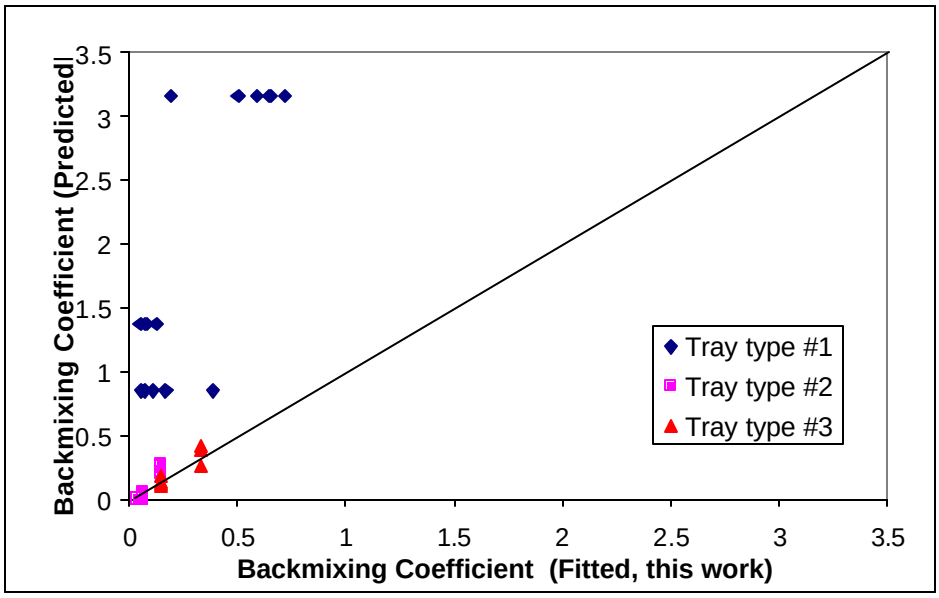

Figure 8.14 Comparison of the Backmixing Coefficient (k) between Fitted Values of this work and Predictions from Correlation (*Kats et al., 1967*) in Multistage Bubble Column with Tray Types #1, #2, and #3.

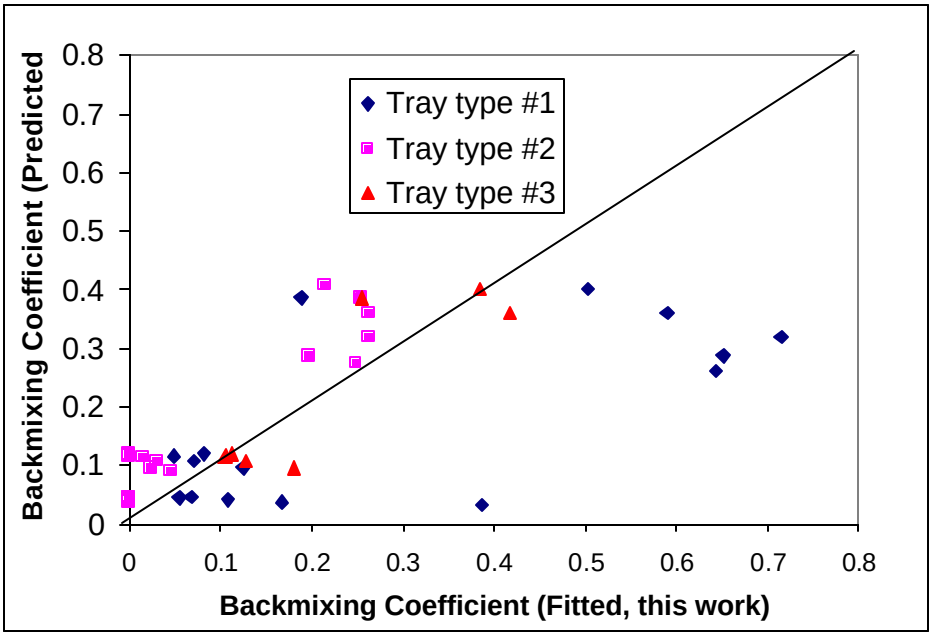

Figure 8.15 Comparison of Backmixing Coefficient (k) between Fitted Values of this Work and Predictions from Correlation (*Sekizawa et al., 1974)* in Multistage Bubble Column with Tray Types #1, #2, and #3.

Table 8.1 Mean Relative Errors between Fitted Values and Correlations.

Reference	Correlation	Mean Relative Error (%)
Kats et al., 1967	Equation 5.20	70
Sekizawa et al., 1974	Equation 5.26	92.8

It is clear that the correlations fail to predict the values of the backmixing coefficient obtained in this work. Moreover, the figures show that the estimations for tray types #2 (d_o=0.6 cm, 5.2% O.A.), and type #3 (d_o=0.6 cm, 10.2% O.A.) are substantially better than for tray type #1 (d_o=1.74 cm, 10.2% O.A.).

8.7 Empirical Expression for the Backmixing Coefficient

We can try to find an empirical relationship between the extent of liquid backmixing with the operating conditions (U_g, and U_l) and the tray design parameters (d_o, and O.A.) studied in this work.

$k=f(U_g, U_l, d_o, O.A.)$

We can write k as a linear function of the studied factors:

$$k = C\, U_l^a\, U_g^b\, d_o^c\, O.A.^d \tag{8.12}$$

Here C is the leading constant; and a,b,c and d are the exponents. All these constants can be determined by a standard multivariable regression approach, using the fitted values of *k* reported in Table A.10.3.

It has been found out that if instead of using the backmixing coefficient directly as the objective function in the regression algorithm, *k* is rearranged into the following form 1/(1+k), and used as the new objective function, then the errors between data points and predictions are lower.

$$\frac{1}{1+k} = 0.67\, U_l^{0.244}\, U_g^{-0.043}\, d_o^{-0.057}\, O.A.^{-0.134} \tag{8.13}$$

A total number of 40 data points were used to develop the above empirical expression. The standard error of the fit (variance) and the mean relative error (Equation 4.7) between data points and predictions are 0.07475 and 18%, respectively.

From Equation 8.13, we can substitute k and write Equation 8.14.

$$k = 1.497\, U_l^{-0.244}\, U_g^{0.043}\, d_o^{0.057}\, O.A.^{0.134} - 1 \tag{8.14}$$

The range of the variables of the data points used to develop Equation 8.14 is the following, U_l=0.5-1.5 cm/s, U_g=1-18 cm/s, d_o=0.6-1.74 cm, and O.A.=5.2%-10.2%, Air-water system.

The parity plot of the backmixing coefficient between data points and predictions (Figure 8.16) shows that Equation 8.14 gives a large error in the prediction of the backmixing coefficient, especially at low values, where the discrepancies can be larger than 100%. However, the predictions are better for larger values of *k*. Equation 8.14 does not pretend to be a general correlation to predict the backmixing coefficient for any given situation, since it was developed using only 50 data points and within a limited set of conditions. Instead, the value of the correlation resides in the fact that it provides the relative effect of the different studied factors. Thus, we can see that superficial liquid velocity ($k\ a\ U_l^{-0.24}$) and tray open area ($k\ a\ O.A.^{0.13}$) have the most important effects on the liquid backmixing, whereas tray hole diameter ($ka\ d_o^{0.057}$) and superficial gas velocity ($ka\ U_g^{0.043}$) are almost independent of it.

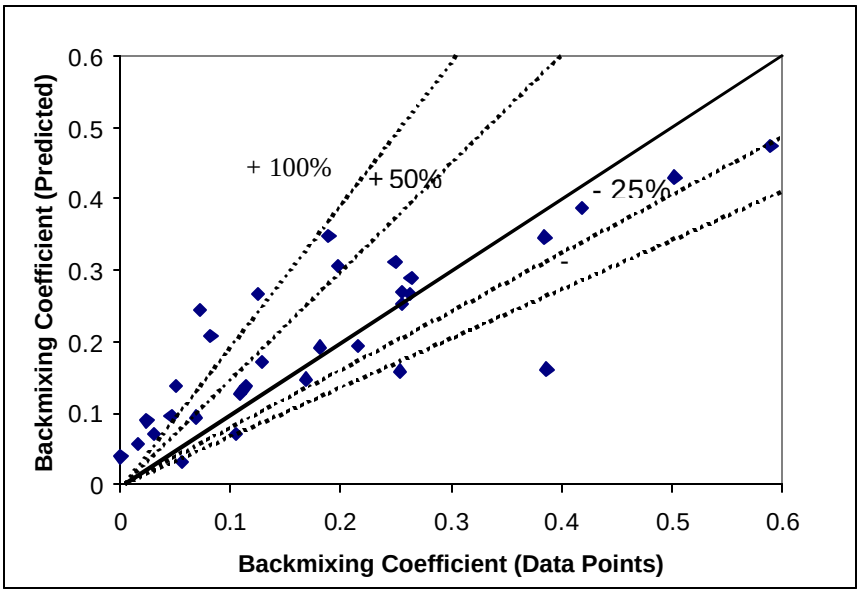

Figure 8.16 Parity Plot of the Backmixing Coefficient (k) between Empirical Expression (Equation 8.14) and Data Points (Table A.10.3) in Multistage Bubble Column with Tray types #1, #2, and #3.

Chapter 9 Summary, Conclusions and Recommendations for Future Work

9.1 Summary and Conclusions

In this study, an experimental co-current trayed bubble column setup has been built to investigate the effect of tray open area, tray hole diameter, superficial gas and liquid velocities, gas sparger, and liquid phase physical properties on overall and staged gas holdup, pressure drop across the trays, and overall liquid phase mixing. Several experimental procedures, such as the Gas Disengagement Technique (GDT) for overall gas holdup determinations, Pressure Drop Method for staged gas holdup and pressure drop across the trays measurements, and the Conductivity Method for liquid-phase tracer studies, have been successfully implemented.

The findings can be summarized as follows:

1. The effect of the trays is to significantly increase the overall gas volumetric fraction as compared to the single stage bubble column. The average increment in gas holdup varies between 20% and 50%, depending upon the gas-liquid system, gas sparger, and superficial liquid velocity used. Furthermore, tray hole diameter is the key parameter, since tray open area has no significant effect on the overall gas holdup. The effect of the tray hole diameter seems to be directly related to the bubble size diameter formed in the trays, and therefore, trays of smaller hole diameter give higher gas holdups.

2. The superficial gas velocity has the strongest effect on the overall gas holdup, which increases with U_g. The transition from Bubbly to Churn-Turbulent Regime occurs at a larger superficial gas velocity when trays are used.

3. The effect of the superficial liquid velocity on the overall gas holdup is negligible under all tested experimental conditions.

4. In the trayed column, the gas sparger has no effect on the overall gas holdup when two different gas spargers, single nozzle sparger (0.375 cm point inlet diameter) and perforated plate sparger (163 holes, 0.4 mm hole diameter, and 0.07% open area), are compared. The trays redistribute the gas phase in each of the stages, and thereby the effect of gas sparger is only noticeable in the first stage. On the other hand, in the single stage column, the perforated tray sparger yields higher gas holdups than the single nozzle sparger in the range of superficial gas velocities U_g=10-20 cm/s. As, U_g if further increased, the effect of the sparger becomes less important.

5. An aqueous surfactant solution consisting of 1% butanol and 0.01% w.t. Sodium Dodecyl Sulfate was used as the liquid phase to simulate the hydrodynamic behavior of the high gas holdup systems encountered in the Visbreaking operation of petroleum residues. Remarkable increases of up to 90% in the overall gas holdup have been observed in the trayed column as compared to the single stage column when this liquid system was used.

6. The following empirical expressions account for the effect of the studied parameters on the overall gas holdup in the Bubbly Regime (Equation 4.5) and in the Churn-Turbulent Regime (Equation 4.6), respectively

$$\varepsilon_g = \exp(9.306)\left[\frac{U_g}{\sqrt{g\,d_o}}\right]^{0.95}\left[\frac{U_l}{\sqrt{g\,d_o}}\right]^{-0.17}\left[\frac{\mu_l^4\,g}{\rho_l\,\sigma_l^3}\right]^{0.29} O.A.^{0.242} \qquad (4.5)$$

$$\varepsilon_g = \exp(10.541)\left[\frac{U_g}{\sqrt{g\,d_o}}\right]^{0.62}\left[\frac{U_l}{\sqrt{g\,d_o}}\right]^{-0.14}\left[\frac{\mu_l^4\,g}{\rho_l\,\sigma_l^3}\right]^{0.48} O.A.^{0.12} \qquad (4.6)$$

7. The axial gas holdup profile was determined by measuring the pressure drop within the stage at four different axial locations by differential pressure transducers. The trays tend to smooth out the axial gas holdup profile as compared to the column without trays.

8. The staged gas holdup measurements confirmed the fact that the effect of the gas sparger on the trayed bubble column is only noticeable in the first stage, because of the gas redistribution by the trays in the upper stages. In general, the perforated plate sparger seems to produce bubbles with an average size smaller than the equilibrium bubble size in the column. This means that there is a decrease in gas holdup in the axial direction until the bubbles reach the secondary bubble size, point after which the profile becomes flat. The opposite effect was observed with the single nozzle sparger, which seems to produce bubbles with average diameters larger than the secondary bubble size, and therefore there was a decrease in the gas holdup until the equilibrium bubble size was reached.

9. An alternative way to estimate the overall gas holdup is from numerical integration of the gas holdup profile along the column's height. It has been observed that in the column without trays, this technique gives values for the overall gas holdup, which are within the experimental error of the values yielded by the Gas Disengagement Technique. However, in the trayed bubble column, the Pressure Drop Technique underpredicts the overall gas holdup determined by the Gas Disengagement Technique by around 20%. This can be explained by noting that in the former method the pressure drop across the trays are not accounted for.

10. The presence of the trays in the column does not introduce a significant increase in the pressure drop due to the flow of the gas and liquid phases across the column. When trays of the same hole diameter and different open areas are compared, the trays with the smallest open area produce the largest pressure drop. On the other

hand, trays of the same open area and different hole diameters do not introduce statistically significant different pressure drops.

11. The placement of perforated trays inside conventional bubble columns significantly reduces the overall liquid backmixing. In some instances, a six-fold reduction was observed as compared to the column without trays.

12. Increasing the superficial gas velocity in the column enhances the gas staging effect, which subsequently increases the degree of internal liquid mixing in the individual stages. In addition, the formation of cushions of gas underneath the trays drives the recirculation of the liquid from the upper to the lower stages. The experimental results showed that there is an almost linear increase in the overall liquid mixing with U_g in the low range of superficial gas velocities (Bubbly Regime), which rapidly shifts towards a constant value when the gas velocity is further increased. The latter effect occurs when the stages become perfectly mixed and the inter-stage backmixing is balanced by the upward momentum of the flowing phases.

13. The superficial liquid velocity causes the strongest effect of all the studied factors on the overall liquid backmixing. As the liquid velocity is increased, the convection term of the mass conservation equation grows faster than the turbulent and molecular diffusion components. This results in a significant reduction of the liquid backmixing.

14. The tray open area has a stronger effect on the liquid phase backmixing reduction than the tray hole diameter. In fact, a 100% increase in the open area with trays of the same hole diameter yielded a 50% reduction in the overall liquid backmixing. On the other hand, a 200% increase in the tray hole diameter in trays of the same open area yielded also a 50% reduction.

15. The N-CSTR in Series with Backmixing Model matches the experimental liquid-phase mixing data obtained in the trayed bubble column better than the Closed-Closed Axial Dispersion Model.

16. The N-CSTR in Series with Backmixing Model can be used to quantify the extent of liquid axial backmixing in tray bubble columns. In the model, the total number of mixed stages *N* can be considered to be equal to the physical number of stages of the column. The effect of superficial gas and liquid velocities and tray geometry on the second parameter of the model, the backmixing coefficient *k*, can be summarized by the following expression:

$$k = 1.497\, U_l^{-0.244}\, U_g^{0.043}\, d_o^{0.057}\, O.A.^{0.134} - 1 \qquad (8.14)$$

Equation 8.14, was obtained by fitting the available experimental data to the model equations.

9.2 Recommendations for Future Work

The effort initiated in this work, with the purpose of acquiring a better understanding of the effect of internals in the hydrodynamics of Trayed Bubble Columns reactors, needs to be further extended. Below, there is a list with some recommendations about the steps that should be taken in the future.

1. Study of the effect of tray spacing. Due to the design constrains of the current experimental setup, the effect of tray spacing was not investigated in this study. Hence, this important design variable should be taken into consideration in future efforts. For instance, one could mount the perforated plates on a central rod, which can be easily introduced and fixed inside the column. Then the trays would slide along the rod, so that the space in between them could be varied. However, several

issues such as the fitting and sealing of the trays to the column walls would have to be resolved.

2. Determination of the radial gas holdup distribution at different axial levels. This can be achieved, for instance, by means of Gamma Ray Computer Tomography. The knowledge of the volumetric distribution of the gas phase can help us to identify issues of flow mal-distribution in the column. For instance, with this technique we could experimentally prove the formation of cushions of gas underneath the trays and study the effect of different tray designs and operating conditions.

3. The liquid flow pattern in bubble columns without trays has been extensively studied and several recirculation models have been proposed. However, in TBC there is a lack of both theoretical model formulation and experimental validation. In this matter, the experimental determination of key properties of the flow structure such as time averaged liquid velocity profiles, turbulent stresses, and eddy diffusivities can be achieved, for instance, by using Computer Automated Radioactive Particle Tracking (CARPT). The implementation of the latter technique in TBC would require the solution of several issues related to the presence of the trays inside the column.

4. Study of the effect of the nature of the liquid and gas phases. In this work, only two liquids and one gas were investigated. In order to gather useful information about the effect of the phases on the studied parameters, a larger number of gas-liquid systems should be considered.

5. Determination of the staged liquid mixing in order to quantify the degree of mixing inside the individual stages of the column. Issues that still need to be resolved include the experimental determination of meaningful tracer responses inside the reactor and model development for proper interpretation of the experimental results.

Appendix A Gas Holdup and Pressure Drop Data

Table A.1 Overall Gas Holdup Measured by the Gas Disengagement Technique.

Single Stage Bubble Column, Single Nozzle Sparger, Air-Water system										
	U_l= 0 cm/s	U_l= 0.5 cm/s			U_l= 1 cm/s			U_l= 1.5 cm/s		
U_g (cm/s)	Run #1 ε_g	Run #2 ε_g	Run #3 ε_g	Average $\bar{e}_g$	Run #1 ε_g	Run #2 ε_g	Average $\bar{e}_g$	Run #1 ε_g	Run #2 ε_g	Average $\bar{e}_g$
1	N.A.D.P	N.A.D.P	0.026	0.026	N.A.D.P	N.A.D.P	N.A.D.P	N.A.D.P	N.A.D.P	N.A.D.P
2	N.A.D.P	N.A.D.P	0.049	0.049	N.A.D.P	N.A.D.P	N.A.D.P	N.A.D.P	N.A.D.P	N.A.D.P
3	N.A.D.P	N.A.D.P	0.067	0.067	N.A.D.P	N.A.D.P	N.A.D.P	N.A.D.P	N.A.D.P	N.A.D.P
4	N.A.D.P	N.A.D.P	0.084	0.084	N.A.D.P	N.A.D.P	N.A.D.P	N.A.D.P	N.A.D.P	N.A.D.P
6	N.A.D.P	N.A.D.P	0.111	0.111	N.A.D.P	N.A.D.P	N.A.D.P	N.A.D.P	N.A.D.P	N.A.D.P
8	0.121	0.120	0.113	0.118	0.111	0.109	0.110	0.104	0.109	0.107
10	0.135	0.135	0.139	0.136	0.129	0.127	0.128	0.122	0.127	0.125
12	0.147	0.145	0.152	0.148	0.139	0.144	0.142	0.136	0.145	0.141
14	0.158	0.164	0.175	0.166	0.157	0.154	0.156	0.154	0.151	0.153
16	0.171	0.172	0.182	0.175	0.166	0.165	0.166	0.164	0.168	0.166
18	0.192	0.189	0.197	0.193	0.177	0.181	0.179	0.171	0.175	0.173
20	0.204	0.206	0.206	0.205	0.197	0.193	0.195	0.188	0.190	0.189
22	0.214	0.218	0.222	0.218	0.208	0.200	0.204	0.201	0.198	0.200
24	0.227	0.227	0.232	0.229	0.214	0.212	0.213	0.207	0.206	0.207
25	0.229	0.272	0.232	0.244	0.222	0.214	0.218	0.213	0.218	0.216

N.A.D.P = No Available Data Point.

Table A.1 Overall Gas Holdup Measured by the Gas Disengagement Technique (Continued).

Trayed Bubble Column with Tray Type #1 (10.2% O.A, d_0=1.74 cm), Single Nozzle Sparger, Air –Water System							
	U_l=0.5 cm/s			U_l=1 cm/s			U_l=1.5 cm/s
U_g (cm/s)	Run #1 ε_g	Run #2 ε_g	Average $\bar{e}_g$	Run #1 ε_g	Run #2 ε_g	Average $\bar{e}_g$	Run #1 ε_g
1	0.029	N.A.D.P	0.029	N.A.D.P	N.A.D.P	N.A.D.P	N.A.D.P
3	0.069	N.A.D.P	0.069	N.A.D.P	N.A.D.P	N.A.D.P	N.A.D.P
4	0.090	N.A.D.P	0.090	N.A.D.P	N.A.D.P	N.A.D.P	N.A.D.P
5	0.106	N.A.D.P	0.106	N.A.D.P	N.A.D.P	N.A.D.P	N.A.D.P
6	0.124	N.A.D.P	0.124	N.A.D.P	N.A.D.P	N.A.D.P	N.A.D.P
8	0.156	0.155	0.156	0.146	0.158	0.152	0.138
10	N.A.D.P	0.179	0.179	0.170	0.183	0.177	0.155
12	0.204	0.198	0.204	0.192	0.205	0.199	0.176
14	N.A.D.P	0.215	0.215	0.213	0.230	0.222	0.188
16	0.245	0.240	0.245	0.231	0.252	0.242	0.204
18	N.A.D.P	0.260	0.260	0.248	0.270	0.259	0.229
20	0.273	0.280	0.273	0.261	0.293	0.277	0.233
22	N.A.D.P	0.313	0.313	0.286	0.307	0.297	0.246
24	N.A.D.P	0.321	0.321	0.293	0.321	0.307	0.258
25	N.A.D.P	0.337	0.337	0.305	0.326	0.316	0.263

N.A.D.P = No Available Data Point

Table A.1 Overall Gas Holdup Measured by the Gas Disengagement Technique (Continued).

Trayed Bubble Column with Tray Type #2 (5.2% O.A, d_0=0.6 cm), Single Nozzle Sparger, Air-Water System						
	U_l=0.5 cm/s	U_l=1 cm/s				U_l=1.5 cm/s
U_g (cm/s)	Run #1 ε_g	Run #1 ε_g	Run #2 ε_g	Run #3 ε_g	Average $\bar{e}_g$	Run #1 ε_g
1	0.029	N.A.D.P	N.A.D.P	N.A.D.P	N.A.D.P	N.A.D.P
2	0.047	N.A.D.P	N.A.D.P	N.A.D.P	N.A.D.P	N.A.D.P
3	0.075	N.A.D.P	N.A.D.P	N.A.D.P	N.A.D.P	N.A.D.P
4	0.092	N.A.D.P	N.A.D.P	N.A.D.P	N.A.D.P	N.A.D.P
5	0.112	N.A.D.P	N.A.D.P	N.A.D.P	N.A.D.P	N.A.D.P
6	0.133	N.A.D.P	N.A.D.P	N.A.D.P	N.A.D.P	N.A.D.P
8	0.163	0.159	0.158	0.155	0.157	0.158
10	0.192	0.186	0.188	0.180	0.185	0.180
12	0.221	0.215	0.214	0.204	0.211	0.198
14	0.247	0.235	0.235	0.225	0.232	0.217
16	0.266	0.250	0.259	0.239	0.249	0.239
18	0.293	0.269	0.276	0.259	0.268	0.255
20	0.318	0.284	0.297	0.279	0.286	0.270
22	0.334	0.307	0.311	0.290	0.303	0.288
24	0.349	0.320	0.329	0.307	0.318	0.300
25	0.355	0.326	0.343	0.312	0.327	0.308

Table A.1 Overall Gas Holdup Measured by the Gas Disengagement Technique (Continued).

Trayed Bubble Column with Tray Type #3 (10.2% O.A, d_0=0.6 cm), Single Nozzle Sparger, Air-Water System			
	U_l=0.5 cm/s	U_l=1 cm/s	U_l=1.5 cm/s
U_g (cm/s)	Run #1 ε_g	Run #1 ε_g	Run #1 ε_g
1	0.031	0.033	0.038
3	0.075	N.A.D.P	N.A.D.P
4	0.095	0.098	0.102
5	0.116	N.A.D.P	N.A.D.P
6	0.136	N.A.D.P	N.A.D.P
8	0.173	0.168	0.167
12	0.227	N.A.D.P	N.A.D.P
14	N.A.D.P	0.245	0.232
16	0.277	N.A.D.P	N.A.D.P
20	0.319	0.309	0.287
24	0.353	0.340	0.323

N.A.D.P = No Available Data Point

Table A.1 Overall Gas Holdup Measured by the Gas Disengagement Technique (Continued).

Single Stage and Multistage Bubble Column, Perforated Tray Sparger, Air-Water System			
U_l=0.5 cm/s	Run #1	Run #1	Run #1
U_g (cm/s)	No Trays ε_g	Tray Type #1 ε_g	Tray Type #3 ε_g
1	0.038	0.028	0.045
3	0.066	0.090	0.089
4	0.094	0.107	0.112
5	0.121	0.134	0.131
6	0.156	0.160	0.152
8	0.181	0.192	0.185
10	N.A.D.P	0.226	0.214
12	0.217	0.263	N.A.D.P
14	N.A.D.P	N.A.D.P	0.261
16	0.230	0.330	N.A.D.P
18	N.A.D.P	N.A.D.P	0.286
20	0.254	0.373	0.302
24	0.274	0.396	0.335

N.A.D.P = No Available Data Point

Table A.1 Overall Gas Holdup Measured by the Gas Disengagement Technique (Continued).

Single Stage Bubble Column, Single Nozzle Sparger, Air-Surfactant Solution System						
	U_l= 0.5 cm/s				U_l= 1 cm/s	U_l= 1.5 cm/s
U_g (cm/s)	Run #1 ε_g	Run #2 ε_g	Run #3 ε_g	Average $\bar{e}_g$	Run #1 ε_g	Run #1 ε_g
8	0.373	0.317	0.313	0.319	0.316	0.290
12	0.530	0.446	0.401	0.438	0.428	0.393
16	0.585	0.529	0.514	0.523	0.522	0.486
20	0.683	0.608	0.590	0.613	0.603	0.564
24	0.786	0.671	0.654	0.679	0.668	0.604

Table A.1 Overall Gas Holdup Measured by the Gas Disengagement Technique (Continued).

Trayed Bubble Column with Tray Type #1 (10.2% O.A, d_0=1.74 cm), Single Nozzle Sparger, Air-Surfactant Solution System						
	U_l= 0.5 cm/s				U_l= 1 cm/s	U_l= 1.5 cm/s
U_g (cm/s)	Run #1 ε_g	Run #2 ε_g	Run #3 ε_g	Average $\bar{e}_g$	Run #1 ε_g	Run #1 ε_g
1	0.052	0.049	0.051	0.050	0.052	0.0462
4	0.234	0.232	0.240	0.235	0.212	0.197
5	N.A.D.P	N.A.D.P	0.336	0.336	0.295	0.269
6	0.461	0.380	0.384	0.409	0.379	0.334
7	N.A.D.P	N.A.D.P	0.490	0.490	0.452	0.400
8	0.544	0.450	0.559	0.534	0.509	0.472
12	0.650	0.654	0.697	0.666	0.647	0.604
16	0.753	0.783	0.749	0.761	0.717	0.691
18	0.755	0.773	0.777	0.768	0.754	0.716
20	0.782	0.784	0.800	0.789	0.780	0.743
24	0.810	0.842	0.851	0.834	0.821	0.785

N.A.D.P = No Available Data Point

Table A.1 Overall Gas Holdup Measured by the Gas Disengagement Technique (Continued).

Trayed Bubble Column with Tray type #2 (5.2% O.A, d_0=0.6 cm), Single Nozzle Sparger, Air-Surfactant Solution System			
	Run #1	Run #1	Run #1
U_g (cm/s)	U_l=0.5 cm/s ε_g	U_l=1 cm/s ε_g	U_l=1.5 cm/s ε_g
1	0.053	0.053	0.051
4	0.247	0.233	0.220
6	0.418	0.402	0.374
8	0.614	0.568	0.518
12	0.787	0.714	0.694
16	0.865	0.803	0.770
18	0.871	0.829	0.783
20	0.890	0.854	0.814
24	0.908	0.877	0.844

Table A.1 Overall Gas Holdup Measured by the Gas Disengagement Technique (Continued).

Trayed Bubble Column Tray Type #3 (10.2% O.A, d_0=0.6 cm), Single Nozzle Sparger, Air-Surfactant Solution System			
	Run #1	Run #1	Run #1
U_g (cm/s)	U_l=0.5 cm/s ε_g	U_l=1 cm/s ε_g	U_l=1.5 cm/s ε_g
1	0.052	0.048	0.048
4	0.236	0.220	0.213
5	0.324	0.303	0.280
6	0.412	0.385	0.351
7	0.518	0.473	0.422
8	0.558	0.538	0.475
12	0.768	0.692	0.659
16	0.826	0.749	0.742
18	0.855	0.820	0.778
20	0.872	0.845	0.805
24	0.906	0.869	0.839

Table A.2 Regime Transition Superficial Gas Velocity

Air-Water system, Single Nozzle Sparger, U_l=0.5 cm/s	**n_1**	**n_2**	**Transition Velocity U_g(cm/s)**
Without Trays	0.85	0.62	4.6
Tray type #1 (10.2% O.A, d_0=1.74 cm)	0.81	0.67	7.2
Tray type #2 (5.2% O.A, d_0=0.6 cm)	0.86	0.69	8.2
Tray type #3 (10.2% O.A, d_0=0.6 cm)	0.82	0.65	9.2

Air-Surfactant system, Single Nozzle sparger, U_l=0.5 cm/s	**n_1**	**n_2**	**Transition Velocity U_g (cm/s)**
Without Trays	0.95	0.64	5.3
Tray type #1 (10.2% O.A, d_0=1.74 cm)	1.14	0.24	9.4
Tray type #2 (5.2% O.A, d_0=0.6 cm)	1.17	0.20	10.1
Tray type #3 (10.2% O.A, d_0=0.6 cm)	1.16	0.24	10.1

Air-Water system, Perforated Plate sparger, U_l=0.5 cm/s	**n_1**	**n_2**	**Transition Velocity U_g (cm/s)**
Without Trays	1.06	0.43	6.5
Tray type #1 (10.2% O.A, d_0=1.74 cm)	0.96	0.45	9.3
Tray type #2 (5.2% O.A, d_0=0.6 cm)	No Data	No Data	No Data
Tray type #3 (10.2% O.A, d_0=0.6 cm)	0.82	0.52	10.2

Table A.2 Regime Transition Superficial Gas Velocity (Continued)

Air-Water system Single Nozzle sparger		n_1	n_2	**Transition Velocity U_g(cm/s)**
Tray type #1 (10.2% O.A, d_0=1.74 cm)	U_l=0.5 cm/s	0.81	0.67	7.2
	U_l=1 cm/s	0.80	0.64	5.8
	U_l=1.5 cm/s	0.81	0.58	4.1
Tray type #2 (5.2% O.A, d_0=0.6 cm)	U_l=0.5 cm/s	0.86	0.69	8.2
	U_l=1 cm/s	0.86	0.62	6.9
	U_l=1.5 cm/s	0.86	0.59	6.3
Tray type #3 (10.2% O.A, d_0=0.6 cm)	U_l=0.5 cm/s	0.82	0.65	9.2
	U_l=1 cm/s	0.78	0.65	8.0
	U_l=1.5 cm/s	0.71	0.60	7.8

Air-Surfactant system Single Nozzle sparger		n_1	n_2	**Transition Velocity U_g(cm/s)**
Tray type #1 (10.2% O.A, d_0=1.74 cm)	U_l=0.5 cm/s	1.14	0.24	9.4
	U_l=1 cm/s	1.1	0.35	9.3
	U_l=1.5 cm/s	1.13	0.38	9.6
Tray type #2 (5.2% O.A, d_0=0.6 cm)	U_l=0.5 cm/s	1.17	0.2	10.1
	U_l=1 cm/s	1.13	0.3	9.6
	U_l=1.5 cm/s	1.11	0.28	10.3
Tray type #3 (10.2% O.A, d_0=0.6 cm)	U_l=0.5 cm/s	1.16	0.24	10.1
	U_l=1 cm/s	1.17	0.35	9.3
	U_l=1.5 cm/s	1.11	0.35	10.3

Table A.3 Axial Gas Holdup Profile

Bubble Column without Trays, Single Nozzle Sparger, Air-Water system												
	U_l=0.5 cm/s				U_l=1 cm/s				U_l=1.5 cm/s			
U_g (cm/s)	PT 1	PT 2	PT 3	PT 4	PT 1	PT 2	PT 3	PT 4	PT 1	PT 2	PT 3	PT 4
	ε_g	ε_g	ε_g	ε_g	ε_g	ε_g	ε_g	ε_g	ε_g	ε_g	ε_g	ε_g
1	0.010	0.023	0.028	0.030	0.013	0.026	0.029	0.031	0.013	0.027	0.025	0.028
2	0.030	0.052	0.061	0.063	0.025	0.043	0.050	0.064	0.027	0.042	0.052	0.049
3	0.052	0.067	0.072	0.081	0.043	0.061	0.068	0.083	0.049	0.053	0.063	0.076
4	0.054	0.083	0.088	0.109	0.057	0.083	0.090	0.100	0.049	0.073	0.080	0.089
6	0.088	0.112	0.125	0.148	0.078	0.104	0.120	0.133	0.081	0.105	0.100	0.118
8	0.110	0.139	0.146	0.161	0.111	0.137	0.138	0.155	0.111	0.122	0.129	0.132
10	0.130	0.144	0.161	0.172	0.124	0.145	0.163	0.171	0.120	0.147	0.136	0.158
12	0.174	0.174	0.166	0.192	0.158	0.175	0.161	0.203	0.169	0.151	0.161	0.161
14	0.181	0.179	0.179	0.212	0.194	0.183	0.190	0.222	0.160	0.159	0.170	0.192
16	0.200	0.196	0.192	0.227	0.210	0.201	0.203	0.223	0.189	0.188	0.203	0.210
18	0.230	0.212	0.225	0.257	0.239	0.203	0.213	0.248	0.197	0.198	0.214	0.217
20	0.247	0.219	0.218	0.253	0.258	0.232	0.217	0.251	0.211	0.214	0.217	0.224
22	0.256	0.230	0.218	0.257	0.264	0.244	0.231	0.260	0.232	0.224	0.233	0.249
24	0.280	0.244	0.257	0.274	0.280	0.241	0.257	0.289	0.252	0.239	0.227	0.238

Table A.3 Axial Gas Holdup Profile (Continued)

Trayed Bubble Column with Tray Type #1 (d_o=1.74 cm, 10.2% O.A) at U$_L$=0.5 cm/s, Single Nozzle Sparger, Air-Water system				
U_g (cm/s)	PT 1	PT 2	PT 3	PT 4
	ε_g	ε_g	ε_g	ε_g
1	0.012	0.022	0.016	0.021
3	0.035	0.051	0.057	0.057
4	0.067	0.079	0.080	0.069
6	0.092	0.109	0.107	0.104
8	0.108	0.122	0.125	0.117
12	0.184	0.147	0.164	0.151
16	0.233	0.189	0.194	0.181
18	0.251	0.201	0.204	0.191

Table A.3 Axial Gas Holdup Profile (Continued)

Trayed Bubble Column with Tray Type #2 (d_o=0.6 cm, 5.2 % O.A) at Ų=1 cm/s, Single Nozzle Sparger, Air-Water System				
U_g (cm/s)	PT 1	PT 2	PT 3	PT 4
	ε_g	ε_g	ε_g	ε_g
1	0.021	0.021	0.027	0.024
3	0.037	0.037	0.070	0.080
4	0.061	0.061	0.085	0.094
6	0.092	0.092	0.116	0.115
8	0.147	0.147	0.136	0.151
12	0.207	0.207	0.178	0.196
18	0.296	0.296	0.232	0.249
20	0.347	0.347	0.246	0.269
24	0.389	0.389	0.258	0.310

Table A.3 Axial Gas Holdup Profile (Continued)

Single Stage Bubble Column at U_l=0.5 cm/s, Perforated Plate Sparger, Air-Water System				
U_g (cm/s)	PT 1	PT 2	PT 3	PT 4
	ε_g	ε_g	ε_g	ε_g
1	0.042	0.032	0.034	0.041
2	0.076	0.057	0.065	0.069
3	0.110	0.095	0.104	0.112
4	0.124	0.120	0.130	0.154
5	0.166	0.159	0.156	0.202
6	0.182	0.158	0.164	0.156
8	0.219	0.216	0.204	0.178
12	0.272	0.259	0.227	0.211
16	0.320	0.240	0.236	0.223
20	0.328	0.263	0.244	0.212
24	0.337	0.268	0.258	0.242

Table A.3 Axial Gas Holdup Profile (Continued)

Trayed Bubble Column with Tray Type #1 (d_o=1.74 cm, 10.2 % O.A) at U_l=0.5 cm/s, Perforated Plate Sparger, Air-Water System.				
U_g (cm/s)	PT 1	PT 2	PT 3	PT 4
	ε_g	ε_g	ε_g	ε_g
1	0.031	0.032	0.027	0.036
3	0.096	0.091	0.075	0.098
4	0.143	0.121	0.103	0.134
6	0.192	0.156	0.126	0.187
8	0.264	0.196	0.175	0.255
12	0.398	0.228	0.219	0.379
20	0.548	0.303	0.310	0.528
24	0.550	0.330	0.371	0.524

Table A.3 Axial Gas Holdup Profile (Continued)

Trayed Bubble Column with Tray Type #2 (d_o=0.6 cm, 5.2 % O.A) at U_l=1 cm/s, Perforated Plate Sparger, Air-Water System.				
U_g (cm/s)	PT 1	PT 2	PT 3	PT 4
	ε_g	ε_g	ε_g	ε_g
1	0.033	0.027	0.024	0.026
3	0.101	0.086	0.074	0.071
4	0.126	0.097	0.085	0.081
6	0.183	0.128	0.114	0.112
8	0.260	0.152	0.152	0.143
12	0.382	0.191	0.194	0.186
20	0.547	0.270	0.315	0.268
24	0.529	0.316	0.361	0.305

Table A.4 Overall Gas Holdup Data from Integration of Axial Gas Holdup Profile

Single and Multistage Bubble Column with Tray Type #1 (d_o=1.74 cm, 10.2% O.A), and Type #2 (d_o=0.6 cm, 5.2% O.A). Single Nozzle Sparger, Air-Water System			
U_g (cm/s)	Without Trays U_l=0.5 cm/s	Tray type #1 U_l=1 cm/s	Tray type #2 U_l=1 cm/s
	ε_g	ε_g	ε_g
1	0.026	0.017	0.025
3	0.046	0.049	0.070
4	0.056	0.072	0.085
6	0.064	0.099	0.113
8	0.084	0.113	0.145
12	0.111	0.149	0.189
18	0.171	N.A.D	0.247
20	0.192	0.183	0.266
24	0.217	0.195	0.295

Table A.4 Overall Gas Holdup Data from Integration of Axial Gas Holdup Profile (Continued)

Single and Multistage Bubble Column with Tray Type #1 (d_o=1.74 cm, 10.2% O.A) and Type #2 (d_o=0.6 cm, 5.2 % O.A.), Perforated Plate Sparger, Air-Water System			
U_g (cm/s)	No Trays U_l=0.5 cm/s	Tray Type #2 U_l=1 cm/s	Tray Type #3 U_l=1 cm/s
	ε_g	ε_g	ε_g
1	0.035	0.026	0.030
2	0.064	N.A.D.P	N.A.D.P
3	0.102	0.082	0.086
4	0.128	0.094	0.118
5	0.164	N.A.D.P	N.A.D.P
6	0.163	0.128	0.153
8	0.207	0.164	0.204
12	0.243	0.216	0.265
16	0.246	N.A.D.P	N.A.D.P
20	0.258	0.321	0.365
24	0.269	0.358	0.397

N.A.D.P = Not Available Data Point

Table A.5 Pressure Drop across the Trays

Trayed Bubble Column with Tray Types #1, #2, and #3 at U_l=0.5 cm/s and 1.5 cm/s. Single Nozzle Sparger, Air-Water System						
	Tray type #1		Tray type #2		Tray type #3	
U_g (cm/s)	U_l=0.5 cm/s	U_l=1.5 cm/s	U_l=0.5 cm/s	U_l=1.5 cm/s	U_l=0.5 cm/s	U_l=1.5 cm/s
	ΔP (inches of water)	ΔP (inches of water)	ΔP (inches of water)	ΔP (inches of water)	ΔP (inches of water)	ΔP (inches of water)
0	4.019	4.114	4.021	4.195	4.004	4.053
1	3.882	4.012	3.861	4.085	3.822	3.933
3	3.595	3.878	3.627	3.925	3.473	3.677
6	3.368	3.566	3.280	3.715	3.214	3.467
12	2.987	3.335	3.085	3.484	2.943	3.181
16	2.810	3.303	3.002	3.442	2.767	3.052
20	2.765	3.163	2.924	3.497	4.004	4.053

* The data reported in the above table is based on the arithmetic mean of the values measured at three different tray locations

Appendix B Calibration and Effect of Temperature in the Conductivity Probes

The observed electrical conductance (inverse of resistance) of a liquid solution depends inversely on the distance between the electrodes *d* and directly on their surface area *A*.

$$\frac{1}{R} = k\frac{A}{d} \tag{B.1}$$

For a given cell with fixed electrodes, the ratio *d/A* is a constant which is called the cell constant *K* (cm^{-1}). The conductivity *k* is then determined by multiplying the measured conductance *1/R* by the cell constant *K*. The MI-900 Series probes used in this work are manufactured to have $K=1cm^{-1}$. However, small variations of the distance between the electrodes, or bare spots on their platinum coating can change the cell constant value. On the other hand, the electrical properties of a cell do vary with the electrolyte concentration and non-linear responses can be expected at high concentration ranges. Therefore, it is necessary to calibrate the probes regularly with their respective conductance meters to always be aware of the exact proportional relationship between the meter output and the tracer concentration.

Solutions of KCl of known concentrations (0, 10^{-5}, $5x10^{-5}$, 10^{-4}, $2.5x10^{-4}$, and $5x10^{-4}$ g/ml) were prepared by dissolving the corresponding amounts of salt into 100 ml of deionized water. The readings of the meters (in volts) were taken after dipping each of the probes into the prepared solutions at room temperature. Thus, the calibration curves for probes #1 and #2 with their respective conductance meters #1 and #2 can be constructed (Figure B.1). Note that the solution of concentration $5x10^{-4}$ g/ml was not used to obtain the equation for the calibration curves since the probes started showing

non-linear behavior beyond this concentration. However, the range of values reached inside the column is always within the linear region of the calibration curves.

The conductivity of a solution is highly sensitive to changes in temperature and thus differences of only a few degrees centigrade can change the measured conductivity by a statistically significant amount. Although the temperature effect on conductivity is non-linear, within small ranges of temperature change, it can be modeled as a linear process. By convention, the conductivity of a solution is defined as the conductivity that it exhibits at 25°C, k_{25}. Then, the conductivity at temperature T, k_T, can be calculated by the following equation *Lide, 1992.*

$$k_T = k_{25}(1+\alpha\Delta T) \qquad \text{(B.2)}$$

Here a is the temperature coefficient of conductivity (change per Celsius degree) and DT is the difference between current temperature T and 25 °C. Since the present setup does not have a temperature control system to keep isothermal conditions, it was decided to correct the conductivity measurements for temperature and refer always to T=25 °C.

In order to calculate a, the conductivity of two solutions of different concentrations ($5x10^{-5}$ and 10^{-4} g/ml) was measured at three different temperatures: 20, 25, and 30°C (Figure B.2). Then, straight lines were fitted and the temperature coefficient a was determined from the slope of the lines. The average a for the two concentrations was taken and the resultant value turned out to be 3% change per degree Celsius. Accordingly, the measured conductivity k_T needs to be corrected by Equation B.3 when the temperature of the liquid phase is not equal to 25 °C.

$$k_T = k_{25}[1+0.03(T-25)] \qquad \text{(B.3)}$$

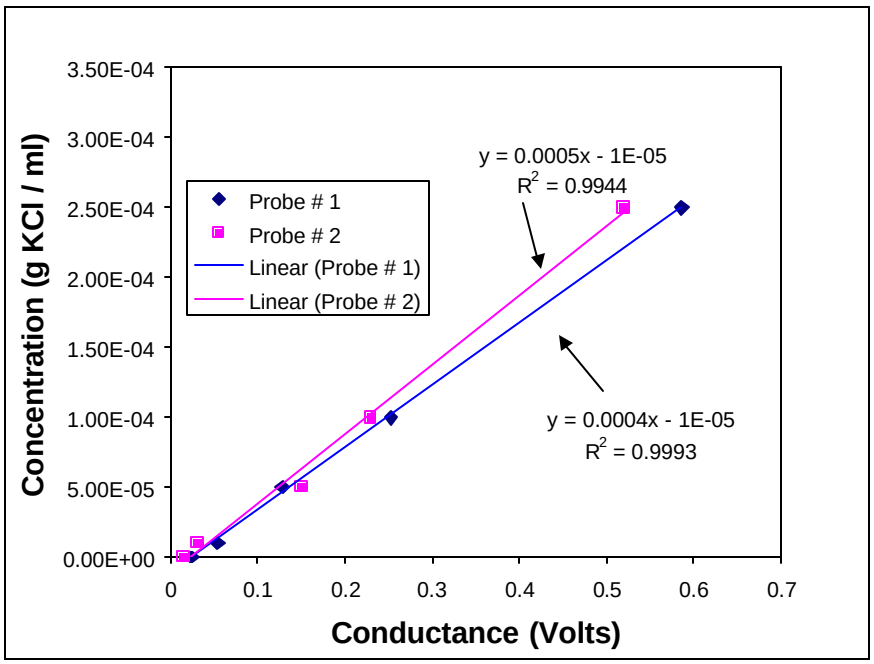

Figure B.1 Calibration Curves for Conductivity Probes #1 and #2 at 25 ^{O}C.

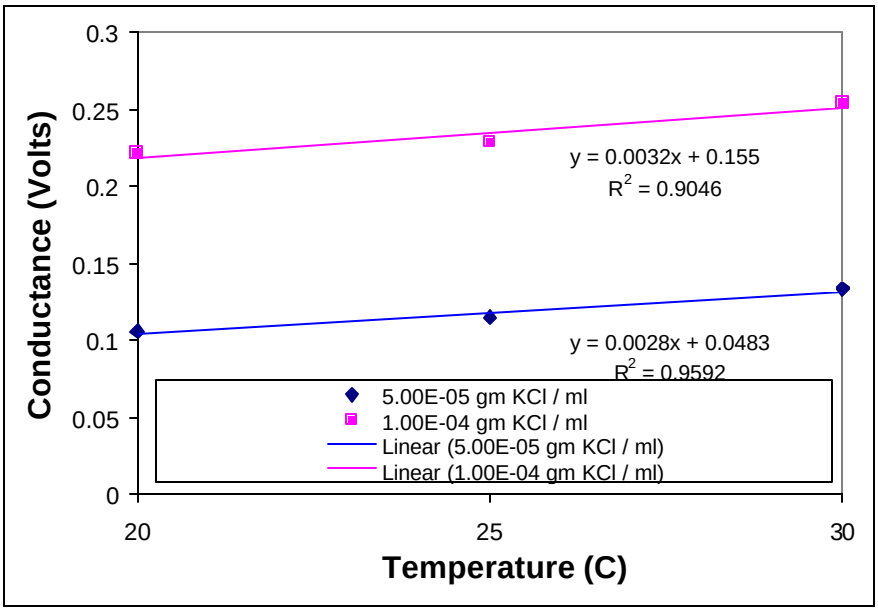

Figure B.2 Estimation of the Coefficient Temperature a..

Appendix C Characteristic Response Time of the Conductivity Probes

When acquiring point liquid phase tracer responses, we need to set the rate at which the conductivity measurements are taken (sampling frequency). It is not wise to sample at a frequency higher than that of the probe characteristic response frequency (inverse of response time), because then one will be just getting an enormous amount of non-significant data. Therefore, the knowledge of the response time of the probe along with the characteristic time of the process that one is interested in capturing (the tracer wash-out curve, in this case) is necessary to select the appropriate sampling frequency.

The approximate characteristic response time of the probes was experimentally determined by modeling the time that it takes for the probe signal to respond to a sudden step change in the medium conductivity by a first order response process (Figure C.1). The conductivity probe, perfectly dried, was dipped into tap water and its response recorded at a sampling frequency of 100 Hz. The described experiment was repeated five times, and the mean value at each sampling time was used to fit a first order response process (modeled response). The model equation for a first order response process is:

$$C=Co\,[1-\exp(-t/\tau)] \qquad (C.1)$$

Co is the final conductivity of the tap water and τ is the response time, which is the time that it takes for the probe to relax up to 63% of its final value.

According to the Nyquist criterion, one can only capture the physical phenomena occurring at a frequency half of the sampling frequency at which it was acquired. One cannot pretend to capture any phenomenon that is occurring at a frequency 3-5 times

faster than the time it takes for the measuring device to relax up to 95-99% of the final value. The time for a 95% relaxation using these probes was 467 milliseconds, which corresponds to a frequency of 2 Hz. Therefore five times this frequency is 10 Hz, and this is the value at which all the tracer experiments were sampled in this work.

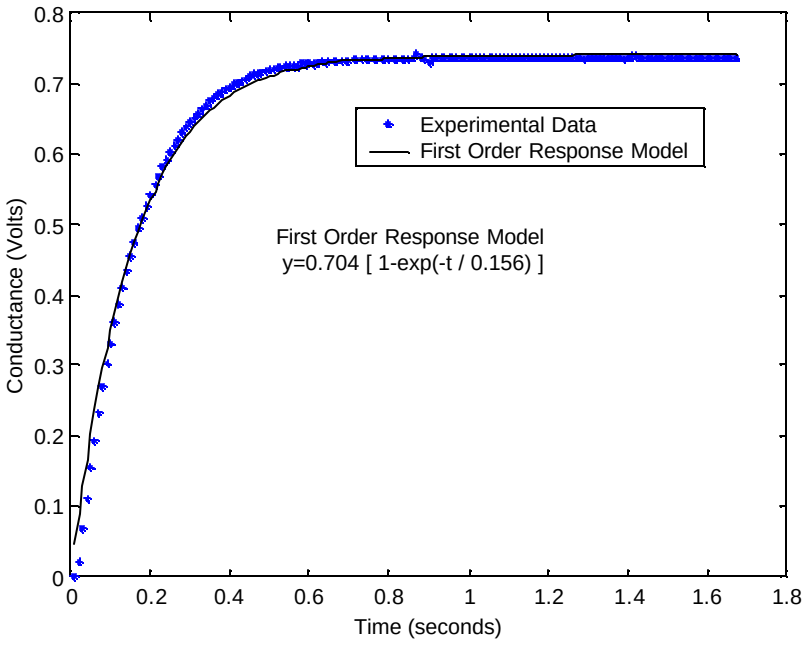

Figure C.1 Experimental Conductivity Probe Signal and First Order Model Fit.

Appendix D Experimental Procedure for Tracer Experiments

The following steps were followed when performing the tracer experiments:

1. The feeding tank was filled half way (~150 gallons) with tap water (city water). Then, the liquid pumps were switch on and the water was circulated through the system in a closed loop until isothermal conditions were reached. Once constant temperature was achieved, the liquid flow was stopped and the liquid outlet hose was removed from the feeding tank and hooked to the room sewer in order to avoid tracer recirculation during the experiments.

2. The gas and liquid flow rates were set at the chosen values with the help of the rotameters.

3. The data acquisition system was programmed to acquire data during the selected sampling period at a sampling frequency of 10 Hz. The total sampling time was varied between 15 to 30 minutes, including a short period of 2 to 3 minutes prior to injection. This was used as base line. In general, the rule of thumb of five times the liquid spatial residence time was observed.

4. The syringe was filled with 10 ml of 0.2 gm of KCl/ml of solution (20 gm of KCl).

5. The acquisition system was started and after the 2-3 minutes left for establishing the base line (this was controlled by a stopwatch), the tracer was injected as a pulse input into the system with the syringe. The injection time was always less than a second.

6. Once the sampling period was over, the data acquisition system stopped acquiring data and generated a text file containing the response of the probes to the tracer pulse

during the corresponding sampling time. Then, the liquid and gas flows were stopped and the liquid in the column was drained.

As mentioned earlier, the presence of the liquid mixing cup device at the top of the column created an extra pressure drop in the liquid outlet pipe that raised the total height of the G-L bed in the column. This increment was a function of the operating conditions and the tray type. Therefore, extreme care was taken when setting the gas and liquid flowrates so as not to flood the column.

Appendix E Ideal Pulse Input Assumption

In Section 7.1, it was explained that the convolution integral (Equation 7.1) can be easily evaluated if the stimulus signal (tracer injection) can be approximated to an ideal δ−Dirac function. The previous is possible because since the system's transfer function is directly given by the probe's response signal measured at the column's outlet.

The introduction of an ideal pulse input signal depends on the speed and reproducibility of the tracer injection. In this sense, it is clear that the longer the residence time of the tracer in the reactor, the closer the signal is to an ideal pulse input.

Prenosil et al., 1968 claimed that for tracer experiments in bubble columns, the ratio of the injection time *Dt* to the tracer's mean residence time $\bar{t}$ has to be smaller than 0.05 in order to consider the approximation to an ideal pulse input acceptable.

$$\frac{\Delta t}{\bar{t}} < 0.05 \qquad \text{(E.1)}$$

The injection time can be estimated from the width of the tracer inlet response signal, whereas the tracer's mean residence time is the first moment of the output response signal. Figure E.1 graphically illustrates this.

As an example, $\Delta t/\bar{t}$ has been estimated for tray type #2 (d_o=0.6 cm, 5.2% O.A.) at U_g=4 cm/s and at three different superficial liquid velocities (U_l=0.5, 1.0, and 1.5cm/s) in Table E.1. The ratio turned out to be always smaller than 0.05, and therefore the approximation of ideal pulse input can be considered acceptable. The above has been also confirmed at different experimental conditions.

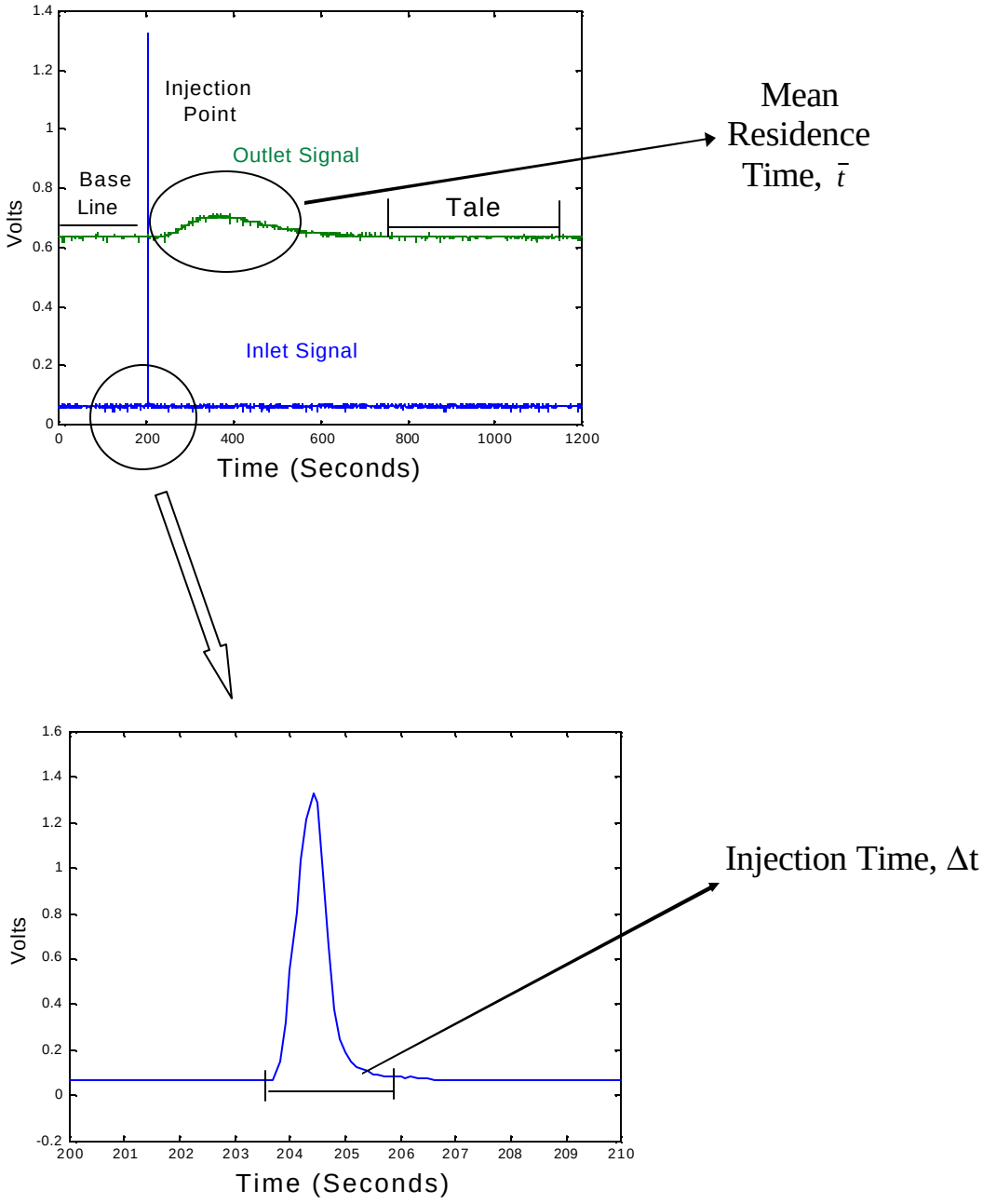

Figure E.1 Schematic Representation of the Estimation of $\Delta t / \bar{t}$ from the Outlet and Inlet Experimental Tracer Responses.

Table E.1 Estimation of $\Delta t / \bar{t}$ for Tray Type #2 (d_o=0.6 cm, 5.2 % O.A.) at U_g=4 cm/s and U_l=0.5, 1.0, and 1.5 cm/s.

$\Delta t / \bar{t}$	**U_l (cm/s)**	**U_g (cm/s)**	**Tray #**
7.8 / 380.97 = **0.02**	0.5	4	2
3.9 / 207.61 = **0.019**	1	4	2
2.6 / 143.39 = **0.018**	1.5	4	2

Appendix F Filtering Methodology to Extract Liquid Phase Tracer Responses in G-L Flows

The extraction of a clean tracer response curve in gas-liquid flows by conductivity methods is not straightforward due to the systematic lowering of the measured signal caused by the continuous bubble passage. The existing standard filtering techniques can easily remove the high frequency components of the signal caused by the so-called white noise, which is random in nature and therefore has a zero time-average value. However, the continuous bubble passage adds a biased contribution to the noise, which can not be removed by the standard filtering algorithms without under predicting the measured conductivity. In general, the standard filtering algorithms are designed based on the assumption that the time averaged value of the noise is zero, and therefore fail to work with signals whose noise contribution does not follow this assumption.

Gupta et al., 1999 came up with a very simple, but powerful scheme to overcome the problem. Their novel idea was to couple the standard Butterworth filters with an iterative methodology, which it is repeated until a tolerance criterion is met. The flowchart of the scheme is presented in Figure F.1.

Basically, the Raw Signal $RS(t)$ is first filtered by a Butterworth filter of order n_B and cutoff frequency f_{cutoff}, from which a Filtered Signal $FS(t)$ is generated. Then, the signals RS and FS are compared at each time step and the following action is taken: if $FS(t_i)$ is larger than or equal to $RS(t_i)$, then the Filtered Signal is accepted, otherwise it is made equal to the Raw Signal. The resulting transformed signal, FTS, is called Filtered plus Thresholded Signal. The next step is to compute the residual value between RS and FTS, called RES. If RES is smaller than a selected tolerance TOL, then the corresponding FTS is taken to be the Final Filtered Signal FFS, otherwise the process is reinitialized

using *FTS* as the new raw signal. The described algorithm was implemented in Matlab™ Ver. 5.3, The Math Works Inc.

The selection of values for the adjustable parameters of the filter is a trial and error procedure. A too strict tolerance could result in a lack convergence or in an excessive smoothing of the signal, with the subsequent loss of information.

In order to show the performance of the new filter, it has been tested with a measured tracer response signal obtained inside the trayed bubble column. Since the probe is now located inside the column, the measured conductivity signal is extremely noisy due to the continuous bubble passage.

The original unfiltered signal, which is presented in Figure F.2, was obtained at U_l=1 cm/s and U_g=1 cm/s using air-water as gas-liquid system. It is worth noting that even at such low superficial gas velocities, the signal disturbances due to the bubble passage are quite significant.

In Figure F.3, the outcome of the new filter algorithm is compared with the conventional filter. The blue line is the resultant signal filtered by a 3rd order lowpass Butterworth filter at a cutoff frequency equal to 0.2 Hz, whereas the black and red lines correspond to the signals processed with the new filtering methodology at the same cutoff frequency with tolerances equal to 6 10^{-4}, and 2 10^{-4}, respectively. From simple visual comparison of Figures A.6.2, and A.6.3, it is clear that the standard Butterworth filter underpredicts the conductivity signal. On the contrary, the novel filter does a much better job not only in not underpredicting the response signal, but also in extracting a smoother signal at the same cut-off frequency.

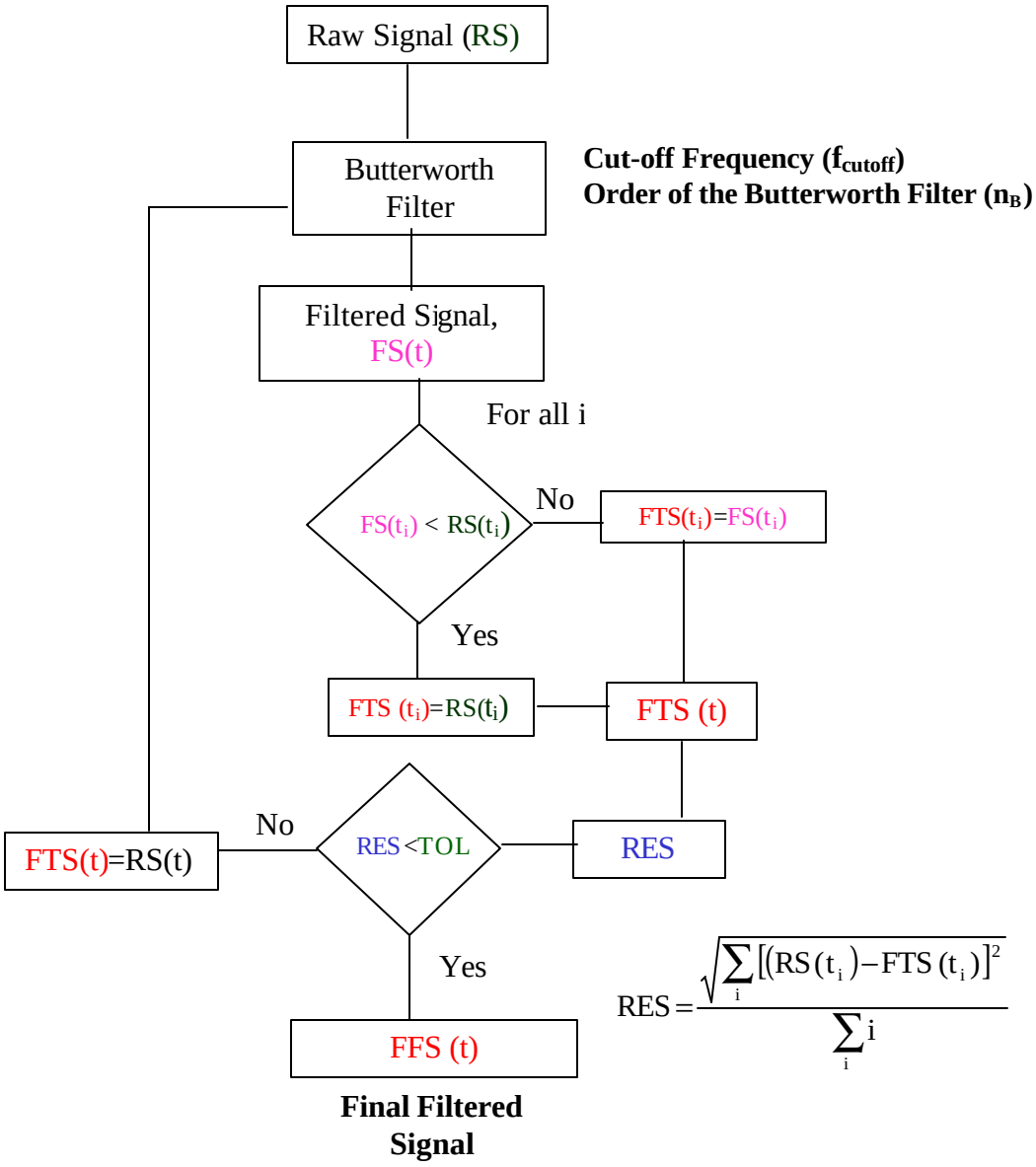

Figure F.1 F1owchart of the New Filter Algorithm Developed by *Gupta et al., 1999*

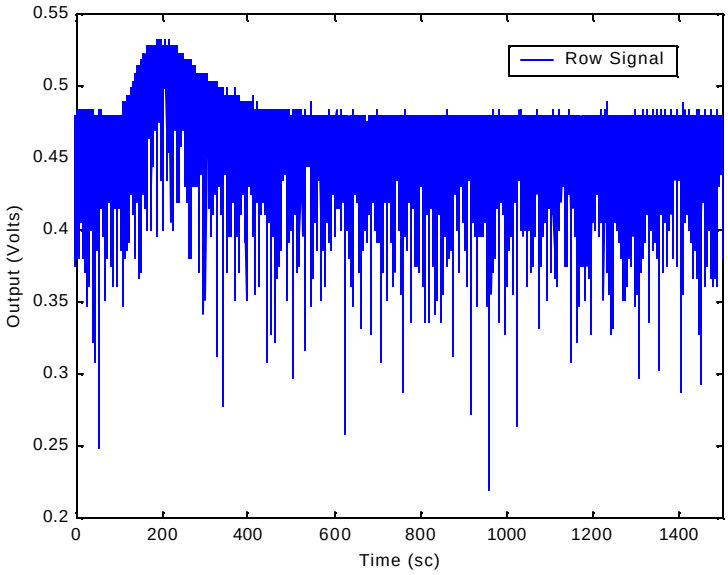

Figure F.2 Tracer Response Curve Obtained in the Trayed Bubble Column at U_g=1cm/s and U_l=1cm/s.

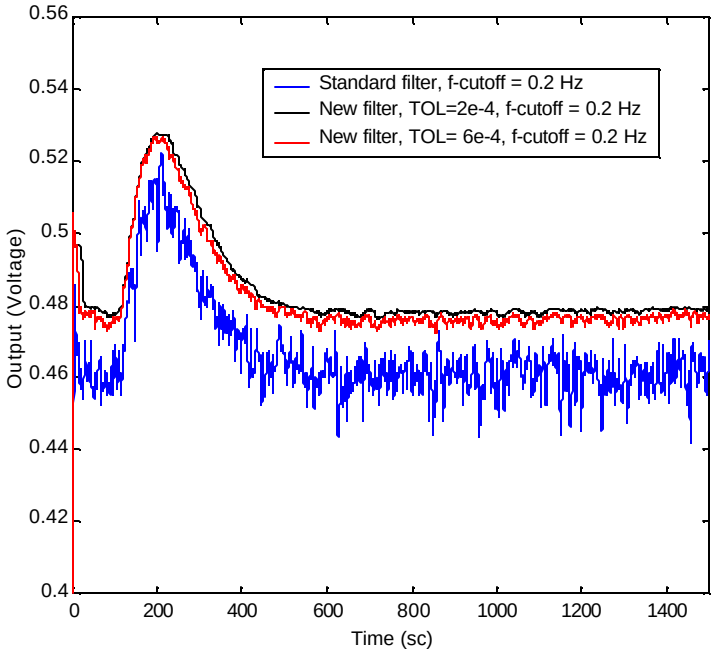

Figure F.3 Performance of the Standard and Novel Filter Algorithms in Filtering the Raw Tracer Response Signal (Figure F.2).

Appendix G Base Line Correction for the Drift in the Experimental Outlet Signal

For some of the experimental runs, a small drift was observed on the tail of the signal with respect to the base line. Since the liquid that has traveled through the column is always discarded and never returned to the system, the tail should always come back to the base line level after a sufficient period of time. The causes of this displacement were numerous and in general it was not possible to eliminate their source. Because even a small displacement of the tail can introduce large errors in the determination of the curve's variance, it was decided to correct it and bring the base line and tail to the same level.

Given the experimental tracer response curve *y(t)* versus t (Figure G.1). Let us assume that the drift of the tracer signal occurs linearly over the time of the experiment. We can draw a straight line, y (drift), between two points located at the end of base line (t_1, y_1) and at the tail section (t_2, y_2), respectively. The equation of the straight line can be written as follows:

$$y\,(drift) = y_1 + \left(\frac{y_2 - y_1}{t_2 - t_1}\right)(t - t_1) \qquad \text{(G.1)}$$

The corrected response signal *y*(t)* can be obtained by subtracting the *y (drift)* from the observed signal *y (t)* as follows:

$$y^*(t) = y(t) - y\,(drift) = y\,(t) - \left[y_1 + \left(\frac{y_2 - y_1}{t_2 - t_1}\right)(t - t_1)\right] \qquad \text{(G.2)}$$

This correction brings both the base line and the tail of the curve to zero.

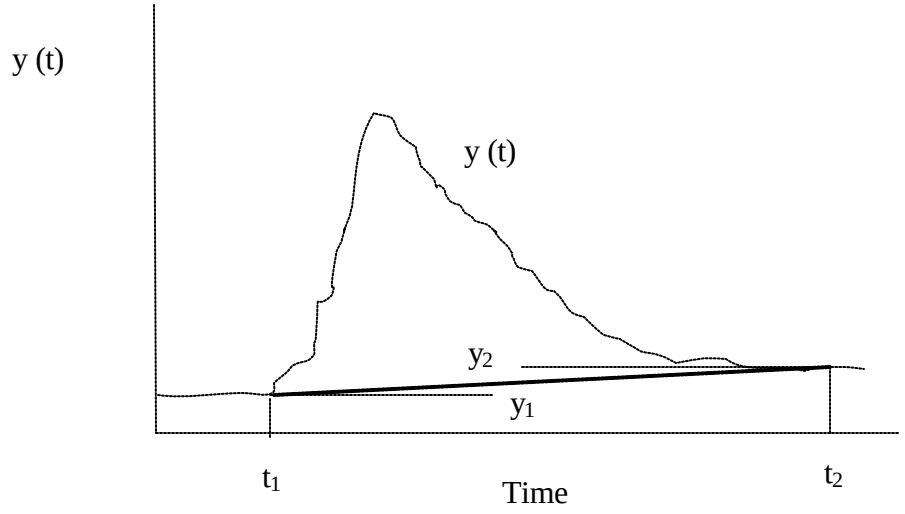

Figure G.1 Schematic Representation of an Experimental Tracer Response Signal y(t), with Tail Displacement.

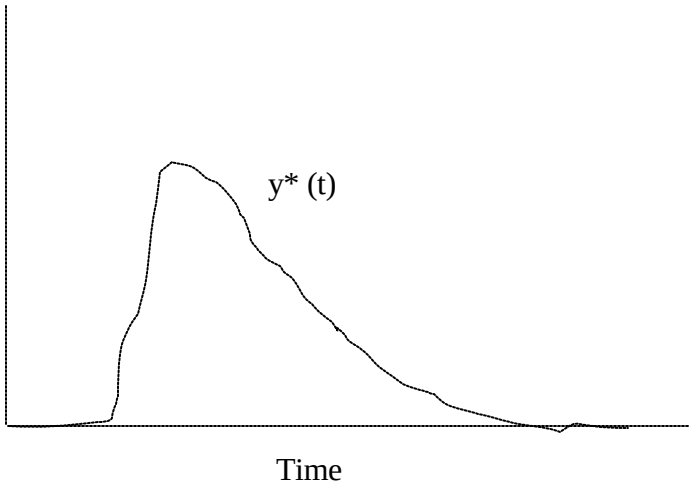

Figure G.2 Schematic Representation of the Corrected Tracer Response, *y*(t).*

Appendix H Parameter Estimation Procedures

Time Domain Fitting

This method fits the model parameters to the experimental data by minimizing the square root of the sum of the squares of the differences between the experimental and the model transfer functions at each time step.

$$R^t(P_j) = \sqrt{\sum_{i=1}^{t_{total}} \frac{\left[E_E(q_i) - E_M(q_i, P_1, P_2, .., P_j, .., P_m)\right]^2}{t_{total} - m}}$$

$$i = 1, .., t_{total}$$
$$j = 1, .., m \qquad \text{(H.1)}$$
$$t_{total} >> m$$

Where $R^t(P_j)$ is the objective function to be minimized (the superindex t stands for time domain); E_E, and E_M are the experimental and model dimensionless exit age density functions, respectively; q_i, is the dimensionless time at the i^{th} time step; P_j, is the j^{th} model parameter; t_{total}, is the total number of sample points; and m is the total number of model parameters. The experimental transfer function E_E is the tracer response signal measured at the outlet of the column, whereas the model transfer function E_M is estimated by solving the corresponding time domain model equations.

The minimization of $R^t(P_j)$ constitutes a non-linear optimization problem, which can be efficiently solved for instance by the Levenberg-Marquardt Method (*Marquardt, 1963 and Levenberg, 1944*), which is a combination of the popular Gauss and the Steepest Descent methods.

Laplace Domain Fitting

The derivation of a time domain analytical expression for the model transfer function E_M is not always possible and in many occasions the model equations have to be solved by numerical methods. Thus, the optimization routine may become very time consuming since it has to find the solution of the model equations at each parameter iteration.

As a matter of fact, for many models it is much easier to estimate the corresponding analytical expression for the transfer functions in the Laplace domain. For instance, the transformation into the Laplace domain of a system of ordinary differential equations yields a system of simple algebraic equations from which the system transfer function can be easily extracted.

Although one needs to evaluate the Laplace transform of the experimental time domain E-curve, this is a straightforward operation carried by integrating the following equation at arbitrary values of the dimensionless Laplace variable s*, defined as $s^* = s\,\bar{t}$.

$$E_E(s*) = \int_0^\infty E_E(q)\exp(-s^* q)\,dq \qquad \text{(H.2)}$$

In the above equation, $E_E(q)$ is the experimental dimensionless outlet tracer response function to a δ-Dirac input function, and $E_E(s^*)$ is the experimental transfer function in the Laplace domain. The evaluation of Equation H.2 can be done numerically by approximating the integral as a summation over a finite domain at selected values of s^* (Equation H.3).

$$\overline{E}_E(s_j^*) = \sum_{i=0}^{\theta_{final}} \overline{E}_E(\theta_i)\,\exp(-s_j^*\theta_i)\Delta\theta_i \qquad \text{(H.3)}$$

Now the objective function that needs to be minimized R^L can be written as follows:

$$R^L(s_i^*, P_j) = \sqrt{\sum_{i=1}^{t_{total}} \frac{\left[\overline{E}_E(s_i^*) - \overline{E}_M(s_i^*, P_1, P_2, .., P_j, .., P_m)\right]^2}{t_{total} - m}}$$

$$i = 1, ..., t_{total} \qquad \text{(H.4)}$$

$$j = 1, ..., m$$

Here, $\overline{E}_E$ and $\overline{E}_M$ are the experimental and model dimensionless transfer functions respectively in the Laplace domain; t_{total} and m are the total number of sample points and model parameters, respectively.

However, the Laplace domain fitting also has some drawbacks. As opposed to the model parameter estimation in the time domain, where the limits of the domain are explicitly given by the initial and the final values of the time series vector, in the Laplace domain the upper and lower limits of the Laplace variable s^* have to be properly selected. *Hopkins et al., 1969* have pointed out that larger errors in the determination of the model parameters can be made if the range of s* is not chosen carefully. In general, too low or too large values of s* are to be avoided.

Appendix I Analysis of Reproducibility

The large amount of different experimental conditions covered in this work made the repetition of tracer experiments at every single condition not feasible due to the time constrain for the completion of the work. Instead, the tracer experiments were repeated eight times at selected conditions, from which the experimental error of the technique was determined. In fact, one can repeat all the data analysis and model fitting estimation (e.g. experimental variances, and model parameters) for the eight-times repetition experiments. Thus, an estimation of the experimental variability based on an eight-sample population is available. Then, one can take the calculated experimental error and approximately extend it to experiments performed at different conditions.

Below, the analysis corresponding to one of the sets of the eight-times repetition experiments performed with tray type #3 (d_o=0.6 cm and 10.2 % O.A.) at U_l = 1 cm/s and U_g = 8 cm/s is presented.

Figure I.1 shows the eight experimental E-curves after the corresponding filtering and transformation into dimensionless form. From the figure, it can be seen how the E-curves overlap in top of each other, thereby proving a good experimental reproducibility.

In Table I.1, the analysis of the experimental tracer E-curves is given (mass of tracer, residence time, and experimental variance), along with the results of the parameter model estimation for the N-CSTR in Series with Backmixing Model (N, k, and R^T_B).

Table I.2 lists the mean values and the standard deviations of the parameters in Table I.1. For a t-distribution with seven degrees of freedom (d.f.=n-1=8-1=7), an interval of $\pm 2.365\ S_d$ around the mean value would bound a 95 % confidence interval. S_d is the

standard deviation based on a population of eight samples. As an approximation, for any given experimental condition in which repetition is not available, we can assign this confidence interval to the corresponding variances, model parameters, and/or residuals obtained from the experimental E-curves and the model parameter estimation procedure.

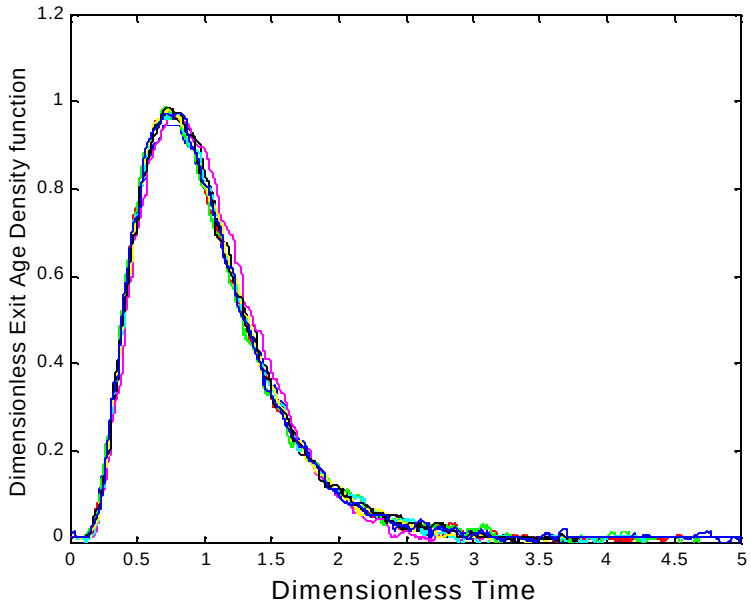

Figure I.1 Dimensionless E-curves of the Eight-Times Repetition Experiments Performed in Trayed Bubble Column with Tray Type #3 (d_o=0.6 cm, 5.2 % O.A.) at U_l = 1 cm/s and U_g = 8 cm/s.

Table I.1 Analysis of the E-curves Corresponding to the Eight-Times Repetition Experiments.

Experimental				**N-CSTR with Backmixing Model**		
Run #	**Mass Tracer (g)**	$\bar{t}$ **(s)**	s^2_E	**N**	**k**	R^T_B
1	2.04	197.70	0.228	5	0.128	9.50E-03
2	2.16	203.86	0.238	5	0.150	1.43E-02
3	2.10	197.68	0.213	6	0.227	8.46E-03
4	2.14	202.43	0.236	6	0.327	9.80E-03
5	1.98	198.06	0.216	5	0.139	1.51E-02
6	2.03	196.75	0.220	6	0.260	1.02E-02
7	2.12	198.32	0.225	6	0.271	7.48E-03
8	2.13	202.03	0.238	6	0.284	9.70E-03

Table I.2 Mean and Standard Deviation Values of the Parameters Listed in Table I.1

	Mean Value	**Standard Deviation**
Mass of Tracer (gm)	2.09	0.063
Residence Time (sc)	199.6	2.71
s^2_E	0.227	0.010
k	0.223	0.075
R^T_B	0.010	0.003

Appendix J Experimental Liquid Phase Mixing Data

Table J.1 Analysis of the Experimental Overall Tracer Response Curves

Tray Type #1 (d_o=1.74 cm, 10.2% O.A), U_l=0.5 cm/s					
U_g (cm/s)	**Mass of Tracer (g)**	**RT (sec)**	**s^2 (sec^2)**	s^2_D	$N = 1/ s^2_D$
1	1.67	420.3	42446	0.240	4.16
4	1.71	406.7	53624	0.324	3.08
8	1.79	388.3	49786	0.330	3.03
12	1.83	373.8	51491	0.368	2.71
16	1.46	337.7	44027	0.386	2.59
20	1.73	310.3	44740	0.389	2.15

Tray Type #1, (d_o=1.74 cm, 10.2% O.A), U_l= 1 cm/s					
U_g (cm/s)	**Mass of Tracer (g)**	**RT (sec)**	**s^2 (sec^2)**	s^2_D	$N = 1/ s^2_D$
1	1.73	226.0	10510	0.206	4.86
4	1.83	214.4	10341	0.225	4.45
8	1.83	202.8	9528	0.232	4.32
12	1.94	188.0	7708	0.218	4.59
16	1.85	190.0	9277	0.257	3.89

Table J.1 Analysis of the Experimental Overall Tracer Response Curves Continued)

Tray Type #1, (d_o=1.74 cm, 10.2% O.A), U_l= 1.5 cm/s					
U_g (cm/s)	**Mass of Tracer (g)**	**RT (sec)**	**s^2 (sec^2)**	s^2_D	$N = 1/ s^2_D$
1	2.03	150.4	3843	0.170	5.88
4	2.28	160.4	4214	0.164	6.11
6	2.60	135.5	3654.	0.199	5.44
8	1.81	131.4	3198.	0.184	5.13
12	1.99	133.6	3479	0.195	4.88
16	2.62	130.8	3505	0.205	5.44

Tray Type #2, (d_o=0.6 cm, 5.2% O.A), U_l= 0.5 cm/s					
U_g (cm/s)	**Mass of Tracer (g)**	**RT (sec)**	**s^2 (sec^2)**	s^2_D	$N = 1/ s^2_D$
0	2.25	466.4	33498	0.154	6.49
1	1.86	428.8	43689	0.238	4.21
2	2.04	431.3	49757	0.268	3.74
4	1.95	402.8	44300	0.273	3.66
6	1.98	390.7	41208	0.270	3.71
8	2.03	369.7	37086	0.271	3.68
12	2.15	361.6	38060	0.291	3.44

Table J.1 Analysis of the Experimental Overall Tracer Response Curves (Continued)

Tray Type #2, (d_o=0.6 cm, 5.2% O.A), U_l= 1 cm/s					
U_g (cm/s)	**Mass of Tracer (g)**	**RT (sec)**	**s^2 (sec^2)**	s^2_D	$N = 1/ s^2_D$
0	2.05	228.7	5837	0.112	8.96
1	2.13	214.7	8809	0.191	5.23
4	2.20	212.4	8755	0.194	5.15
6	2.16	202.2	8180	0.200	5.00
8	2.17	196.4	7946	0.206	4.85
12	1.86	187.4	7483	0.213	4.69
14	2.11	179.0	7337	0.229	4.36

Tray Type #2, (d_o=0.6 cm, 5.2 %O.A), U_l= 1.5 cm/s					
U_g (cm/s)	**Mass of Tracer (g)**	**RT (sec)**	**s^2 (sec^2)**	s^2_D	$N = 1/ s^2_D$
0	2.21	151.7	2462	0.107	9.35
1	2.00	147.8	3846	0.176	5.68
4	1.99	141.4	3457	0.173	5.78
6	2.04	137.3	3379	0.179	5.58
8	2.04	132.1	2984	0.171	5.85
12	2.01	127.9	3185	0.195	5.14

Table J.1 Analysis of the Experimental Overall Tracer Response Curves (Continued)

Tray Type #3, (d_o=0.6 cm, 10.2% O.A.), U_l= 0.5 cm/s					
U_g (cm/s)	**Mass of Tracer (g)**	**RT (sec)**	**s^2 (sec^2)**	s^2_D	$N = 1/ s^2_D$
1	1.90	401.2	35555	0.221	4.53
4	1.78	381.0	38090	0.262	3.81
8	1.75	355.2	37602	0.298	3.36

Tray Type #3, (d_o=0.6 cm, 10.2% O.A.), U_l= 1 cm/s					
U_g (cm/s)	**Mass of Tracer (g)**	**RT (sec)**	**s^2 (sec^2)**	s^2_D	$N = 1/ s^2_D$
1	2.14	215.3	8832	0.191	5.25
4	2.08	218.3	10495	0.220	4.67
8	2.04	197.7	8911	0.228	4.39
12	2.05	188.3	8794	0.248	4.03

Column without Trays, U_l= 0.5 cm/s					
U_g (cm/s)	**Mass of Tracer (g)**	**RT (sec)**	**s^2 (sec^2)**	s^2_D	$N = 1/ s^2_D$
0	2.44	486.9	29751	0.126	7.97
1	2.43	471.8	128215	0.576	1.74
8	2.00	375.0	95625	0.680	7.97
20	2.04	331.8	77265	0.702	1.47

Table J.1 Analysis of the Experimental Overall Tracer Response Curves (Continued)

Column without Trays, U_l= 1 cm/s					
U_g (cm/s)	**Mass of Tracer (g)**	**RT (sec)**	**s^2 (sec^2)**	s^2_D	$N = 1/ s^2_D$
0	2.28	223.8	6877	0.137	7.28
1	2.06	224.9	28264	0.559	1.79
4	2.30	212.8	27432	0.606	1.65
8	2.24	202.9	25820	0.627	1.59

Column without Trays, U_l= 1.5 cm/s					
U_g (cm/s)	**Mass of Tracer (g)**	**RT (sec)**	**s^2 (sec^2)**	s^2_D	$N = 1/ s^2_D$
1	1.95	150.80	11370.3	0.500	2.00
4	1.95	149.82	11380.1	0.507	1.97
8	1.89	135.76	10505.5	0.570	1.75

Table J.2 Experimental Parameter Estimation of the N-CSTR with Backmixing Model in the Time Domain (Fitted N and k)

Tray Type #1 (d_o=1.74 cm, 10.2 %O.A.), U_l = 0.5 cm/s					
U_g (cm/s)	**N**	**k**	**R^T_B**	**$s^2_{D,B}$**	**$s^2_{D,E}$**
1	5	0.189	0.0148	0.258	0.240
4	5	0.503	0.0118	0.341	0.324
8	6	0.851	0.0116	0.366	0.330
12	7	1.282	0.0101	0.391	0.369
16	7	1.196	0.0085	0.379	0.386
20	7	1.187	0.0091	0.376	0.389

Tray Type #1 (d_o=1.74 cm, 10.2% O.A.), U_l = 1 cm/s					
U_g (cm/s)	**N**	**k**	**R^T_B**	**$s^2_{D,B}$**	**$s^2_{D,E}$**
1	6	0.142	0.0167	0.205	0.206
4	6	0.232	0.0130	0.228	0.225
8	6	0.220	0.0124	0.225	0.232
12	6	0.286	0.0108	0.242	0.218
16	6	0.377	0.0107	0.264	0.257

Table J.2 Experimental Parameter Estimation of the N-CSTR with Backmixing Model in the Time Domain (Fitted N and k) (Continued)

Tray Type #1 (d_o=1.74 cm, 10.2 %O.A.), U_l = 1.5 cm/s					
U_g (cm/s)	**N**	**k**	**R^T_B**	**$s^2_{D,B}$**	**$s^2_{D,E}$**
1	6	0.055	0.0148	0.182	0.170
4	6	0.068	0.0191	0.185	0.164
6	6	0.148	0.0867	0.207	0.199
8	6	0.108	0.0176	0.196	0.184
12	6	0.168	0.0223	0.212	0.195
16	8	0.387	0.0335	0.205	0.205

Tray Type #2 (d_o=0.6 cm, 5.2% O.A.), U_l = 0.5 cm/s					
U_g (cm/s)	**N**	**k**	**R^T_B**	**$s^2_{D,B}$**	**$s^2_{D,E}$**
0	13	0.364	0.0904	0.127	0.154
1	6	0.286	0.0256	0.242	0.238
2	6	0.395	0.0114	0.268	0.268
4	5	0.236	0.0069	0.271	0.273
6	5	0.256	0.0082	0.277	0.270
8	5	0.264	0.0091	0.279	0.271
12	5	0.271	0.0151	0.281	0.291
16	6	0.381	0.0107	0.264	0.235
18	5	0.250	0.0126	0.275	0.266

Table J.2 Experimental Parameter Estimation of the N-CSTR with Backmixing Model in the Time Domain (Fitted N and k) (Continued)

Tray Type #2 (d_o=0.6 cm, 5.2% O.A.), U_l = 1 cm/s (Fitted N and k).					
U_g (cm/s)	**N**	**k**	**R^T_B**	**$s^2_{D,B}$**	**$s^2_{D,E}$**
0	24	0.773	0.1021	0.101	0.112
1	5	0.001	0.0101	0.200	0.191
4	6	0.148	0.0892	0.206	0.194
6	6	0.153	0.0841	0.208	0.200
8	6	0.171	0.0073	0.212	0.206
12	6	0.181	0.0074	0.215	0.213

Tray Type #2 (d_o=0.6 cm, 5.2% O.A), U_l = 1.5 cm/s					
U_g (cm/s)	**N**	**k**	**R^T_B**	**$s^2_{D,B}$**	**$s^2_{D,E}$**
1	6	0.080	0.0166	0.189	0.176
4	6	0.056	0.0092	0.182	0.173
6	6	0.083	0.0083	0.189	0.179
8	6	0.057	0.0089	0.182	0.171
12	6	0.119	0.0067	0.189	0.195

Table J.2 Experimental Parameter Estimation of the N-CSTR with Backmixing Model in the Time Domain (Fitted N and k) (Continued)

Tray Type #3 (d_o=0.6 cm, 10.2% O.A), U_l = 0.5 cm/s					
U_g (cm/s)	**N**	**k**	**R^T_B**	**$s^2_{D,B}$**	**$s^2_{D,E}$**
1	4	0.052	0.0250	0.246	0.221
4	4	0.151	0.0184	0.256	0.262
8	4	0.179	0.0171	0.301	0.298

Tray Type #3 (d_o=0.6 cm, 10.2% O.A.), U_l = 1 cm/s					
U_g (cm/s)	**N**	**k**	**R^T_B**	**$s^2_{D,B}$**	**$s^2_{D,E}$**
1	5	0.105	0.0113	0.233	0.191
4	6	0.273	0.0112	0.237	0.214
8	5	0.128	0.0095	0.240	0.228
12	6	0.353	0.0102	0.258	0.248

Column without Trays, U_l = 0.5 cm/s					
U_g (cm/s)	**N**	**k**	**R^T_B**	**$s^2_{D,B}$**	**$s^2_{D,E}$**
1	6	7.80	0.0364	0.496	0.576
8	5	7.92	0.0175	0.542	0.680
20	4	6.07	0.0230	0.789	0.702

Table J.2 Experimental Parameter Estimation of the N-CSTR with Backmixing Model in the Time Domain (Fitted N and k) (Continued)

Column without Trays, U_l = 1 cm/s					
U_g (cm/s)	**N**	**k**	**R^T_B**	**$s^2_{D,B}$**	**$s^2_{D,E}$**
1	3	0.997	0.0341	0.601	0.559
4	3	1.577	0.0273	0.645	0.606
8	3	1.78	0.0275	0.672	0.627

Column without Trays, U_l =1.5 cm/s					
U_g (cm/s)	**N**	**k**	**R^T_B**	**$s^2_{D,B}$**	**$s^2_{D,E}$**
1	5	1.742	0.0313	0.456	0.500
4	6	2.674	0.0375	0.459	0.507
8	6	2.723	0.0323	0.506	0.570

Table J.3 Experimental Parameter Estimation of the N-CSTR with Backmixing Model in the Time Domain (Fitted k and N=5)

Tray Type #1 (d_o=1.74 cm, 10.2 %O.A.), U_l = 0.5 cm/s, N=5				
U_g (cm/s)	**k**	**R^T_B**	**$s^2_{D,B}$**	**$s^2_{D,E}$**
1	0.189	0.0148	0.258	0.240
4	0.503	0.0118	0.341	0.324
8	0.590	0.0132	0.361	0.330
12	0.715	0.0105	0.389	0.369
16	0.651	0.0124	0.375	0.386
20	0.643	0.0105	0.373	0.389

Tray Type #1 (d_o=1.74 cm, 10.2 %O.A.), U_l = 1.0 cm/s, N=5				
U_g (cm/s)	**k**	**R^T_B**	**$s^2_{D,B}$**	**$s^2_{D,E}$**
1	0.050	0.0197	0.216	0.206
4	0.082	0.0187	0.226	0.225
8	0.071	0.0132	0.222	0.232
12	0.125	0.0105	0.239	0.218

Table J.3 Experimental Parameter Estimation of the N-CSTR with Backmixing Model in the Time Domain (Fitted k and N=5) (Continued)

Tray Type #1 (d_o=1.74 cm, 10.2 %O.A.), U_l = 1.5 cm/s, N=5				
U_g (cm/s)	**k**	**R^T_B**	**$s^2_{D,B}$**	**$s^2_{D,E}$**
1	0.055	0.0148	0.217	0.170
4	0.068	0.0191	0.221	0.164
8	0.108	0.0176	0.234	0.184
12	0.168	0.023	0.252	0.195
16	0.387	0.035	0.312	0.205

Tray Type #2 (d_o=0.6 cm, 5.2 %O.A.), U_l = 0.5 cm/s, N=5				
U_g (cm/s)	**k**	**R^T_B**	**$s^2_{D,B}$**	**$s^2_{D,E}$**
1	0.254	0.0150	0.276	0.238
2	0.25	0.0126	0.265	0.268
6	0.255	0.0082	0.276	0.270
8	0.263	0.0091	0.279	0.271
12	0.64	0.0091	0.279	0.291
16	0.197	0.0087	0.260	0.235
18	0.249	0.0099	0.275	0.266

Table J.3 Experimental Parameter Estimation of the N-CSTR with Backmixing Model in the Time Domain (Fitted k and N=5) (Continued)

Tray Type #2 (d_o=0.6 cm, 5.2 %O.A.), U_l = 1.0 cm/s, N=5				
U_g (cm/s)	**k**	**R^T_B**	**$s^2_{D,B}$**	**$s^2_{D,E}$**
1	0	0.0128	0.200	0.112
4	0	0.0145	0.200	0.191
6	0.016	0.0135	0.205	0.194
8	0.030	0.0122	0.210	0.200
12	0.024	0.0154	0.208	0.206
14	0.046	0.0136	0.215	0.229

Tray Type #2 (d_o=0.6 cm, 5.2 %O.A.), U_l = 1.5 cm/s, N=5				
U_g (cm/s)	**k**	**R^T_B**	**$s^2_{D,B}$**	**$s^2_{D,E}$**
1	0	0.0239	0.200	0.176
4	0	0.0563	0.200	0.173
6	0	0.0239	0.200	0.170
8	0	0.0079	0.200	0.179
12	0	0.0156	0.200	0.195

Table J.3 Experimental Parameter Estimation of the N-CSTR with Backmixing Model in the Time Domain (Fitted k and N=5) (Continued)

Tray Type #3 (d_o=0.6 cm, 10.2 %O.A.), U_l = 0.5 cm/s, N=5				
U_g (cm/s)	**k**	**R^T_B**	**$s^2_{D,B}$**	**$s^2_{D,E}$**
1	0.255	0.0253	0.276	0.221
4	0.385	0.0211	0.311	0.262
8	0.418	0.0193	0.319	0.298

Tray Type #3 (d_o=0.6 cm, 10.2 %O.A.), U_l = 1.0 cm/s, N=5				
U_g (cm/s)	**k**	**R^T_B**	**$s^2_{D,B}$**	**$s^2_{D,E}$**
1	0.105	0.0193	0.232	0.191
4	0.113	0.0112	0.235	0.214
8	0.128	0.0095	0.240	0.228
12	0.181	0.0150	0.255	0.248

Table J.4 Experimental Parameter Estimation of the ADM with Closed-Closed Boundary Conditions in the Laplace Domain

Tray Type #1 (d_o=1.74 cm, 10.2% O.A)					
U_l (cm/s)	**U_g (cm/s)**	**Pe_{ADM}**	**R^L_{ADM}**	**$s^2_{D,ADM}$**	**$s^2_{D,,E}$**
0.5	4	4.31	1.67E-03	0.358	0.324
0.5	12	3.69	1.07E-03	0.398	0.368
1	1	9.17	4.60E-03	0.231	0.206
1	16	6.06	8.56E-04	0.276	0.257
1.5	12	8.09	1.87E-03	0.217	0.195

Tray Type #2 (d_o=0.6 cm, 5.2% O.A)					
U_l (cm/s)	**U_g (cm/s)**	**Pe_{ADM}**	**R^L_{ADM}**	**$s^2_{D,ADM}$**	**$s^2_{D,,E}$**
0.5	0	12.34	2.63E-03	0.149	0.154
0.5	4	5.50	1.69E-03	0.298	0.273
0.5	8	5.40	1.81E-03	0.302	0.271
1	4	7.92	1.47E-03	0.221	0.194
1	8	7.39	1.86E-03	0.234	0.206
1	12	7.30	1.52E-03	0.237	0.213
1.5	1	9.10	8.93E-04	0.196	0.176
1.5	8	9.18	1.23E-03	0.194	0.171
1.5	12	8.16	1.15E-03	0.215	0.195

Table J.4 Experimental Parameter Estimation of the ADM with Closed-Closed Boundary Conditions in the Laplace Domain (Continued)

Tray Type #3 (d_o=0.6 cm, 10.2 %O.A)					
U_l (cm/s)	**U_g (cm/s)**	**Pe_{ADM}**	**R^L_{ADM}**	$s^2_{D,ADM}$	$s^2_{D,,E}$
0.5	1	6.15	4.52E-03	0.273	0.221
0.5	8	5.01	2.03E-03	0.320	0.298
1	4	6.96	1.08E-03	0.246	0.220
1	12	6.26	7.19E-04	0.269	0.248

Column Without Trays					
U_l (cm/s)	**U_g (cm/s)**	**Pe_{ADM}**	**R^L_{ADM}**	$s^2_{D,ADM}$	$s^2_{D,,E}$
0.5	20	0.79	6.05E-03	0.782	0.702
1	1	1.49	1.30E-03	0.645	0.559
1	8	1.16	1.58E-03	0.704	0.627
1.5	4	1.81	1.04E-03	0.594	0.507

Appendix K Comparison of the Residuals of the Fit between N-CSTR with Backmixing Model and ADM

In Sections 8.2 and 8.3 the fitting procedures used to determine the model parameters of the N-CSTR with Backmixing model and ADM, respectively, were reported. Further, the comparison of the residuals of the fit between the two models can help us to determine whether one of the models fits the experimental data better than the other. However, in order for the comparison between the two models to be meaningful, the residuals of the fit have to be evaluated in the same frame of reference. We can compare the value of the residuals in the time domain or in the Laplace domain. In either case, if the residuals for one of the two models are statistically smaller than the other, then it can be concluded that this model fits the experimental data better than the other.

First, let us try to conduct the comparison in the Laplace domain since an approximate analytical transfer function for the N-CSTR with Backmixing model has been derived by *Zitny et al., 1996*.

$$\overline{E}_B(s*,1) = \frac{2^N (1+k)^{N-1} H(s*)}{J_+(s*) - J_-(s*)} \tag{K.1}$$

$$H(s*) = \sqrt{\left(1 + \frac{s*}{N}\right)^2 + \frac{4\,k\,s*}{N}} \tag{K.2}$$

$$J_{\pm}(s*) = \left(1 + \frac{s^*}{N} + 2k \pm H(s^*)\right)^{N-2} \left(1 + \frac{s^*}{N} \pm H(s^*)\right)\left[\left(1 + \frac{s^*}{N} + k\right)\left(1 \pm H(s^*)\right) + \frac{s^*}{N}\left(1 + \frac{s^*}{N} + 3k\right)\right] \tag{K.3}$$

The residual objective function for the model can be written in the Laplace domain, Equation K.4, where $\overline{E}_E(s_i^*)$ and $\overline{E}_B(s_i^*)$ are experimental and model transfer functions, respectively.

$$R_B^L(s_i^*, k, N) = \sqrt{\sum_{i=1}^{S_{total}} \frac{\left[\overline{E}_E(s_i^*) - \overline{E}_m(s_i^*, k, N)\right]^2}{t_{total} - 2}} \qquad \text{(K.4)}$$

$i = 1, \ldots, t_{total}$

As pointed out in Section H.2 of Appendix H, the values of the dimensionless Laplace variable *s** have to be carefully selected. In general, too low or too large values need to be avoided *(Hopkins et al., 1969).* By trial and error, it was found that in this case there are almost no differences in the estimation of the model parameter values as long as s* is kept within the range bounded by s*=1, and s*=10.

Figure K.1 shows the Parity Plot of the residuals, from where it is very hard to conclude which of the models does a better job in fitting the experimental data since the residuals are approximately equally spread above and below the diagonal line.

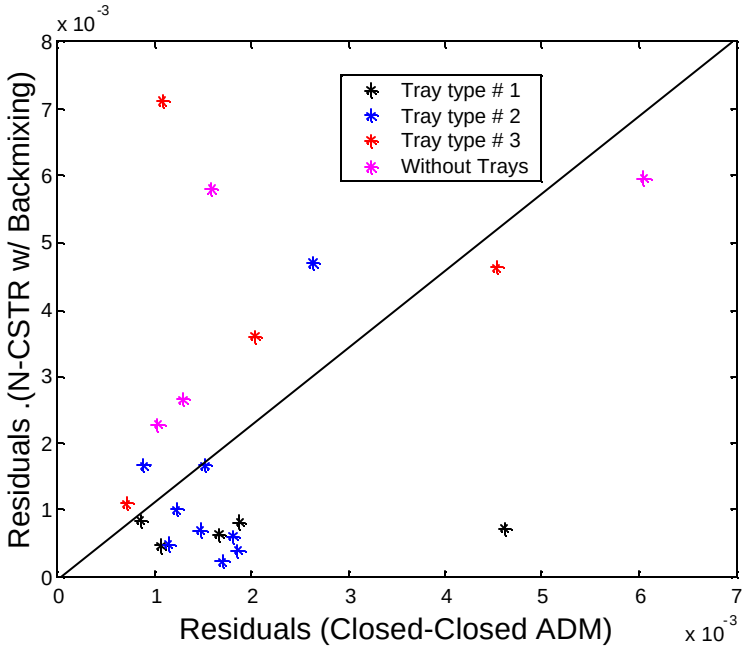

Figure K.1 Parity Plot of the Residuals of the ADM and the N-CSTR with Backmixing Model in the Laplace Domain.

Accepting the hypothesis of random sampling of the differences between the residuals of the two models, d_i, from a normal distributed population with mean d and variance s; then we can use a student or t-distribution to compare the mean value of the sample of differences $\bar{d}$ with the real mean of the distribution δ. If there are n differences, then $(\bar{d} - d)/(S_d/\sqrt{n})$ is t-distributed with n-1 degrees of freedom, where S_d^2 is the population sample variance defined as follows:

$$S_d^2 = \frac{\sum_{i=1}^{n} (d_i - \bar{d})^2}{n-1} \qquad \text{(K.5)}$$

We can test the hypothesis that the real mean of the differences of the residuals between the two models are not statistically different (Null hypothesis, δ=0), against the mean value of the population of available samples, $\bar{d}$. On behalf of the Null Hypothesis, we can write:

$$t = \frac{(\bar{d} - 0)}{s_d / \sqrt{n}} \qquad \text{(K.6)}$$

If the probability that t is smaller or equal than 5%, then we can reject the Null hypothesis at the 5% significant level (1-side test). In this case, it can be stated that there is a statistically significant difference between $\bar{d}$ and δ. In other words, $\bar{d}$ is statistically different than zero and the residuals given by the models can be said be different.

Let us apply the above test to our sample population of differences of residuals, where n=22, $\bar{d} = R_B^L - R_{ADM}^L = 2.48x10^{-4}$, S_d=2.046 x10^{-3}, $S_d / \sqrt{n}$ = 4.362 x10^{-4}, and t = $\frac{\bar{d} - 0}{S_d / \sqrt{n}} = 0.568$

Looking at the tables for a t-distribution with n-1=21 degrees of freedom, then the probability that t is larger than 0.568 is equal to 28.8%, which is larger than the 5% significant level, and thereby the Null Hypothesis can not be rejected.

Therefore, the residuals, which are a measure of goodness of the fit, are not statistically different. As a result, neither the N-CSTR with Backmixing Model nor the Axial Dispersion Model can be said to fit the experimental data better than the other when they are used and compared in the Laplace domain.

How do the two models behave when they are compared in the time domain? Are the differences in the residuals insignificant as it was the case in the Laplace domain?

As it was mentioned in Section 8.3, *Brenner (1962)*, derived an analytical solution for the one-dimensional Axial Dispersion Model with closed-closed boundary conditions

(Equation 8.6). However, the series does not converge for small times and therefore it cannot be used to generate the complete E-curve.

One valid alternative is to numerically invert the model's Laplace transfer function (Equation 8.18) into the time domain by a proper numerical algorithm. The Quotient Difference Method with Accelerated Convergence for the Continued Fraction Expansion (*De Hoog et al., 1982*) has been found to do the job very efficiently. Using this approach, we can convert the Laplace's transfer function into the time-domain E-curves, estimate the residuals in this frame, and finally compare the residual values yielded by the two models at the same experimental conditions. The model parameter values used in this case are the fitted Peclet numbers, which were previously estimated from the minimization of the objective function in the Laplace domain (Equation H.4).

Figure K.2 shows the Parity Plot of the residuals in the time domain for both models.

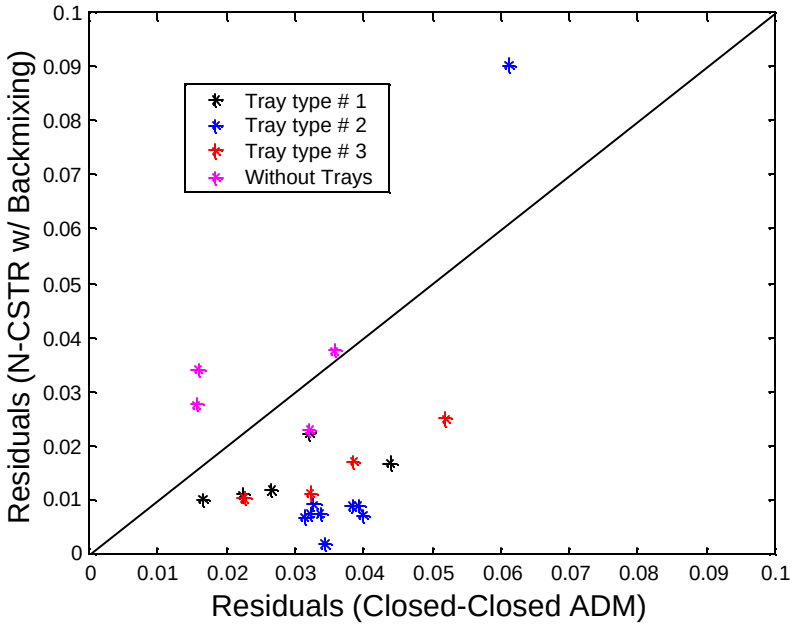

Figure K.2 Parity Plot of the Residuals of the ADM and the N-CSTR with Backmixing Model in the Time Domain.

It can be seen how in this case most of the points are now located below the diagonal line, indicating the better performance of the N-CSTR with Backmixing model over the ADM in fitting the experimental data.

In order to numerically prove the above statement, let us do the same statistical analysis that was previously conducted for the differences in the residuals estimated in the Laplace domain.

n=22, $\bar{d} = R_B^T - R_{ADM}^T = -0.0148$, S_d=0.0170, $S_d/\sqrt{n} = 3.617\ 10^{-3}$, and t = $\dfrac{\bar{d} - 0}{S_d/\sqrt{n}}$ =-4.091

Looking at the tables for a t-distribution with n-1=21 degrees of freedom, then the probability that t is smaller than –4.091 is equal to 0.026%, which is much smaller than the 5% significance level. Hence, the Null Hypothesis can be very comfortably rejected. Therefore, there is a real effect here and the residuals given by the N-CSTR with Backmixing model are significantly smaller than the values given by the ADM when both models are compared in the time domain frame.

References

Bakopoulos, A., "Scale-up of Three Phase Photo-biochemical Reactors for Algae Microorganisms Production", Presented at 1998 AIChE Annual Meeting, Scale-up/Scale-down of Multiphase Reactors session, Miami Beach, FA, Nov. 15-20, (1998).

Blass, E., and Cornelius, W., "The Residence Time Distribution of Solid and Liquid in Multistage Bubble Columns in the Co-current Flow of Gas, Liquid, and Suspended Solids", *Multiphase Flow*, **3**, 459-469 (1977).

Box, G.E.P., Hunter, and W.G., Hunter, J.S., "Statistics for Experimenters", Wiley Series in Probability and Mathematical Statistics, John Wiley & Sons, Inc., 1979.

Brenner, H., "Diffusion Model of Longitudinal Mixing in Beds of Finite Length-Numerical Values", Chem. Eng. Sci., **17**, 229-243 (1962).

Buffham, B. A., and Gibilaro, L.G., "A Generalization of The Tanks-in-Series Mixing Model", *AIChE J*., **14**, 805-806 (1968).

Chen, B.H., and Yang, N.S., "Characteristics of a Co-current Multistage Bubble Column", *Ind. Eng. Chem. Res*., **28**, 1405-1410 (1989)

Chen, B.H, Yang, N. S., and Mc Millan, A.F., "Gas Holdup and Pressure Drop for Air-Water flow through Plate Bubble Columns", *Can. J. Chem. Eng.* **64**, 387-392 (1986).

Chiang, D., Cholette, A., and Bang, V., "Optimum Attenuation of Inlet Fluctuations in a Flow System for Imperfectly Mixed Tanks in Series", *Can. J. Chem. Eng*, **53** (5), 521-526 (1975)

Cholette A., and Cloutier, Z., "Mixing Efficiency Determinations for Continuous Flow Systems", *Can. J. Chem. Eng*., **37**, 105-112 (1959).

Danckwerts, P.V., "Continuous Flow Systems: Distribution of Residence Times", *Chem. Eng. Sci*., **2**, 1-18 (1953)

Dassori G., Personal Communication, Intevep-PDVSA (1999)

De Hoog, F. R., Knight, J. H., and Stokes, A. N. "An Improved Method for Numerical Inversion of Laplace Transforms", *S.I.A.M. J. Sci. and Stat. Comput*., **3**, 357-366, (1982).

Dreher A.J., and Krishna, R., "Liquid Phase Backmixing in Bubble Columns, Structured by Introduction of Partition Plates", *Catalysis Today*, **69**, 165-170, (2001).

Dudukovic, M. P., Chen, J.C., Fan., L., Degaleesan, S., Guptan, P., Al-Dahhan, H.A., and Toseland, A. B., "Fluid Dynamic Parameters in Bubble Columns with Internals", *Chem. Eng. Sci.* **54**, 2187-2197 (1999).

Eickhoff, H., and Schutte, R., "Design of Perforated Trays for use in Bubble Column Reactors, especially for use in manufacture of Hydrogen Peroxide", *PCT Int. Appl*. (2000).

Fan, L.T., and Wen, C.Y., "Models for Flow Systems and Chemical Reactors", Marcel Dekker, Inc., New York, (1975).

Guitián, J., and Joseph, D., "How Bubbly Mixtures Foam and Foam Control Using a Fluidized Bed", *Int. J. Multiphase Flow Vol.* **24** (1), 1-16 (1998).

Gupta, P., Muthanna, M.H., Dudukovic M.P., and Mills, P.L.A.,"A Novel Signal Filtering Methodology for Obtaining Liquid Phase Tracer Responses from Conductivity Probes", Flow Meas. Instrum., **11,** 2, (1999).

Hewitt, G., F., "Measurement of Drops and Bubble Sizes", Handbook of Multiphase Systems, Chapter 10, Hemisphere Pub Corp, New York (1982).

Hoeller, V., Radevik, K., Lioubov, K., and Renken, A., "Bubble Columns Staged with Structured Fibrous Catalytic Layers: Residence Time Distribution and Mass Transfer Bubble Columns Staged with Structured Fibrous Catalytic Layers: Residence Time Distribution and Mass Transfer", *Ind. Eng. Chem. Res.* **40** (6), 1575-1579 (2001).

Hopkins, M. J., Sheppard, A.J., and Eisenklam, P., "The Use of Transfer Functions in Evaluationg Residence Time Distribution Curves", Chem. Eng., Sci., **24**, 1131-1136 (1969).

Houzelot, J.L., Thiebaut, M.F., Charpentier, J.C., and Shicber, J., *Entropie*, N^{o} 113-114, (1983).

Ichikawa, Y., Y. Akachi, and K. Makino, "On the Longitudinal Mixing Charactiristics of Gas Bubble Column with Perforated Plates", *Kagaku kogaku* (abridged ed.) **5**, 179-182 (1967).

Joshi, J.B., Veera, U.P., Prasad, C. V., Phanikumar, D.V., Deshphande, N.H., Thakre, S.S., and Thorat, B.N., "Gas Holdup Structure in Bubble Column Reactors", PINSA, **64** (4), 441-567 (1998).

Joshi, J.B., and Sharma, M. M., "A Circulation Cell Model for Bubble Columns", *Trans. I. Chem. E.*, **57**, 245 (1979).

Karr, A.E., "Performance of a Reciprocating-Plate Extraction Column", *AIChE J.*, **5** 446-452 (1952).

Kastánec, F., Zahradnik, J., Kratochvil, J., and Cermak, J. "Chemical Reactions for Gas-Liquid systems", Ellis Horwood Series in Chemical Engineering, ACADEMIA ed., 1993.

Kato, Y., Kago, T., and Morooka, S., "Longitudinal Concentration Distribution of Droplets in Multi-Stage Bubble Columns for Gas-Liquid Systems", *J. Chem. Eng. Japan*, **17**, 429-435 (1984).

Kato, Y., Kago, T., Morooka, S., and Nishiwaki, A., "Longitudinal Dispersion of Droplet Phase in Single and Multi-Stage Bubble Columns for Gas-Liquid-Liquid Systems", *J. Chem. Eng. Japan*, **18**, 154-158 (1985).

Kats, M.B., and Genin, L.G., "Study of Longitudinal Mixing of Liquid in Co-current Sparged Reactors Sectionalized with Sieve Trays", *Int. Chem. Eng*., **7** (2), 246-252 (1967).

Kitai, A., Shinji, G.,Ozaki, A., "The Performance of Perforated Column as a Multistage Continuous Fermentor", *J. Ferment. Technol*., **47** (6), 340-347 (1969).

.

Letzel, H. M., Schouten, J.C., Krishna, R., and Van den Bleek, C.M., "Characterization of Regime Transitions in Bubble Columns by Chaos Analysis of Pressure Signals", *Chem. Eng. Sci*., **52** (24), 4447-4459 (1996).

Levenberg, K., "A Method for the Solution of Certain Problems in Least Squares", *Quart. Apl. Math.*, **2**, 164-168 (1944).

Levenspiel, O., "Chemical Reaction Engineering", 2nd ed., John Wiley and Sons., Inc., New York, (1962).

Liang, S.H., Bavarian, R.L., Gorowara, R.L., and Kreischer, B.E., "Hydrodynamics of Gas-Liquid-Solid Fluidization Under High Gas Holdup Conditions", Powder Technology, **53**, 285-293 (1987).

Lide, R.D., "CRC Handbook of Chemistry and Physics", CRC Press Inc., 72nd Ed., New York, 1992.

Lucke J., Schugerl, K., Oels, U., "Bubble Column Bioreactors", Advances in Biochemical Engineering **(7)**, 1-83 (1977).

Magnussen, P., and Schumacher, V., "Axial Mixing of Liquid in Packed Bubble Columns and Perforated Plate Columns of Large Diameter", *Ger. ACS Symp. Ser*., 337-347 (1978).

Maretto C., and Krishna, R., "Design and Optimization of a Multi-Stage Bubble Column Slurry Reactor for Fischer-Tropsch Synthesis", 3rd International Symposium on Catalysis in Multiphase Reactors; Naples, Italy, 29-31 May (2000).

Marquardt, D., "An Algorithm for Least-Squares Estimation of Non-linear Parameters", *SIAM J. Appl. Math.*, **11**, 431-441 (1963).

Mecklenburgh J.C., Hartland S., The Theory of Backmixing. J. Wiley, London 1975.

Miyauchi,T., "Ryukeisosa to Kongotokusei", *Nikkan-Kogyo-Shinbunsha*, (1960).

Munter, R., Kamenev, S., and Sarv, L., "Design of a Staged Downflow Bubble Reactor", *Ozone: Sci. Eng.*, **12** (4), 437-455 (1990).

Myers, J., K., "Liquid-Phase Mixing in Churn Turbulent Bubble Columns", D.Sc. Thesis, Department of Chemical Engineering, Washington University, St. Louis, MO, USA, 1986.

Nauman, E.B., and Buffham, B.A., "Mixing in Continuous Flow Systems", John Wiley & Sons, New York, 1983.

Nishiwaki, A., and Kato, Y., "Longitudinal mixing of liquids in multistage bubble columns", *Kagaku Kogaku*, **36** (10), 1112-1116 (1972).

Nishikawa, M., Shino, K., Kayama, T., Nishioka, S., and Hashimoto, K., "Gas Absorption in a Multi-Stage Gas-Liquid Spouted Vessel", *J. Chem. Eng. Japan*, **18**, 496-501 (1985).

Ostergaard, K., and Michelsen, M.L., "On the Use of the Imperfect Tracer Pulse Method for Determination of Holdup and Axial Mixing", *Can. J. Chem. Eng.*, **47**, 107-112 (1969).

Palaskar, S. N., De, J. K., and Pandit, A.B., "Liquid Phase RTD Studies in Sectionalized Bubble Column", *Chem. Eng. Technol.*, **23** (1), 61-69 (2000).

Patil, V. K., Joshi, J.B., and Sharma, M., "Sectionalized Bubble Column: Gas Holdup and Wall Side Solid-Liquid Mass Transfer Coefficient", Can. J. Chem. Eng., **62**, 228-232, 1984.

Poncin, S., Midoux, N., and A. Laurent, "Hydrodynamics and Residence Time Distribution in a Counter Current Slurry Bubble Column Partitioned with Sieve Plates", *Proc. World Congress IV*", Sect. 8.2-11 (1990).

Prenosil, J., and Novosad, Z, *Coll. Czech. Chem. Commum.*, **33**, 376 (1968).

Raghuraman, J., Varma, B.G., "A Model for Residence Time Distribution in Multistage Systems with Cross-flow between Active and Dead Regions", Chem. Eng. Sci., **28**, 585-591 (1973).

Reháková, M., and Novosad, Z.,"Residence Time Distribution and Fractional Conversion for a Multistage Reactor with Backmixing between Real Stages", *Chem. Eng. Sci.*, **23**, 139-145 (1967).

Roemer, M., H., and Durbin, L., D., "Transient Response and Moments Analysis of Backflow Cell Model for Flow Systems with Longitudinal Mixing", I. & E. Fundamentals, **6** (1), 120-129 (1967).

Schugerl, K., Todt, J., Lucke, J., and Renken, A., "Gas Holdup and Longitudinal Dispersion in Different Types of Multiphase Reactors and their possible Application for Microbial Processes", *Chem. Eng. Sci.*, **32**, 369-375 (1977).

Sekizawa, T., and Kubota, H., " Liquid Mixing in Multistage Bubble Column", *J. Chem. Eng. Japan* **7**, 441-446 (1974).

Sekizawa, T., and Kubota, H., "Effect of Partition Plate on Dispersion of Suspended Solid Particles in Multistage Bubble Columns", *J. Chem. Eng. Japan* **18**, 14-19 (1975).

Shah, Y.T., Kelkar, B.G., Godbole, S.P., and Deckwer, W.D., "Design Parameters Estimations for Bubble Column Reactors", *AIChE J.* **28** (3), 353-379 (1982).

Thyn, J., Zitny, R., Kluson, J., and Cechak, T., "Analysis and Diagnostics of Industrial Processes by Radiotracers and Radioisotope Sealed Sources", Vydavatelstvi CVUT, Praha, 2000.

Urseanu, M., I., Ellenberger, J., and Krishna, R., "A Structured Catalytic Bubble Column Reactor: Hydrodynamics and Mixing Studies", *Catalysis Today*, **69**, 105-113 (2001).

Vinaya, M., "Multistage Bubble Column, and Liquid Pulsed Column", D.Sc. Thesis, Department of Chemical Engineering, Indian Institute of Technology Madras, India (1994).

Vinaya, M., and Varma, Y.B.G., "Some Aspects of Hydrodynamics in Multistage Bubble Columns", Bioprocess Eng., **2**, 231-237 (1995).

Wakao, N., and Chen, B.H., "Frictional Gas in Multiplate Bubble Columns", *Can. J. Chem. Eng.*, **66**, 145-149 (1988).

Yamada, H., and Goto, S., "Gas and Liquid Holdups in Multi-Stage Bubble Columns for Gas-Liquid-Liquid-Solid Four-Phase System", *J. Chem. Eng. Japan*, **31** (5), 813-817 (1998).

Yang, N.S., and Chen, B.H., “Characteristics of a Cocurrent Multistage Bubble Column”, Ind. Eng. Chem. Res., **28**, 1405-1410 (1989).

Zitny, R., and Thyn, J., “Residence Time Distribution Software Analysis”, Computer Manual Series No. 11, IAEA, Vienna (1966).

Vita

Javier Alvaré was born on July 22, 1973 in Avilés, Spain. He attended the University of Oviedo in Oviedo, Spain from 1992-1997 and earned a B.S. in Chemical Engineering. He worked in the Manufacturing Department of Asturiana de Zinc, S.A. in Avilés, Spain as a summer intern from July to August 1999. Javier is currently employed at Air Products and Chemicals, Inc. in Allentown, PA. He has been working as an engineer in the Research and Development Department since 2001. He is also completing his M.S. degree in Chemical Engineering from Washington University in St. Louis, MO. His M.S. work on Gas Holdup and Liquid Phase Mixing in Trayed Bubble Columns has been presented at two American Institute of Chemical Engineers (AIChE) National Meetings. Javier has been an AIChE member since 1999.

August 2002